# Fresh Groundwater Resources in Coastal Deltas

**by**

**Aspen Anderson**

B.Sc. (Geophysical Engineering), Colorado School of Mines, 2017

Thesis Submitted in Partial Fulfillment of the
Requirements for the Degree of
Doctor of Philosophy

in the
Department of Earth Sciences
Faculty of Science


SIMON FRASER UNIVERSITY
Spring 2023

## Declaration of Committee

| | |
|---|---|
| **Name:** | **Aspen Anderson** |
| **Degree:** | **Doctor of Philosophy** |
| **Title:** | **Fresh Groundwater Resources in Coastal Deltas** |
| **Committee:** | **Chair:** Brent Ward<br>Professor, Earth Sciences |
| | **Diana Allen**<br>Supervisor<br>Professor, Earth Sciences |
| | **Jeremy Venditti**<br>Committee Member<br>Professor, Environmental Science |
| | **Carl Mendoza**<br>Examiner<br>Professor Emeritus, Earth and Atmospheric Sciences<br>University of Alberta |
| | **Holly Michael**<br>External Examiner<br>Professor, Earth Sciences<br>University of Delaware |

# Abstract

Coastal deltas house more than 335 million people worldwide in some of the largest population centers in the world, including growing megacities such as Shanghai, Dhaka, and Bangkok. These populations often rely heavily upon groundwater resources to meet domestic, agricultural, and industrial water demands—making the sustainability of fresh groundwater resources critical to ensuring the longevity of coastal communities. This research uses delta morphology as a tool for understanding the distribution of fresh and saline groundwater within coastal deltas.

Morphodynamic modeling simulating the formation of coastal deltas is used to explore how delta morphology impacts hydrogeologic characteristics within deltas. Data from deltas around the world are used to create 207 unique models that span the full range and combination of fluvial and marine influences. Simulated landforms depict the characteristics expected in fluvial, wave, and tidal influenced deltas; these landforms are used to generate spatially varying permeability profiles for each simulated delta. High permeability areas within coastal deltas are often associated with the river network and are highly connective. A distance-based sensitivity analysis shows that deltaic permeability, hydraulic gradient, and groundwater flow rates are sensitive to changes in delta morphology and geomorphic characteristics.

Two-dimensional density-dependent groundwater flow and solute transport modeling is used to simulate the horizontal fresh-saline water distribution within the shallow subsurface in representative fluvial, wave, and tidal deltas. The volume of saline water in the shallow subsurface within deltas is estimated to vary between 36% and 89% of the total groundwater volume, depending on the morphodynamic influences and the amount of recharge the delta receives. Results show that deltas located in dry climates are most susceptible to salinity and that wave or fluvial delta are especially susceptible. The generic groundwater models of the three delta types are used to understand the vulnerability of 55 real deltas to groundwater salinization. The result of this research provides an initial estimate of the amount of freshwater within deltas, identifies where salinity is most likely to occur within a delta, and suggests which delta types are most vulnerable to groundwater degradation.



**Keywords:** coastal groundwater; delta morphology; permeability; salinity.

*For the teachers, family, and friends*

*who have inspired*

*my knowledge, love, and curiosity of the natural world.*

# Acknowledgements

This research would not have been possible without the support, patience, and encouragement of Dr. Diana Allen. Thank you for guiding me throughout this pursuit and for your confidence in me. I would also like to thank Dr. Jeremy Venditti for always proving insightful comments, reminding me to ground everything in the fundamentals, and engaging with me in interesting scientific discussions.

I believe it is also important to recognize all the teachers, educators, and mentors who have inspired my pursuit of science and engineering; I would not be here without them. Although I could never list every person this applies to, I want to specifically acknowledge a few. Dr. Terri Houge, thank you for showing me the importance of water resources and believing in me. Your guidance and support were invaluable. Dr. Brandon Dugan, thank you for advising me and being the first to introduce me to hydrogeology. I also want to thank Dr. Gwenn Flowers, Dr. Stephanie Fanslow, Dr. Andrei Swidinski, Dr. Toby Ault, Nicholas Horianopoulos, Abby Davidson, Nathan Kirkley, Nick True, John Thayer, and Steven Walder. I am deeply appreciative of the knowledge and wisdom each of you has shared with me.

Most importantly, I want to thank my parents and my teachers in life: **Ann Murphy** and **Dr. Steven Anderson**. These two incredible people have given me more support, guidance, and love than I could have ever imagined. Words will never be enough to express my gratitude and love for you.

# Table of Contents

# List of Tables

# List of Figures

# Chapter 1.

# Introduction

## 1.1. Introduction

Coastal deltas house more than 335 million people worldwide in some of the largest population centers in the world, including growing megacities such as Shanghai, Dhaka, and Bangkok (Edmonds et al., 2020). Deltas that do not house large population centers are often productive agricultural hubs and marine ecosystem sanctuaries—conservative estimates report deltas collectively have a multi-trillion-dollar value in terms of economic revenue and ecosystem services (Giosan et al., 2014). Populations living on costal deltas often rely heavily upon groundwater resources to meet domestic, agricultural, and industrial water demands—making the sustainability of fresh groundwater resources critical to ensuring the longevity of these coastal communities (Post and Abarca, 2010; van Weert and van der Gun, 2012; Custodio and Bruggeman, 2013). Furthermore, submarine groundwater discharge supplied through deltas is critical for the surrounding marine ecosystems (Kolker et al., 2013). Deltas are widely recognized as highly vulnerable systems, with anthropogenic activities associated with climate change and urbanization impacting the structural integrity of these coastal landforms as well as the groundwater systems (Lee et al., 2021).

Much of the recent research surrounding delta sustainability has focused on future structural and geomorphic changes within deltas arising from relative sea level rise and upstream stressors, most notable of which is river damming (Syvitski, 2008; Elliott, 2009; Giosan et al., 2014; Ingebritsen and Galloway, 2014; Elliott et al., 2019; Hoitink et al., 2020). Globally, about 3,700 hydroelectric dams are under construction or planned; these dams impact some of the largest river systems in South America, South and East Asia, and Africa (Mulligan et al., 2020). Changing land management practice and river damming is projected to reduce sediment flux to coastal deltas significantly (up to 83% reduction) by the end of the century (Dunn et al., 2019). Sediment starvation and relative sea level rise are expected to increase erosion of deltaic lands and could provoke extensive ecosystem loss, economic and social crises, and large-scale migration (Syvitski, 2008; Mazzotti et al., 2009; Overeem and Syvitski, 2009; Syvitski et

al., 2009, 2010; Giosan et al., 2014; Tessler et al., 2015; Davis et al., 2018). It is estimated that approximately 5% of global deltaic land will be lost by 2100, with 85% of the loss caused by sea level rise (Nienhuis and van de Wal, 2021).

The sustainability of deltaic land and coastal groundwater resources have closely linked feedbacks—changes that occur on the land surface affect groundwater quantity and quality while changes within the groundwater system can impact land surface elevation. In the Mekong Delta, land subsidence driven by groundwater extraction is the primary mechanism accelerating relative sea level rise; the extraction-induced subsidence threatens to displace the 18 million inhabitants in addition to compromising a large source of Southeast Asia's agri- and aquaculture production (Minderhoud et al., 2017, 2020). One proposed method for counteracting relative sea level rise is to reduce human-induced land subsidence through the limitation of groundwater withdrawal in coastal cities (Nicholls et al., 2021). While coastal engineering efforts help counteract deltaic land loss, these engineering structures can have detrimental effects on the groundwater system. One of the most notable examples of this is the creation of the polders in The Netherlands—a practice that resulted in the upwelling of deep saline groundwater and contamination of near surface groundwater reserves (Oude Essink et al., 2010). Research evaluating the availability of fresh groundwater in deltas is a relatively recent field of study that has gained attention out of necessity. Degradation of groundwater resources through anthropogenic activities associated with climate change and urbanization (i.e. groundwater overdrafts, coastal engineering, and urban loading) have highlighted the need for hydrogeologic evaluation of deltaic systems.

The present subsurface fresh-salt water distribution in deltas is a product of geomorphic evolution over thousands of years (Stanley and Warne, 1994). Transgressive and regressive sea level regimes resulted in the formation of aquifer/aquitard structures that are highly heterogeneous and often discontinuous across the delta plain (Michael and Khan, 2016; Larsen et al., 2017). The resulting semi-confined leaky aquifers experience both groundwater freshening and salinization over geologic timescales as sea level varies, resulting in complex mixing patterns between paleowater and fresh recharge (Post and Abarca, 2010; Delsman et al., 2016; Kim et al., 2017; Larsen et al., 2017; Van Pham et al., 2019). Understanding how heterogeneous deltaic aquifer systems and the resulting subsurface salinity distributions have evolved to

their present status is paramount to estimating how much freshwater is currently available in deltas.

In the future, the biggest threat to the quality of deltaic groundwater resources globally is from seawater intrusion and interactions with saline paleowater; paleowater is defined as groundwater emplaced under previous climatic and hydrogeologic settings (Oude Essink, 1996; Custodio, 2002; Vandenbohede et al., 2008; Wada et al., 2010; Custodio and Bruggeman, 2013). Seawater intrusion and the upwelling of saline paleowater are expected to increase as sea levels rise and groundwater pumping is relied upon more as a source of freshwater. For example, in the Mekong Delta, groundwater abstraction has increased steadily since 1980 to meet the growing industrial, agricultural, and domestic demand; daily groundwater abstraction rates are estimated at 2.5 million $m^3$ throughout the delta (Wagner and Mahrwald, 1980; Wagner et al., 2012; Minderhoud et al., 2017, 2020). Although mixing of saline paleowater with fresh groundwater often plays a more important role in coastal salinization than saltwater intrusion, very few studies have focused on understanding how these paleowaters formed and how they may respond in the future to natural and anthropogenically induced change (Oude Essink et al., 2010; Delsman et al., 2014; Antonellini et al., 2015; Larsen et al., 2017; Van Pham et al., 2019). Furthermore, coastal aquifers with high groundwater use are more vulnerable to groundwater salinization due to abstraction than to sea level rise, suggesting that efforts to adapt to sea level rise at the expense of better water management are misguided (Ferguson and Gleeson, 2012). Understanding the amount of freshwater available within coastal deltas is the first step to sustainable use of freshwater resources and protection of deltaic lands.

This research employs morphodynamic and hydrogeologic modeling to explore how delta morphology impacts the permeability distribution, and ultimately, the distribution of fresh and saline groundwater within deltas around the world. Morphodynamic modeling is used to simulate the formation of coastal deltas and explore how delta morphology impacts the hydrogeologic properties within deltas. The permeability distribution, connectivity of high permeability material, hydraulic gradient, and specific discharge are characterized for three classic end-member morphologies (fluvial, wave, and tidal influenced deltas) to understand how morphology impact hydrogeology in coastal deltas. Groundwater modeling is then used to understand the fresh/saline water distribution present within each of the delta types, furthering our

understanding of how much fresh groundwater is available within coastal deltas globally. The models developed in this study are used to investigate the vulnerability of 60 deltas around the world to groundwater salinization. The modeling approach used in this research deviates from the majority of current hydrogeologic research, which has been carried out on a case-by-case basis. The approach is intended to be applicable to generic systems, and therefore, can aid in understanding the factors controlling salinity in coast deltas on a global scale. The result of this research provides an initial estimate of the amount of freshwater within deltas globally, pinpoints where salinity is most likely to occur within a delta, and identifies which deltas are most vulnerable to groundwater degradation.

## 1.2. Background and previous research

### 1.2.1. Delta formation

Deltas are complex depositional landforms that develop when a sediment-bearing river loses transport competence as it enters a standing or slow-moving body of water. Coastal deltas form where a river discharges into an ocean if the deposition rate of continental debris supplied by the river is greater than the erosion rate from marine influences (traditionally identified as waves, tides, and longshore currents). A coastal delta will only form if there is space available along the coastal margin for sediment to accumulate. The following overview of coastal delta formation around the world is primarily summarized from (Davis, 1983; Davis and Fitzgerald, 2003; Elliott, 2005). The potential for sediment accumulation along a coastline is closely linked to plate tectonics, the regional geologic setting, and climate. The locations of most major modern coastal deltas are associated with passive continental margins that have extensive drainage basins (Wright et al., 1974). Passive margins are an ideal place for sediment deposition because they are typically associated with gently sloping continental shelves. The shallow slope is more effective at dissipating marine energy, ultimately limiting sediment loss and allowing for delta formation (Wright and Coleman, 1972, 1973). Active continental margins, on the other hand, are often not associated with delta formation because the drainage areas are typically much smaller due to the presence of coastal mountains and do not create enough sediment to form a delta. Additionally, the narrow and steep continental shelves of active margins hinder delta growth because sediment is

rapidly removed from the river mouth because marine influences are not effectively dissipated. Deltas that have managed to form along active margins include the Fraser Delta, Canada, and the Copper Delta, Alaska.

Interdecadal and interannual climate variability can impact delta stability by disrupting average sediment transport rates to the delta. For example, a drainage basin that experiences several years of abnormally low winter precipitation may undergo a significant decrease in annual sediment load because of a decrease in the spring freshets. At millennial time scales, climate change and associated eustatic changes in sea level also impacted delta stability. Rapid sea level rise following the last glacial maximum suppressed delta formation because sediment accumulation was outpaced by shoreline transgression and increasing accommodation space. The initiation of Holocene delta formation across the world is correlated with the deceleration in sea level rise that occurred between 8.5 and 6.5 thousand years ago (kya) (Stanley and Warne, 1994).

## *Deltaic Processes*

Sediment transport and deposition within the delta are primarily controlled by fluvial processes, encompassing interactions between the river effluent and basin waters at the river mouth. Sediment accumulation patterns are modified by marine processes including tidal and wave action, and longshore currents. Wright (1977, 1978) provides a synthesis of the research describing the forces at work within a delta and uses this to explain sediment deposition patterns witnessed in deltas; this seminal work is summarized in the Fluvial Processes and Marine Processes sections.

### Fluvial Processes

Once sediment is transported into the distributary network, it is deposited according to interactions between the effluent and basin waters. The three fluvial forces that govern interactions between the effluent and basin waters are the outflow inertia, turbulent bed friction, and outflow buoyancy. When outflow velocities are high and the density contrast between the effluent and basin water is low, the effluent's inertial forces create a jet that carries plumes of suspended sediment into the ocean basin. Lateral spreading and deceleration of effluent jets is caused by turbulent eddies that form at the boundary of the effluent and basin water. Sediment deposited by effluent jets typically has limited lateral spreading and fines seaward (Bates, 1953).

Purely effluent jets are primarily associated with newly created river mouths along open coasts because the continued progradation and aggradation of effluent deposits cause a decrease in water depth, thereby increasing the influence of bed friction. Increased bed friction enhances lateral spreading and deceleration of the jet, resulting in the deposition of a triangular shoal with adjacent bifurcating channels. The angle at which the channels diverge, known as the bifurcation angle, increases as the depth-to-width ratio of the river mouth decreases. Basins with a shallow gradient and high outflow velocity can exhibit multiple channel bifurcations with numerous middle-ground shoals.

When the river effluent is significantly less dense than the basin water, a buoyant plume will exist above the underlying salt water. A saltwater wedge will form where the discharge exceeds the tidal prism (defined as the volume of water in an estuary between the mean high and low tide), but the outflow velocity is not strong enough to completely flush the seawater from the channel mouth. Buoyant effluent sediment deposition patterns consist of subaqueous levees and the formation of distributary-mouth bar crests. The subaqueous levees result in minimal channel bifurcation.

**Marine Processes**

Marine processes modify fluvial transport and the subsequent sediment is deposited both directly and indirectly. Direct modification of effluent redirects sediment before deposition through rapid mixing and momentum exchange between effluent and ambient waters. Indirect modification redistributes sediment after the initial deposition. Waves and tides are the main marine processes that impact sediment distribution and are therefore the processes considered in this research. Although longshore currents influence sediment deposition within deltas, these currents primarily move sediment parallel to the shoreline, creating a zero-net sediment flux. Longshore currents have been largely neglected in evolutionary deltaic modeling (Seybold et al., 2007; Geleynse et al., 2011; Caldwell and Edmonds, 2014). Similarly, longshore currents are not considered in this research.

In high wave-energy environments, outflow from the river mouth refracts incident waves and causes waves to break in deeper water. Wave breaking enhances mixing, causing rapid deceleration and mixing of effluent and ambient waters (Davis, 1983). Lack of a consistent vertical density gradient at the mixing front negates buoyancy

effects and leads to sediment deposition. Sediment accumulation in high-wave energy environments occurs closer to the river mouth because the stronger wave energy is more effective at pushing the mixing landward. Crescentic river mouth bars are formed as waves redistribute sediment after deposition by pushing material back toward the shore. Subaqueous levees are formed along the lateral flanks of the effluent where bed load is deposited due to steep velocity gradients. The symmetry of the channel banks is often dictated by wind direction and longshore currents.

Tides add complexity to delta formation by modulating the location of the mixing zone where the upstream fluvial effluent merges with the ambient marine water (Hoitink et al., 2011). Flood tides carry marine water into the basin, leading to the mixing front moving landward and confining sediment to the basin. Ebb tides enhance river discharge, moving the mixing front seaward and carrying sediment away from the basin.

The effects of tides are most prominent where the tidal range is large or where tides are fast moving. Microtidal environments often do not have enough marine influence to significantly overcome river-mouth processes because there is still a continuous outflow. Tidal dominance occurs when the tidal flow amplitude in a distributary exceeds the river flow. This causes bidirectional sediment transport during flood tides and leads to the formation of linear shoals with the long axis parallel to the flow direction (Wright et al., 1975; Davis, 1983). Strong ebb tides reinforce the formation of parallel structures by lengthening levees and elongating channels.

### *Morphological classification*

Fisher et al. (1969) was the first to classify deltas based on their morphology and proposed that three basic delta morphologies (cuspate, lobate, and elongated deltas) result from constructive (riverine) and destructive (marine, not including tidal) processes. Galloway (1975) expanded upon Fisher's model by including tidal action (estuarine deltas) within destructive processes. This model, often referred to as Galloway's ternary diagram (Figure 1.1A), is used to qualitatively classify the dominant morphodynamic influences acting within a particular deltaic system and has been used routinely to describe defining geomorphic features within end-member deltas.

Deltas formed primarily by constructive influences, commonly referred to as river or fluvial dominated deltas, are located at the top of the ternary diagram. Deltas that fall

within this region of the ternary diagram are primarily influenced by river-mouth processes in addition to incoming sediment flux. Outflow in a fluvial delta is largely unopposed by marine influences, allowing the effluent to carry sediment into the basin, resulting in basin-ward progradation of the delta plain. The Mississippi Delta in the United States (US) is often pointed to as the representative morphological architype for fluvial deltas, making the iconic “bird’s foot” shape of the delta plain (Figure 1.1B)—a prominent feature of fluvial deltas (Wright and Coleman, 1973). Constructive deltas typically carry abundant sediment load from large drainage basins and debouch into a shallow sloping marine environment devoid of strong marine influences (Fisher et al., 1969). The Mississippi Delta has evolved primarily through constructive influences partly because the Gulf of Mexico’s gentle slope dissipates wave energy, and the gulf provides protection from tides.

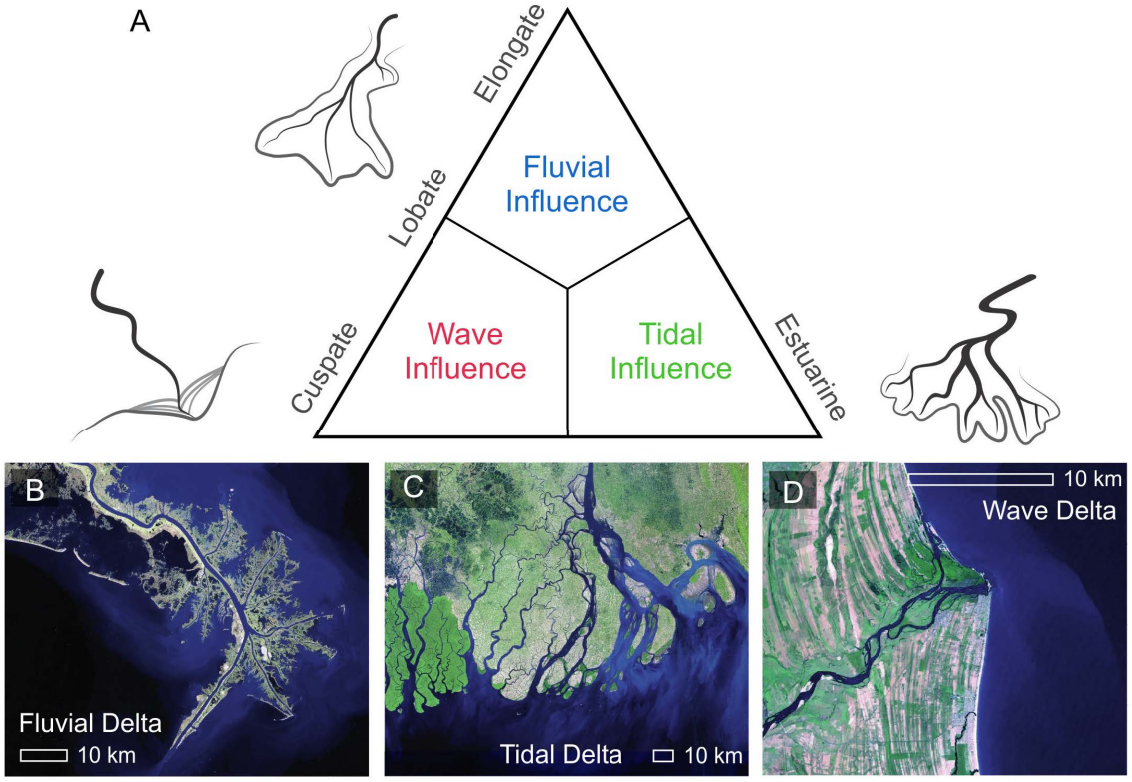


**Figure 1.1. A) Galloway’s ternary diagram with examples of a B) fluvial delta (Mississippi, USA), C) tidal delta (Fly, Papua New Guinea), and D) wave delta (Sao Francisco, Brazil).**

Strong tidal currents in the absence of abundant wave energy result in the formation of deltaic landscapes characterized by elongated islands separated by

abundant distributary and tidal channels (Hoitink et al., 2017). The number of channels in a tidally dominated region is often greater than number found in fluvial dominated deltas. The islands within tidal influenced regions generally have smoother shore boundaries compared to interdistributary islands in the fluvial dominated deltas (Elliott, 2005). Rossi et al. (2016) also suggest that increased tides change the delta-front profile from a concave structure seen in fluvial deltas to a convex structure. Additionally, increases in tidal amplitude may result in deeper channels (Rossi et al., 2016). Many of these features are witnessed in the Fly River Delta in Papua New Guinea (Figure 1.1C), and Ganges-Brahmaputra Delta in Bangladesh. The Ganges-Brahmaputra Delta is the world's most extensive tidal influenced delta. The tidal region of the Ganges-Brahmaputra Delta has high channel density, is absent of oxbow lakes, and has small island shape factors (defined as the ratio of the wetted perimeter and the square root of the island area) (Hoitink et al., 2017).

Deltas dominated by destructive influences are located at the bottom of the ternary diagram and are split into two categories: those with a higher proportion of wave energy (wave influenced) and those with more tidal energy (tidal influenced). Abundant wave energy generally occurs where river mouths are fronted by steep nearshore slopes. Wave action in these environments rework sediment back toward the shoreline, often creating a barrier island system with beaches and dunes where the delta plain does not protrude into the basin. Wave dominated deltas are often significantly smaller than fluvial deltas due to the increase in destructive influences and trend toward no delta formation if waves are strong enough. The Sao Francisco Delta, in Brazil, is often cited as the morphological architype for wave deltas due to its large distributary channel and smooth cuspate shape (Figure 1.1D) (Wright and Coleman, 1973). The Sao Francisco is relatively symmetric compared to other wave dominated deltas such as the Senegal River Delta in West Africa. Wave dominated deltas are also often noted to have fewer distributary channels compared to fluvial and tidal deltas (Fisher et al., 1969).

Although there is a tendency to pigeon-hole deltas into one of the end-member classifications, assigning a single classification to an entire deltaic system often results in oversimplification of the spatial and temporal variability. This does not fully capture the complex morphodynamic balance shaping the hierarchical features often witnessed in large deltas (Dalrymple and James, 2010). Nevertheless, studying end-member

morphologies provides a necessary simplification to help understand how fluvial, wave, and tidal processes influence geomorphic behavior at the basin scale.

### Second-order morphology

Research expanding upon Galloway's classification scheme has accounted for second-order differences in delta morphology that offers an explanation between deltas that have similar morphodynamic ratios but exhibit different depositional features. Second-order morphologies considered in this body of research include incoming sediment size and antecedent basin shape.

Orton and Reading (1993) extended the ternary classification to include sediment type by showing that deltas primarily dominated by fine-grained sediments have a planform delta front while medium-grained sediments produce semicircular deltas. Increased sediment cohesion in deltas results in greater channel progradation due to the formation of stronger levees (Edmonds and Slingerland, 2010). Additionally, higher ratios of fine-grained cohesive sediments in the subsurface elongates deltaic depositional structures and creates deeply incised distributaries (Geleynse et al., 2011; Rossi et al., 2016).

An observable link exists between delta formation and bathymetry, which is often influenced by regional tectonics (Pratson et al., 2007). Caldwell et al. (2019) showed that the likelihood of delta formation in each area decreases as bathymetric slope increases due to a greater accommodation space and increased marine influences. However, deltas are also more likely to form when the slope steepens past 0.006 m/m. Steep sloping bathymetry is most commonly found along active tectonic margins; deltas that form in these conditions have high transport rates of coarse-grained sediment due to increased mountain erosion and shortened transport distances (Caldwell et al., 2019).

## *Quantification of morphodynamics in deltas*

Many studies have used Galloway's classification to compare the relative morphodynamic regimes of global deltas based on the identification of distinguishing deltaic structures and sediment deposition patterns. Thus, defining delta morphology remains largely qualitative.

Recent work has made progress toward a goal of quantifying the ternary diagram. Nienhuis et al. (2015) made a distinction between fluvial and wave dominated deltas by comparing the delivered fluvial sediment flux $Q_{river}$ [$MT^{-1}$] to the combined maximum possible littoral transport to the left or right of the river mouth $Q_{s,max}$ [$MT^{-1}$]:

$$R = \frac{Q_{river}}{Q_{s,max}} \qquad (1.1)$$

If the fluvial dominance ratio $R$ [-] is greater than 1, destructive wave influences are not strong enough to negate delta construction from riverine processes and the delta is classified as fluvial dominated. If $R$ is less than 1, destructive influences can remove sediment, and consequently, a cuspate delta forms. Applying this method to real world deltas, the Sao Francisco was calculated to have a fluvial ratio of 0.3 while the Mississippi has a fluvial ratio of 7. Nienhuis et al. (2015) notes that this ratio assumes a simplified linear relation between the retained fluvial flux and the fluvial dominance. This linearity does not account for wave spreading and asymmetry in waves and only predicts delta morphology in a steady state.

Nienhuis et al. (2018) defined a tidal dominated delta as one where the tidal discharge amplitude at the river mouth $\hat{Q}_{tide}$ [$L^3T^{-1}$] is greater than the mean annual fluvial discharge $Q_{river}$ [$L^3T^{-1}$]:

$$T = \frac{\hat{Q}_{tide}}{Q_{river}} \qquad (1.2)$$

A tidal-dominance ratio $T$ [-] less than 1 signifies river or wave dominance, whereas a ratio greater than 1 signifies tidal dominance. Nienhuis et al. (2018) notes that an end-member tidal delta (formed as $T$ approaches infinity) is the same as a self-formed estuary, making a distinction between self-widening channels and underfilled drowned valleys. In Equation 1.2, $Q_{tide}$ is a function of the tidal angular frequency and the tidal prism (a product of the tidal range amplitude and the distance of tidal influence into the channel).

Nienhuis et al. (2020) combined the fluvial dominance ratio (Nienhuis et al., 2015) and the tidal dominance ratio calculations (Nienhuis et al., 2018) to compare the relative impact of fluvial, wave, and tidal influences using a normalized three-way ratio (Equation 1.3):

$$Realtive\ Q_i = \frac{Q_i}{Q_{river}+Q_{wave}+Q_{tide}} \qquad (1.3)$$

In this equation, $i = [river, wave, tide]$, $Q_{river}$ is the delivered fluvial sediment flux [MT$^{-1}$], $Q_{wave}$ is the potential for waves to move sediment away from the river mouth [MT$^{-1}$], and $Q_{tide}$ is the tidal sediment flux [MT$^{-1}$]. By calculating the sediment flux within a delta produced through fluvial, wave, and tidal influences, Nienhuis et al. (2020) was able to compare the morphodynamics of deltas around the world on the ternary diagram (Figure 1.2).

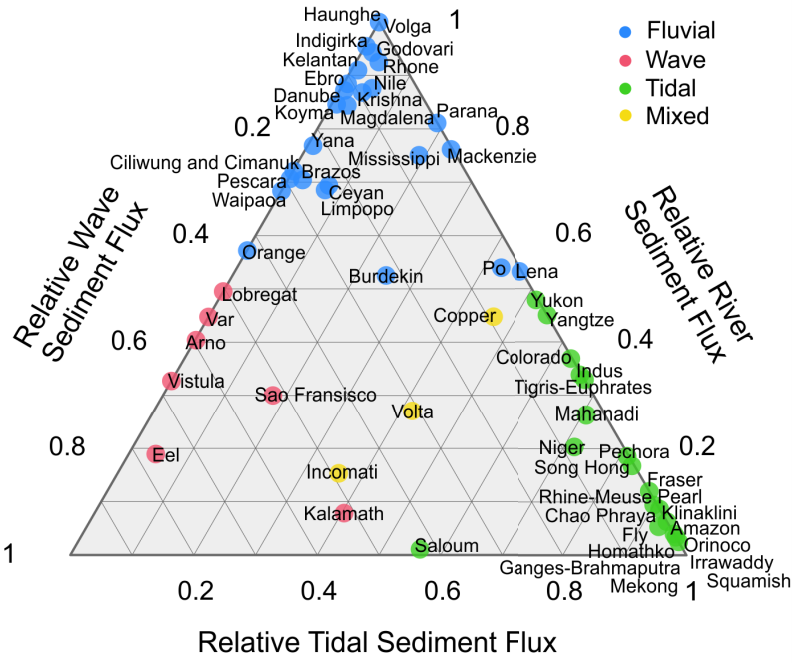


**Figure 1.2. The ternary diagram populated with 51 of the world's largest deltas using Nienhuis et al. (2020) classification of relative river (fluvial), wave, and tidal sediment flux ratios. The data and codes used to create this figure are provided by Nienhuis et al. (2020).**

Syvitski and Saito (2007) evaluated the relative morphodynamic regimes of 51 deltas from around the world using satellite imagery and created a database of deltaic parameters including delta area, incoming fluvial discharge, sediment flux, maximum wave height, tidal range, and bathymetric slope. These parameters were used by Syvitski and Saito (2007) to compare the relative destructive marine influences to constructive riverine influences within deltas. They used a proxy of marine power, $P_m$ [L$^2$], which is a combination of the maximum monthly wave height $W_a$ $[L]$ and the tidal range $T_i$ $[L]$:

$$P_{marne} = {W_a}^2 + {T_i}^2 \quad (1.4)$$

The proxy for marine power was compared to a proxy for river power $P_r$ [$L^3T^{-1}$]:

$$P_{river} = 11 Q_{av} D_{grd} \quad (1.5)$$

where $Q_{av}$ [$L^3T^{-1}$] is the average monthly discharge and $D_{grd}$ $[-]$ is the gradient of the delta plain.

Equation 1.6 computes the relative impact of fluvial, wave, and tidal influences using the power method, where $i = [river, wave, tide]$.

$$Realtive\ P_i = \frac{P_i}{P_{river} + P_{wave} + P_{tide}} \quad (1.6)$$

In this equation, wave and tidal power are defined by each of the components in Equation 1.4:

$$P_{wave} = {W_a}^2 \quad (1.7)$$

$$P_{tide} = {T_i}^2 \quad (1.8)$$

It is critical to note that Syvitski and Saito (2007) did not provide a relative power comparison for fluvial, wave, and tidal influences. Equations 1.6-1.8 are provided here so that the ternary diagram can be populated with deltas according to their relative fluvial, wave, and tidal power (Figure 1.3).

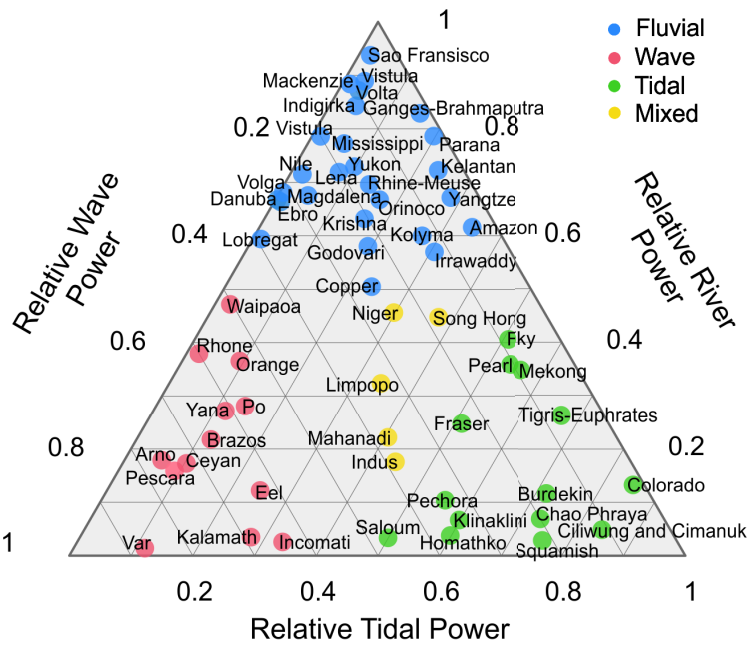


**Figure 1.3. The ternary diagram populated with 51 of the world's largest deltas using Syvitski and Saito (2007)classification of relative river (fluvial), wave, and tidal power ratios. Data used to create this figure is from Table 1 in Syvitski and Saito (2007).**

Upon visual analysis, the proposed delta morphologies in Figure 1.2 and Figure 1.3 do not fully align with qualitative morphodynamic features of certain deltas. For instance, the Po Delta and the Sao Francisco Delta both exhibit a cuspate shape, have a smooth shoreline, and only have a few channels cutting through the delta plain, suggesting that both deltas are primarily wave influenced. Figure 1.2 shows that the Po Delta is primarily a fluvial delta and has secondary tidal and wave influences. Similarly, Figure 1.3 indicates that the Sao Francisco Delta has the largest fluvial influence in the entire dataset. Syvitski et al. (2022) point out that the computed sediment fluxes calculated in Nienhuis et al. (2020) are "unreliable" due to the use of converging-flow theory, which is often not applicable in coastal deltas where there is divergence in river flow through the distributary channels. Converging-flow theory predicts the sediment flux over all the distributary channels in a delta and assumes this flux occurs at one distributary mouth, concentrating the fluvial sediment fluxes in a narrow portion of the delta. This allows for the other distributary mouths to be overwhelmed by marine influences. A better quantification system that aligns with the qualitative nature of the ternary diagram would be beneficial for quantitatively comparing delta morphology in deltas around the world.

### *Quantification of delta morphometrics*

In addition to quantifying the relative morphodynamics shaping deltas, recent research has also aimed to quantify the geomorphic characteristics of a delta, often referred to as morphometrics. Commonly used morphometrics include the shape of the delta plain, elongation and skewness of the plain, the number of distributary channels, shoreline rugosity, channel sinuosity, and channel shape (Wright and Coleman, 1973; Syvitski and Saito, 2007; Caldwell and Edmonds, 2014).

Although Syvitski and Saito (2007) developed a series of analytical formulas to predict when certain morphologies will be present based on the morphodynamics within the receiving basin, there are no studies that quantify the morphodynamic influence ratios at which certain distinguishing deltaic landforms (such as tidal channel deepening, delta front elongation, increased bifurcation ratios, etc.) emerge. However, Syvitski and Saito (2007) warn that studies using a simple ternary diagram may not being able to capture all the morphodynamic variations that occur within deltas and are particularly limited by scaling effects between small and large deltas.

### *Morphodynamic modeling of deltas*

An increasing number of studies have used numerical modeling to understand delta morphology through the simulation of delta formation. Although some modeling studies focus on a specific delta of interest, most morphodynamic modeling is generic and does not pertain to a particular delta. Generic modeling studies often aim to understand how delta morphology is impacted by variations in the system feeding the delta or changes occurring in the ocean; examples include evaluating morphological changes due to antecedent stratigraphy (Geleynse et al., 2010), sediment properties (Edmonds and Slingerland, 2010; Rossi et al., 2016; Caldwell et al., 2019), and relative sea level rise (Hariharan et al., 2022).

Many of the models used to investigate delta formation are conservation-based models that solve conservation of mass and momentum equations. These equations are most often solved in two dimensions (2D), with cross sectional models aiming to study avulsion and delta lobe progradation while planform models typically look at delta formation, morphology, and channel dynamics (Edmonds et al., 2021). One of the most popular conservation-based numerical models is Delft3D (Deltares, 2013). Delft3D is an

open-sourced, physically based, hydro-morphodynamic model that solves the shallow water equations (Deltares, 2013). Delft3D has been used to simulate the evolution of landscape-scale fluvial and tidal deltas over long time periods (Edmonds and Slingerland, 2010; Geleynse et al., 2010, 2011; Caldwell and Edmonds, 2014; Rossi et al., 2016). Even though many of the 2D and 3D morphodynamic models have the capability to include fluvial, wave, and tidal processes within the modeling framework (Overeem et al., 2011), Edmonds et al. (2021) stated that “we are unaware of any single model that can reproduce the diversity of river, wave, and tide dominated features that Galloway tried to explain”.

### 1.2.2. Connecting the surface to the subsurface in coastal deltas

It is well known that the aquifer/aquitard structure within the subsurface of a delta is highly heterogenous and often discontinuous (Michael and Khan, 2016; Larsen et al., 2017) due to the episodic nature of sea level transgression and regression (Figure 1.4A). Deltas can only form when sediment deposition along coastal margins outpaces shoreline transgression (Figure 1.4B). Between approximately 120 and 20 thousand years ago (kya), fluvial sediments were deposited along coastlines; sea level declined during this Pleistocene recession allowing for the deposition of fluvial sediments, primarily silt and sand-sized particles, and the building of deltaic aquifer structures (Syvitski and Saito, 2007). During the marine transgression between 20 and 10 kya, sea level rise resulted in the submergence of coastal margins and the deposition of fine-grained marine sediment (Figure 1.4C). While the marine sediment was deposited atop the previously exposed delta, saline ocean water was generally able to seep into the subsurface, resulting in the salinization of deeper aquifer structures. Sea level decline approximately 8 kya resulted in the construction of the modern deltas that appear along coastlines today (Figure 1.4D). Thus, modern deltas sit atop aquifers that were salinized at the end of the Pleistocene. The ongoing deposition of fluvial sediments forming the delta is paired with erosion of underlying marine sediments from river incision and erosive marine action. This erosion allows freshwater in the delta distributary network to once again seep into the lower aquifer structure, this time resulting in freshening. The spatial variability of the aquifer/aquitard structures is dependent on where deposition and erosion occur, and ultimately, the relative strength of the morphodynamic influences within the delta.

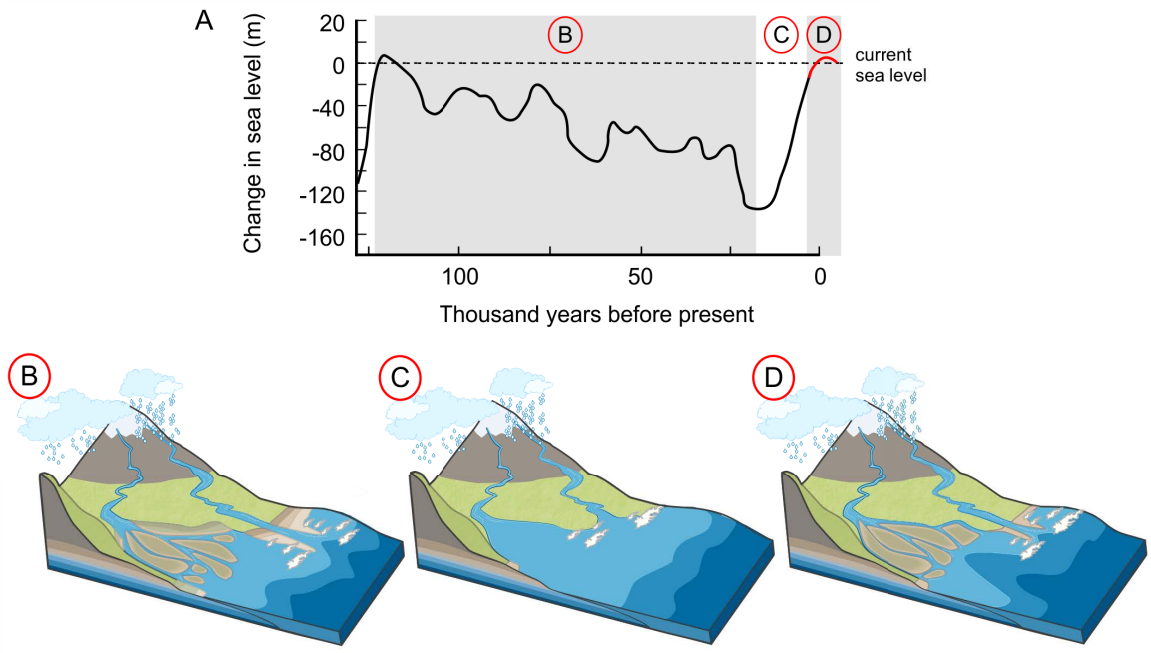


**Figure 1.4.** **A) Representitive sea level change curve (redrawn from Wagner et al., (2012), after Waelbroeck et al., (2002)). Conceptualization of deltaic aquifer/aquitard formation during B) Pleistocene regression (approximately 120 to 20 kya), C) late Pleistocene/early Holocene transgression (approximately 20 to 10 kya), and D) modern delta formation (approximately 8 kya to present).**

Spatial quantification of the subsurface permeability has been thoroughly studied in a handful of deltas, including the Ganges-Brahmaputra (Michael and Voss, 2009; Khan et al., 2016; Michael and Khan, 2016), Mekong (Minderhoud et al., 2015; Van Pham et al., 2019), Song Hong (Red River) (Tran et al., 2012; Larsen et al., 2017), Nile (van Engelen et al., 2019), Po (Mollema et al., 2013; Antonellini et al., 2015), and Rhine-Meuse (Post et al., 2003; de Louw et al., 2010; Oude Essink et al., 2010; Delsman et al., 2014). However, considering that there are likely over 2,000 coastal deltas estimated to exist around the world (Syvitski et al., 2022), a more generalized approach is needed inform the expected permeability distribution in these systems and how thousands of years geomorphic evolution have shaped the subsurface.

Linking surface features (such as islands and river channels) to the subsurface permeability in a delta through generalized modeling efforts has only been considered in primarily fluvial deltaic environments (Kolker et al., 2013; Hariharan et al., 2021; Xu et al., 2021; Steel et al., 2022a). Kolker et al. (2013) suggested that water in the Mississippi Delta flows from the surface water network through the deltaic subsurface via

paleochannels and other buried sand bodies that were identified with seismic imaging. The link between horizontal subsurface groundwater flow in deltas and presence of permeable flow pathways through paleochannels was further confirmed in two companion papers that used numerical morphodynamic and groundwater modeling (Hariharan et al., 2021; Xu et al., 2021). Steel et al. (2022) also used a physical delta model to characterize the connectivity of sand bodies within the delta and suggested that groundwater flow in a delta may be controlled by the lower permeability sediments rather than the connective sand bodies. There has yet to be a study investigating how combined morphodynamic influences within a delta impact the subsurface permeability.

### 1.2.3. Groundwater salinity in coastal deltas

The distribution of groundwater salinity in coastal deltas reflects the complex geologic history of these systems. Types of groundwater salinity found in these environments include 1) salinity derived from natural wedges along the coastal margin, 2) saline groundwater emplaced under previous climatic and hydrogeologic settings (paleowater), and 3) salinity due to mixing (either natural mixing or mixing caused by human alterations (e.g., pumping)). Less common sources of groundwater salinity may be related to 4) dissolution of salts either at depth (e.g., mineral salts) or near surface (road salt application or evapoconcentrated salts, particularly in irrigated areas in arid and semi-arid regions). The research presented in this thesis focuses on physical processes impacting the preservation and transport of saline paleowater. Other salinity sources and the hydrochemical processes that may alter the groundwater chemistry are not considered.

To understand the proportion and distribution of salinity contained within deltaic groundwater globally, it is imperative to define what “fresh” means in a groundwater context. This research uses chloride concentration as a proxy for salinity and refers to the following classification: fresh ($Cl \leq 300$ mg/L), brackish ($300 > Cl \leq 1000$ mg/L), or saline ($Cl > 1000$ mg/L) (Oude Essink et al., 2010).

#### *Groundwater salinity in deltas around the world*

Globally, coastlines average one delta for every ~300 km of shoreline (Caldwell et al., 2019). However, there are only 32 deltas where deltaic saline paleowater has been reported in the scientific literature (Figure 1.5) (Larsen et al., 2017; van Engelen,

2020). The number of deltas in which paleo-hydrologic modeling has attempted to explain the evolution of groundwater salinity is even more limited. It is likely that the discrepancy between the number of major coastal deltas and the number of deltas where paleowater has been reported is due to a lack of research on the topic rather than a physical lack of saline water itself.

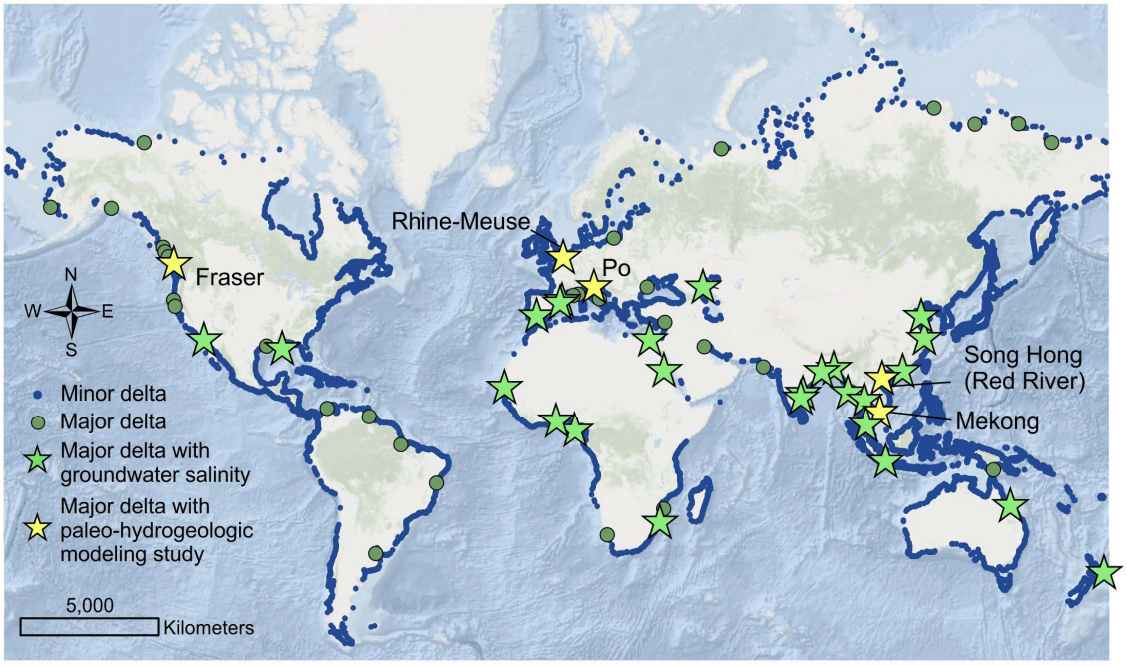


**Figure 1.5. Major river deltas around the world with reports of saline paleowater, as indicated in literature reviews by Larsen et al. (2017) and Van Englen (2020). Over 10,000 minor river deltas are included from Nienhuis et al. (2020).**

The remainder of this section examines the scientific literature surrounding paleo-hydrogeologic modeling of groundwater salinity in three deltas: 1) the Rhine-Meuse Delta, 2) the Mekong Delta, and 3) the Song Hong (Red River) Delta (locations shown in Figure 1.5). These three tidal deltas are chosen because they have an extensive body of literature investigating the origin and groundwater flow through the deltaic subsurface. These deltas also have a long history of anthropogenic alternations, making them fascinating case studies that allow us to look at what the future may hold for those living on coastal deltas.

## Rhine-Meuse Delta, Netherlands

### Geomorphic and hydrogeologic evolution

Post et al. (2003) developed a conceptual model of the genesis of the current subsurface salinity distribution in The Netherlands using geological, chemical, and geophysical data. Their conceptualization suggests that marine aquitards deposited during the Pleistocene originally contained saline water and subsequently underwent freshening during the regressive period between the Eemian and Holocene transgressions. Salinization during the Holocene transgression resulted in saline fluvial Pleistocene layers overtopping less saline Pleistocene marine layers. Significant freshening since the beginning of the Holocene transgression did not commence until 5.5 kya during the formation of coastal dunes. Before this time, freshening deeper than tens of metres was unlikely because shallow topographic variations resulted in low hydraulic gradients. Dune formation along the coast allowed freshening to occur up to 120 m deep due to enhanced recharge.

The development of polders and other coastal engineering structure have altered topography in The Netherlands and has resulted in a complex shallow groundwater system (Post et al., 2003). Infiltration of fresh water takes place from surface water in elevated areas, while upwelling of saline water occurs in the polders due to the land being several metres below sea level. Preferential pathways through the marine Holocene confining layer facilitates the rapid transfer of chloride between the Pleistocene aquifer and the upper Holocene aquifer (de Louw et al., 2010). The paleo-hydrogeologic modeling performed by Delsman et al. (2014) supports the conceptual model developed by Post et al. (2003).

### Paleo-hydrogeologic modeling methods

Delsman et al. (2014) used SEAWAT (Langevin, 2009) to model the evolution of Holocene-aged groundwater salinity in The Netherlands along a two-dimensional transect intersecting the coast. The model used a specified head boundary on the western seaward model edge and a no flow boundary at the eastern land side. The model spanned 65,100 km in the horizontal direction and had 102 vertical layers with variable thickness (all less than 10 m). Geographical changes throughout the Holocene were simulated using 10 times steps in which boundary conditions were changed to

represent changes in land surface elevation and sea level. Overall, the model ran for 8.5 ky.

The model was not calibrated, and a rigorous sensitivity analysis was not preformed due to the long computational times. The authors noted that the model was less sensitive to dispersivity and was more sensitive to the initial subsurface salinity distribution in the deeper aquifers. Although calibration was not performed, model validity was still assessed by comparing hydraulic heads and chloride concentrations with observed measurements. The normalized root mean squared (NRMS) error for the hydraulic head comparison was 11% and the chloride measures were 16%.

### Outlook of the delta

The Rhine-Meuse Delta is one of the only locations where future impacts of climate change, sea level rise, and coastal engineering on paleowater exfiltration have been examined. Oude Essink et al. (2010) evaluated the impacts of climate change and anthropogenic activities on the Rhine-Meuse Delta using a 3D MOCDENS3D model (Oude Essink, 1998, 1999, 2001). The research showed that future land subsidence will cause the water table in unconfined aquifers to drop more than hydraulic heads in the underlying aquifers, promoting the exfiltration of saline groundwater and increasing salinity under deep polders by double the current concentrations. Sea level rise is also projected to raise hydraulic heads in the deeper aquifers but is only expected to be influential within 10 km of the coast and estuaries.

## Mekong Delta, Vietnam

### Geomorphic and hydrogeologic evolution

Paleo-hydrogeologic modeling by (Van Pham et al., 2019) suggests that the Mekong Delta underwent significant groundwater freshening driven by sea level regression between 60-18 kya. Fresh groundwater replaced saline water up to 500 metres below sea level (mbsl). This freshening persisted until 18-12 kya, at which time the model had the largest volume of freshwater in the subsurface. The rapid Holocene transgression that occurred from 12-2.5 kya drove saline water into deeper aquifers through density-dependent flow, illustrating a pattern of seawater fingering. The Holocene aquitard material that accumulated at the top of the model during the last stress periods inhibited the freshening of the groundwater system, even though the sea

level dropped slightly from 2.5 kya to present. Van Pham et al. (2019) noted that recharge in the basin is currently inhibited by sedimentation of the top clay layer and that this mechanism is one of the main factors resulting in the decrease in total freshwater volume. This salinization is perpetuated by over-exploitation of groundwater resources in the Mekong Basin.

### Paleo-hydrogeologic modeling methods

Van Pham et al. (2019) followed a similar approach to paleo-hydrogeologic modeling as Delsman et al. (2014) using a two-dimensional “Mekong like” cross section to conceptually model the evolution of groundwater within in the delta. Salinization and freshening within the delta were simulated over a 60 ky period. This time period was divided into eight stress periods to account for changing sea level, recharge, and landscape. Four different geologic realizations were used to change the connectiveness and thickness of the aquitards. Model sensitivity to hydraulic conductivity was tested by changing the hydraulic conductivity of each sediment size in the realizations within a range of plausible values. A sensitivity analysis visually comparing modeled and observed salinity and groundwater age was used to conclude that the model results are reasonable. The study did not attempt to quantify the uncertainties in the model.

### Outlook of the delta

Minderhoud et al. (2017) modeled land surface subsidence in relation to groundwater extraction in the Mekong Delta over the past 25 years. The study used the MODFLOW-based environment, iMOD, to create a 3D groundwater flow model to simulate groundwater extraction within the basin (Vermeulen et al., 2006; Minnema et al., 2013; Deltares, 2021). Lower water pressures from the hydrogeologic modeling were used to determine subsidence using SUB-CR, a geotechnical subsidence model (Kooi et al., 2018). The modeling suggests that 25 years of groundwater pumping in the delta induced subsidence that caused the land surface to sink an average of approximately 18 cm, with some areas up to 30 cm. Minderhoud et al. (2020) used the 3D coupled hydrogeologic and geotechnical model developed in Minderhoud et al. (2017) to investigate six mitigation and non-mitigation scenarios for the delta. The study found that although the Vietnamese Government hopes to end groundwater use in the country by 2100, the delta is nearing a tipping-point. Effective mitigation strategies to reduce subsidence and salinization from groundwater extraction include using alternative water

sources (piped water, high quality surface water, or desalinized water), relocating/distributing groundwater extraction to areas that are less exploited or where subsidence is less harmful, and employing managed aquifer recharge/groundwater injection.

## Song Hong (Red River) Delta, Vietnam

### Geomorphic and hydrogeologic evolution

Tran et al. (2012) used geophysical methods to infer that saline paleowater occupies the Holocene aquifers in the Song Hong Delta up to 50-75 km inland. Although fresh groundwater occupies the underlying Pleistocene aquifers in some locations, elevated total dissolved solids and chloride concentrations in other locations result from saline paleowater in the overlying Holocene aquitard. At the time of the publication, Tran et al. (2012) suggested that more research should be conducted to determine if leaching of the saline paleowater is occurring diffusively or through density-driven flow.

Hydrogeologic modeling from Larsen et al. (2017) showed that diffusion controls leaching of sediment porewater when the hydraulic conductivity of the marine clay is less than $10^{-8}$ m/s. Hydraulic conductivities greater than $10^{-8}$ m/s result in density-dependent flow being the primary driver of freshening in the delta. It is likely that saline paleowater is still present in the Holocene marine aquitards but has been flushed from the marine clays deposited during the Eemian transgression, assuming that more saline water has not been introduced into the system through infiltration or diffusion.

Although the results of 2D paleo-hydrogeologic modeling in Larsen et al. (2017) do not reconstruct a timeline of events influencing salinization and freshening throughout the modeled time, the discussion in the paper provides information regarding the simulated present-day salinity distribution in the Song Hong Delta and factors that may influence groundwater salinity in coastal deltas. The modeled current salinity distribution is similar to the conceptual model of the saline distribution proposed by Tran et al. (2012), suggesting that saline paleowater in the Song Hong Delta extends inland 50-75 km from the coast. Broader implications of the work suggest that low-permeability aquitards can take up to 40-50 ky to adjust to sea level change, resulting in delta disequilibrium regarding salinity.

### Paleo-hydrogeologic modeling methods

Larsen et al. (2017) investigated the evolution of the current salinity distribution in the Song Hong Delta using SEAWAT (Langevin et al., 2007). Pseudo 1D column modeling was used to assess the impact that hydraulic conductivity and marine clay thickness have on the flushing of saline connate water from marine clay. In these three-layer column models, a marine clay layer filled with saline porewater water is overtopped by a sand-till layer and underlain by a sand-gravel layer, both saturated with fresh porewater. This modeling exercise showed that diffusion is the main transport mechanism occurring when the hydraulic conductivity is less than $10^{-8}$ m/s and that marine porewater should still be present in the Holocene clays (Larsen et al., 2017).

Two-dimensional modeling along a generalized cross section from the delta apex to the shoreline was used to further understand the development of the current salinity distribution in Holocene sediment within the Song Hong Delta (Larsen et al., 2017). Boundary conditions maintained the horizontal hydraulic gradient toward the sea at 0.03%, which is representative of the current hydrogeologic regime. The initial chloride concentration was selected by process of elimination—a chloride concentration representing a saline subsurface did not yield results comparable to observations, so a concentration representing a fresh groundwater used. Both models were run over 11 ky with 1000-year stress periods. The output from each stress period was used as the input for the subsequent stress periods, and new hydrogeologic units were incorporated in the model to simulate the building of the delta.

The study did not mention the use of calibration techniques nor attempts to quantify the uncertainty within the model. The modeled salinity patterns at the end of the simulation were visually compared to the salinity distribution derived from geophysical borehole logs and transient electromagnetic (TEM) soundings, but no quantitative comparison was performed.

## 1.2.4. Modeling and uncertainty

Currently, physically-based (or process-based) numerical modeling is one of the only methods available for understanding the evolution of both past and future Earth systems on geologic timescales. Modeling techniques are used to investigate the dynamics at work in specific locations, in addition to evaluating feedbacks within

hypothetical idealized scenarios. However, no matter the application of a model, uncertainty within the model results is always present. Uncertainty analysis can estimate the uncertainty surrounding a modeled forecast as well as convey the information regarding how well the model can be expected to address the modeling purpose. Adequate documentation and communication of uncertainty allows modeling results to be useful, despite being uncertain. This is particularly important in studies that aim to integrate science and society.

Within models used for forecasting, there are two main forms of uncertainty; uncertainty associated with the model and uncertainty associated with the specifications of the future conditions. Uncertainty associated with the model includes assumptions made within the conceptual model (e.g., the dominant processes and how they are represented, boundary conditions, model structure), measurement error within data and observations, simplifications required by calibration, and simplification error resulting from parameterization (Anderson et al., 2015). Uncertainty associated with specifications of future conditions can be split into intrinsic and epistemic uncertainty. Intrinsic uncertainty cannot be reduced by the addition of more knowledge and is well described using probabilities. Epistemic uncertainty stems from the uncertainty of not knowing what may happen in the future. This uncertainty is not well described probabilistically because the creation of probability distributions requires assumptions about the future conditions; making the distribution incomplete, imprecise, and liable to change with time (Anderson et al., 2015).

Although there are many approaches that can be used to quantify uncertainty associated within a model, sensitivity analysis of alternative realizations is among the most common types of advanced (non-linear) uncertainty analysis used in hydrological modeling. One of the most robust ways of producing alternative realizations is using Monte Carlo methods. Monte Carlo uses many forward forecast simulations with randomly sampled variable parameterizations to explore uncertainty without first making predictions about the relation between model inputs and outputs. Monte Carlo methods typically require thousands to millions of simulations to define an uncertainty profile that can statistically characterize the results. In addition to understanding how parameterization within a single model structure can affect results, Monte Carlo methods can also be used to be used to determine uncertainty derived from the model structure (nodal spacing, boundary conditions, initial conditions, model domain, etc.). The result of

Monte Carlo methods is a range of expected outcomes that can be expressed by a probability density function or a cumulative density function. Realizations included in the density functions only include forecasts that meet modeler-specified criteria and are consistent with what is known about the system. Therefore, the bounds of the function represent the range of possible outcomes, and the resulting probability conveys the uncertainty surrounding the model output of interest assuming that the PDFs of the inputs are correct. Although Monte Carlo methods can be applied to a modeling framework informally, models specifically tailored to preforming Monte Carlo simulations for uncertainty analysis do exist. Within groundwater modeling, the General Likelihood Uncertainty Estimation (GLUE) model is most widely used to facilitate Monte Carlo methods on both model parameterization within a given model structure and across varying conceptualizations of model structure (Beven and Binley, 1992). One of the biggest drawbacks to preforming Monte Carlo methods, and perhaps the most common reason Monte Carlo methods are not used more widely, is because of the computational time and storage needed to preform thousands of modeling simulations.

Once alternative realizations are produced, sensitivity analysis is used to understand how the variation of uncertain input parameters impacts the uncertainty of the forecast/response of interest (Scheidt et al., 2018). There are many methods for preforming sensitivity analysis; some of the most popular include the Morris method, the Sobol method, and the response surface methodology (RSM) (Fenwick et al., 2014). A popular technique for sensitivity analysis in the geosciences is a generalized sensitivity analysis (GSA), which was originally proposed by Spear and Hornberger (1980). GSA split models into discrete classes. The theory behind GSA is that if there is a difference between the distributions in each class for a certain parameter, that parameter is influenced in the model. However, if there is no difference between the distributions in each class, the parameter does not impact the model results (Spear and Hornberger, 1980). Using a sensitivity analysis can aid in reducing the uncertainty in the forecast by 1) identifying which parameters have a high impact on the results, 2) reducing complexity of the problem by identifying parameters that have little influence on the forecast, and 3) quantifying the combined (non-linear) effect of parameters on variations in the response (Scheidt et al., 2018).

### 1.2.5. Future sustainability of deltas

Given the high population density of deltas and the importance of these landscapes from an ecological perspective, many recent review papers have summarized the current risk to deltas and evaluated the sustainability of these landscapes (Syvitski, 2008; Giosan et al., 2014; Ingebritsen and Galloway, 2014; Elliott et al., 2019). The prominent risk discussed in these studies is the risk of land loss due to relative sea level rise, defined as the combination of natural and anthropogenically driven coastal subsidence and sea level rise. Natural processes impacting the location of the coastline include a change in the global volume of ocean water (eustasy), changes in regional earth-source load changes (isostasy), sediment supply, and sediment compaction (Ericson et al., 2006). Natural sediment compaction and eustatic changes in sea level are often comparable within an order of magnitude (Syvitski, 2008). However, both contributors are often significantly less than the land surface elevation change due to isostasy (Syvitski, 2008).

The most studied causes of anthropogenic coastal subsidence are dewatering of aquifers due to over pumping or urban loading. Subsidence due to groundwater pumping is caused by the collapse of the pore space within the porous media and is generally considered irreversible because compaction in aquifer-aquitard systems can be inelastic. Erban et al. (2014) found that groundwater pumping in the Mekong Delta may be responsible for 90 percent of the relative sea level rise expected by 2050. Offshore pumping has also been shown to cause land subsidence onshore in coastal settings (Yu and Michael, 2019). Subsidence due to urban loading refers to increased sediment compaction rates derived from the construction of heavy infrastructure. In the Fraser Delta, rapid subsidence rates due to urban loading was estimated to augment relative sea level rise by as much as 130% (Mazzotti et al., 2009). In additional to coastal subsidence, upstream water management and damming practices have resulted in a decrease in the amount of sediment being supplied to deltas by up to half compared to prehuman times (Syvitski and Saito, 2007; Syvitski, 2008; Giosan et al., 2014). When combined with the increased erosive effects of more frequent and intense climate extremes, most deltas are on course to drown (Syvitski et al., 2009; Giosan et al., 2014).

Tessler et al. (2015) and Day et al. (2019) surveyed deltas around the world to determine the future sustainability of these highly populated area. Although these

studies took differing approaches to quantifying sustainability, both studies found that deltas located in countries with poor economic conditions are most at risk for land loss because of the lack of financial means to invest in costly and timely land-loss mitigation strategies and engineering solutions. The enclosure of the Rhine-Meuse Delta in The Netherlands cost $6.3 billion USD while restoration of the Mississippi Delta is expected to run for the next 50 years and is projected to cost between $500 million and $1.5 billion USD per year (Giosan et al., 2014). Wealthier countries, such as The Netherlands and the United States, have the financial means to invest in protecting delta stability in addition to tackling growing costs associated with climate change, energy production, and food security (Giosan et al., 2014; Tessler et al., 2015; Day et al., 2019). However, upwelling of saline water in The Netherlands after land reclamation, creating the polder system, outlines just one unintended negative consequence that land management strategies can have on water resources in deltaic systems (Oude Essink et al., 2010).

As Day et al. (2019) state, “deltaic sustainability refers to the persistence through time of the structure and function of deltaic systems”. Only considering the effect of natural and anthropogenic changes on deltaic structure neglects the function of life on these landforms. Additionally, Day et al. (2019) identifies the quantity of freshwater as a key factor impacting the sustainability of deltas. However, the study by Day et al. (2019) is limited by exclusively considering deltas where hypersaline conditions exist and only recognizes the Nile, Indus, and Cauvery deltas as having detrimental saline conditions. Although recognizing that salinity degrades freshwater resources is a step in the right direction, the lack of awareness of the risk saline paleowater poses to freshwater availability within deltas is alarming and clearly outlines the need for further investigation.

## 1.3. Research goal and objectives

The overarching goal of this research is to characterize the amount and spatial distribution of fresh groundwater resources in coastal deltas and determine the vulnerability of deltaic groundwater to salinization. The research hypothesis is that the amount of fresh groundwater within a delta is dependent on the permeability distribution within the subsurface of the delta, which is ultimately controlled by the morphodynamic influences within the deltaic basin. Guiding questions for the research and the objectives completed to address each question include:

***Question 1:*** *How do morphodynamics impact the distribution of subsurface permeability within a delta?*

- Determine the range of fluvial, wave, and tidal influence that results in the formation of coastal deltas.
- Characterize the hydrogeologic properties that exist within deltas.
- Determine the sensitivity of hydrogeologic properties to changes in morphodynamics.

***Question 2:*** *How much fresh groundwater is currently contained within deltas and how does the distribution of subsurface permeability impact the preservation of groundwater salinity?*

- Assess the proportion of fresh and saline groundwater that exists within fluvial, wave and tidal influenced deltas.

***Question 3:*** *How vulnerable are fresh groundwater resources in deltas to salinization?*

- Evaluate the vulnerability of large coastal deltas around the world to groundwater salinization.

## 1.4. Thesis overview

This thesis is composed of five chapters. Chapter 1 introduces the scientific literature upon which this research builds in addition to defining the research hypothesis, questions, objectives, and approach. Chapters 2 through 4 were prepared as stand-alone papers with the intention of submitting these papers for publication. Chapter 5 presents the conclusions to the thesis.

All papers were co-authored with my senior supervisor, Dr. Diana Allen. Dr. Jeremy Venditti is also listed as a co-author on the paper included in Chapter 2. Although Dr. Allen and Dr. Venditti are co-authors on these publications, I am the main contributor to these works—I preformed all analyses and prepared the publications. Dr. Allen and Dr. Venditti provided technical input, guidance, and editing to the publications. An overview of the scope of work completed in Chapters 2 through 4 is provided:

***Chapter 2:*** *Controls on coastal delta formation under varying morphodynamic and basin conditions.*

- Data from 51 of the world's largest and most populated deltas are collected from previous scientific publications to determine the range of fluvial discharge, wave height, and tidal amplitude that exist within deltas around the world. Additionally, bathymetric gradient, incoming sediment concentration, and median grain size are also analyzed.

- The numerical morphodynamic model Delft3D-Flow is used to simulate the formation of coastal deltas under varying morphodynamic and basin conditions. The models mimic a sediment bearing river debouching into an ocean basin. A total of 207 models are used to span the full range and combination of fluvial and marine influence.

- A distance-based generalized sensitivity analysis is used to determine the sensitivity of delta formation to changes in fluvial discharge, bathymetric gradient, wave height, and sediment concentration.

***Chapter 3:*** *Sensitivity of subsurface permeability and groundwater flux in coastal deltas to their morphodynamic and geomorphic characteristics.*

- Two-dimensional morphodynamic models are used to explore the range of subsurface permeability, hydraulic gradient, and groundwater flux within three end-member delta types (fluvial, wave, and tidal).

- The connectiveness of the subsurface permeability is quantified in addition to estimating the horizontal heterogeneity and anisotropy that exists within deltaic permeability.

- A distance-based generalized sensitivity analysis is used to investigate the impact morphodynamic influences (fluvial, wave, and tidal), basin conditions (sediment concentration, bathymetric gradient), and geomorphic characteristics (number of channels, shape of the delta plain, delta from rugosity) have on the subsurface permeability, hydraulic gradient, and connectivity.

***Chapter 4:*** *Impact of delta morphology on vulnerability to groundwater salinization in large coastal deltas.*

- The numerical modeling code iMOD-WQ is used to determine the susceptibility of shallow deltaic aquifers to groundwater salinity in fluvial, wave, tidal deltas.
- The role of the river network and recharge in freshening of the shallow subsurface is investigated.
- Numerical modeling, along with previously published information on morphodynamics, climate, and population, is used to determine the vulnerability of large coastal deltas around the world to future groundwater salinization.

# Chapter 2.

# Controls on coastal delta formation under varying morphodynamic conditions and basin characteristics

## 2.1. Abstract

Delta morphology is primarily classified qualitatively through visual analysis, leading to the development of ternary diagrams indicating the degree of fluvial-, tidal-, and wave-influence on delta morphology. Recently, global datasets quantified morphodynamic and basin characteristics for deltas around the world. Here, we use data from 51 of the world's largest and most populated deltas to develop numerical morphodynamic models that simulate the formation of coastal deltas. Models span the full range of fluvial and marine influence by varying the fluvial discharge, wave height, and tidal amplitude according to the published parameter ranges. Additionally, bathymetric gradient, incoming sediment concentration, and median grain size are varied to explore their influence on delta formation in varying morphodynamic settings. Using 207 models, we find that 82% of parameter combinations produce deltas that display the morphological characteristics expected in fluvial, wave, and tidal environments. Some models that formed a delta have the same proportion of fluvial, wave, and tidal influence as models that do not form a delta; changes in sediment concentration and bathymetric gradient can control if a delta forms. A distance-based generalized sensitivity analysis shows that delta formation is most sensitive to changes in fluvial discharge, bathymetric gradient, wave height, and sediment concentration. Although delta formation is insensitive to tides in most environments, fluvial and wave interactions with tides have a constructive effect on delta formation. Our results identify the conditions in which delta formation is most likely to occur and which parameters are most important in creating new deltaic land.

## 2.2. Introduction

Coastal deltas form where rivers debouch into the ocean, depositing continental sediment eroded from drainage basins. Delta formation and the depositional morphology of a delta depend on the balance of sediment delivery (Caldwell et al., 2019) and

deposition from fluvial discharge and erosion from the ocean (Fisher et al., 1969; Galloway, 1975; Caldwell et al., 2019). Fluvial forces, including inertia, buoyancy, and bed friction, act upon river effluent to disperse and accumulate sediment entering the delta (Wright, 1977). Tides and waves interact with the effluent to change the amount and spatial location of sediment deposition. The impact of these three morphodynamic forces on sediment deposition in coastal deltas has been examined qualitatively, focusing on the link between delta morphology and the relative strength of discharge, waves, and tides within the depositional basin. For example, Fisher et al. (1969) described delta morphology as a balance between constructive fluvial influences and destructive marine influences. Galloway (1975) further distinguished the role of tides and waves on delta morphology. This distinction led to the formation of a ternary diagram with three distinct end-member delta archetypes: a fluvial, wave- and tidal influenced delta. Deltas are often categorized into one of these end-member types based on qualitative analysis of depositional characteristics including the geometry of the delta plain, shoreline rugosity, channel sinuosity, channel shape, and bulk composition of the depositional system (Galloway, 1975).

Recently, focus has shifted to quantifying the relations between morphodynamics, depositional basin conditions, and delta morphology. Data on morphodynamics and basin conditions in over 10,800 global deltas were collected through point source and remote sensing methods (Syvitski and Saito, 2007; Caldwell et al., 2019; Nienhuis et al., 2020). This information led to the development of empirical relations describing delta morphology (Syvitski and Saito, 2007) and the likelihood of delta formation (Caldwell et al., 2019). Recently, numerical modeling has been used to evaluate the morphological response to variations in morphodynamics and basin conditions. The integration of both fluvial and wave influences showed that fluvially-dominated environments result in protruding deltaic landforms while wave action results in sediment build up along the shoreline (Seybold et al., 2007; Geleynse et al., 2010). The inclusion of tides produces relatively stable distributaries with interbedding of sand and silts (Geleynse et al., 2010). Changes in delta morphology can also stem from variations in antecedent stratigraphy (Geleynse et al., 2010), sediment properties such as incoming median grain size and sediment cohesiveness (Edmonds and Slingerland, 2010; Caldwell and Edmonds, 2014; Rossi et al., 2016), and relative sea level rise (Liang et al., 2015).

While previous studies have examined the link between delta morphodynamics and morphology, how the magnitude and combination of morphodynamic influences impact delta formation has not been examined. It is widely accepted that deltas can not form when destructive forces overpower constructive properties (Fisher et al., 1969; Galloway, 1975; Caldwell et al., 2019; Nienhuis et al., 2020). However, consensus on which factors are constructive and which are destructive remains elusive. Syvitski and Saito (2007) proposed that river power is a result of fluvial discharge and bathymetric gradient while marine power is a result of waves and tides. Caldwell et al. (2019) developed an equation to predict delta formation with 75% accuracy using fluvial and sediment discharge as constructive factors and wave and tidal action for destructive factors. Caldwell et al. (2019) recognized that the combined effect of tidal and wave processes on altering constructive properties in deltas is largely unknown. Furthermore, studies have yet to explore the effect of basin conditions on the interaction and competition of morphodynamics.

Here, we explore how the competition between morphodynamic influences (e.g., fluvial discharge, waves, and tides) and interactions with basin characteristics (e.g., sediment concentration, bathymetric gradient, median grain size of incoming sediment) affect delta formation. We use an aggregation of global datasets to establish the range of morphodynamic and basin characteristics for deltas globally. The upper and lower limits of parameter distributions for 51 of the world's largest and most populated deltas are used to constrain numerical models to simulate the formation of coastal deltas. We use 229 unique combinations of morphodynamic and basin characteristics to explore which combinations produce viable and realistic deltas, and importantly, which do not. A distanced-based sensitivity analysis is used to quantify which parameters and parameter interactions are most important for delta formation and how this may change in various morphodynamic environments.

## 2.3. Methods

### 2.3.1. Data

We combine three previously published global datasets (Syvitski and Saito, 2007; Caldwell et al., 2019; Nienhuis et al., 2020) to constrain the ranges of parameters for a suite of numerical morphodynamic models used to simulate delta formation (Figure

2.1; See Appendix A for more details on the preparation and comparison of datasets). We select 51 deltas representing the largest and most populated deltas on Earth (Syvitski and Saito, 2007). The selected deltas are not representative of all deltas around the world due to a biased sampling of large deltas; i.e., the dataset excludes small deltas that are typically wave dominated and that are often little more than a small extrusion from the shoreline (Nienhuis et al., 2020). Syvitski et al. (2022) proposed a stringent criterion of features that a delta must have and state that many of the “deltas” in the Nienhuis et al. (2020) dataset are only river mouths. Information gathered for each of the 51 deltas includes incoming river discharge (Qav), wave height (Wa), tidal range (Ti), incoming sediment concentration (Cs), bathymetric gradient (Dgrd), and median grain size (Dmm).

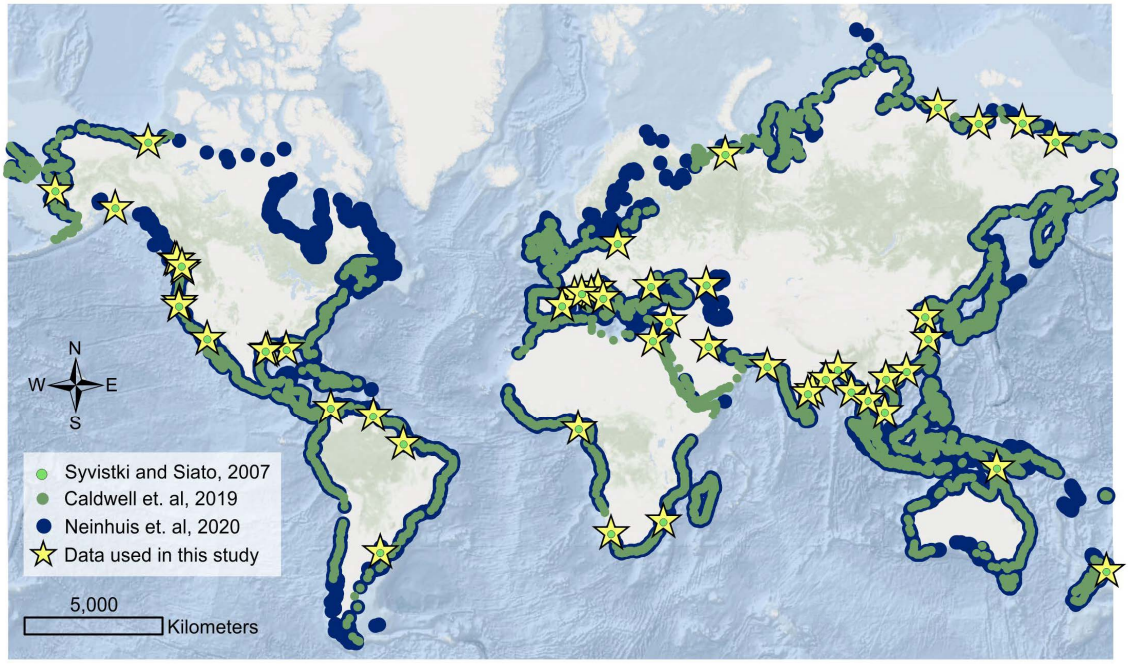


**Figure 2.1. Location of deltas identified by Syvitski and Saito (2007), Caldwell et al. (2019), and Nienhuis et al. (2020). Stars show the locations of large deltas from which the data are used in this study.**

The distribution of Qav, Wa, Ti, Cs, Dgrd, and Dmm for the 51 deltas are compared to all 13,073 observations in the global datasets (Figure 2.2). A distribution is fit to each parameter in the 51 deltas dataset as a means for defining parameter input ranges for the numerical modeling. A normal distribution is used when a Shapiro Wilks test for Normality was confirmed at a 95% confidence interval (BenSaïda, 2021); a log-normal distribution is used when the Shapiro Wilks test for Normality was accepted at a

95% confidence interval after the data were log-transformed (BenSaïda, 2021); and an exponential distribution is used when the One-sample Kolmogorov-Smirnov was accepted at a 95% confidence interval using an exponential cumulative density function with a mean equal to the mean of the data. The fit distributions are then used to calculate the 25th, 50th, 75th, and 90th percentiles of each parameter (Table 2.1).

The 51 deltas used in this study have a larger median Qav than the aggregated datasets, because we self-selected the largest deltas; the range in area of the 51 deltas is 5 to 470,000 $km^2$. Qav, measured herein as the mean annual discharge, for the 51 deltas is log-normally distributed, with a range from 30 to 200,000 $m^3/s$, and a median of 2000 $m^3/s$ (Table 2.1). Wa, Dgrd, and Cs are also log-normally distributed. Ti is the only variable that is exponentially distributed. Wave height values range from 0.42 to 3.63 m, with a median of 1.36 m, while the Ti ranges from 0.004 to 4.1 m, with a median of 1.1 m. Cs and Dmm are only available for the 51 selected deltas. Cs ranges from 0.02 to 23 $kg/m^3$, with a median of 0.6 $kg/m^3$. Dmm ranges from 0.01 to 10 mm, with a median 0.2 mm. Data for Dmm did not fit any of the tested distributions. Dgrd ranges from $6x10^{-5}$ to $2x10^{-2}$ m/m with a median of $8x10^{-4}$ m/m. Although some deltas can form with Dgrd > $2x10^{-2}$ m/m (Figure 2.2), the 51 deltas selected for this study do not form in basins with a Dgrd > $2x10^{-2}$ m/m.

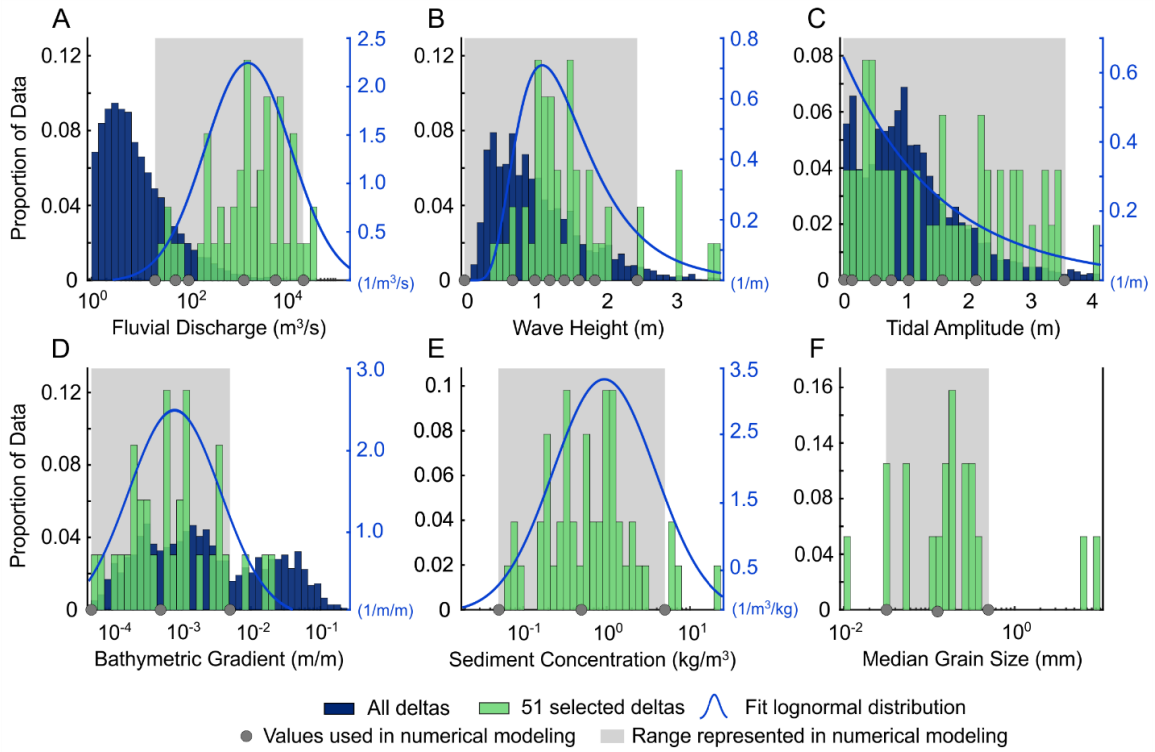


**Figure 2.2.** **Distribution of A) fluvial discharge (Qav), B) wave height (Wa), C) tidal range (Ti), D) bathymetric gradient (Dgrd), E) sediment concentration (Cs), and F) median grain size (Dmm) for all deltas in the combined dataset (blue bars) and the largest 51 deltas (green bars). A fit distribution is not included for Dmm because the data did not fit any of the distributions tested.**

**Table 2.1.** **Minimum, maximum, and percentile values for six morphodynamic and basin characteristics for 51 selected global deltas.**

| Parameter | Minimum | Percentile of Distribution 25 | 50 | 75 | 90 | Maximum | Number of data points |
|---|---|---|---|---|---|---|---|
| **Qav ($m^3/s$)** | 30 | 500 | 2000 | 7000 | 22000 | 200000 | 51 |
| **Wa (m)** | 0.42 | 1.0 | 1.4 | 1.9 | 2.5 | 3.6 | 51 |
| **Ti (m)** | 0.004 | 0.45 | 1.1 | 2.2 | 3.6 | 4.1 | 51 |
| **Cs ($kg/m^3$)** | 0.02 | 0.25 | 0.60 | 1.5 | 3.2 | 24 | 51 |
| **Dmm (mm)** | 0.01 | 0.06 | 0.2 | 0.3 | 4 | 10 | 19 |
| **Dgrd (m/m)** | $6x10^{-5}$ | $3x10^{-4}$ | $8x10^{-4}$ | $2x10^{-3}$ | $5x10^{-3}$ | $2x10^{-2}$ | 33 |

## 2.3.2. Numerical modeling

This study developed 229 unique models to explore how changes in morphodynamic and basin characteristics influence delta formation. Seventy-five models are used to explore varying proportions of fluvial discharge, wave height, and tidal amplitude (analysis 1), 56 models are used to determine the minimum Qav and Cs

needed to produce a delta in various morphodynamic environments (analysis 2), and 98 models are used to examine the combinations of varying Cs, Dgrd, and Dmm in various morphodynamic environments (analysis 3).

### *Base case model setup*

We simulate the formation of coastal deltas using Delft3D, an open source, physically based, numerical morphodynamic modeling software. The morphodynamic models are 2D and use a depth-averaged approach to solving the flow and sediment transport equations (Deltares, 2012). We used depth-averaged flow to reduce model runtimes and because we are not expecting the horizontal flow field to have significant variation in the vertical direction (which can arise from wind forcing, bed stress, Coriolis force, and bed topography).

The initial model setup is based on the modeling protocol described in Caldwell and Edmonds (2014). The models mimic a sediment-carrying river debouching into an oceanic basin that increases in depth away from the initial shoreline (Appendix A, Figure A1). The initial shoreline, located along the southern boundary of the model, consists of an erodible beach 5 meters above sea level (m asl) and protrudes 5 km into the basin. The beach and the basin floor are 0.5 m thick and consist of homogenously mixed sediments that have the same distribution of sizes as the incoming sediment. A channel cuts through the initial shoreline half-way along the southern boundary. Bathymetry in the basin is shallowest at -5 m asl in the channel at the southern boundary and deepens to the north with a uniform gradient.

The modeling domain is 80 km x 100 km resulting in a 8,000 $km^2$ domain. The grid cell size is 200 m x 200 m. Other delta modeling used studies using Delft3D have used a much smaller domain. The domain in Caldwell and Edmonds (2014) was 7.5 km x 5.625 km with grid cells of 25 m x 25 m while the domain in Broaddus et al. (2022) used a domain of 9 km x 21 km with grid cells of 25 m x 25 m. Although the domain in this study is significantly larger than what has been used in previous studies, we choose a larger domain to produce deltas on a similar scale to the 51 global deltas and to accommodate with largest modeled deltas while minimizing the amount of sediment that gets deposited along the eastern and western boundaries.

To accommodate the large domain size, a larger cell size (200 m x 200 m) is required to reduce computational time. The increased cell size means that features smaller than 200 m are not distinguished within the model. For instance, all river channels within the model are at least 200 m wide (one grid cell), which neglects the finer resolution features within the delta such as thin tidal channels or some channels within smaller fluvial deltas. Some of the branches within the Nile Delta are approximately 250 m wide at the thinnest sections near the shoreline. The width of the Fraser River is approximately 1 km wide at the delta apex and 250 m wide on some of the smaller sections of river near the shoreline. The smallest river width in the Fraser Delta is approximately 150 m and occurs in a side channel where a fluvial island forms in the river. Choosing a cell size of 200 m x 200 m was necessary to reduce the computational time but may impact the ability of deltas to form at very low fluvial discharge rates.

A total discharge boundary located in the channel represents the fluvial input to each model and is specified with a constant Qav and Cs. In all models, there are six sediment types ranging in size from clay ($2x10^{-3}$ mm) to coarse sand (2 mm) (Appendix A Table A2). The incoming grain size distribution is normal, with the mean of the distribution varying for each analysis (Appendix A Figure A3). The northern boundary represents ocean conditions and is specified as constant water level boundary or a harmonic boundary in models that incorporate tidal action. In models that include waves, wave action is also specified at the northern boundary. In all models, the northern boundary has a Cs = 0 $kg/m^3$ to promote the deposition of sediment coming into the basin while the eastern and western boundaries are no-flux boundaries with a Cs = 0 $kg/m^3$ (see Appendix A for more justification on the types of boundary conditions selected). Specific values for Qav, Wa, Ti, Cs, and Dmm used in each analysis are described below.

### *Analysis 1: Changes in morphodynamic influences*

The effect of changes in morphodynamic influences on delta formation is explored by varying the proportion of fluvial discharge, wave height, and tidal amplitude within the models. These parameters are varied according to the percentiles for fluvial discharge (Pf), wave height (Pw), and tidal range (Pt) for the 51 deltas (Table 2.1). Changes in fluvial influence are simulated by varying Qav entering the basin; we used

fluvial discharge as a proxy for the fluvial force present within the model. Incoming Qav is varied between Pf = 0.5, 0.75, and 0.9 (e.g., Pf = 0.9 represents the 90$^{th}$ percentile of Qav = 21,793 m$^3$/s). Qav below Pf = 0.5 is not simulated because initial sensitivity testing indicated that Qav below Pf = 0.5 did not consistently produce model deltas with an active river channel. The initial channel width varies proportionally with Qav; i.e., 600 m, 1200 m, and 2200 m, respectively. Variations in Ti are used to represent changes in tidal influence between Pt = 0, 0.25, 0.50, 0.75, and 0.9. Tides are simulated in the model using a harmonic water level boundary imposed at the northern boundary with a frequency of 30 degrees/hour, creating semidiurnal tides. Changes in wave influence are accounted for by varying the Wa at the northern boundary. Wave height vary between Pw = 0, 0.25, 0.5, 0.75, 0.9. All waves enter the basin at 0 degrees from the north and have a peak period of seven seconds. Variations in fluvial discharge, tidal range, and wave height result in 75 unique models (see Supplemental Information for input parameters on all models used in this study). In these 75 models, there is a uniform gradient of Dgrd = 5x10$^{-4}$ m/m and a constant Cs = 0.5 kg/m$^3$ specified at the river boundary; the incoming sediment has a median Dmm = 0.13 mm. Values used for Cs and Dgrd in this analysis represent the median values listed in Table 1 but are altered slightly for ease in modeling and sensitivity analysis.

### *Analysis 2: Changes in discharge and sediment concentration*

To determine the minimum discharge and sediment concentration needed to produce a delta in various environments, Qav and Cs are varied for four environments representing the three end-member morphodynamic conditions as well as one environment with all three morphodynamic influences: 1) fluvial (no wave or tidal influence), 2) wave (Wa equivalent to Pw = 0.9), 3) tidal (Ti equivalent to Pt = 0.9), and 4) mixed (Wa, and Ti equivalent to Pw = Pt = 0.9). These models are run with Qav values of Pf = 0.1, 0.25, 0.375, 0.5, 0.625, 0.75, and 0.9. Cs values of 0.5 kg/m$^3$ and 0.05 kg/m$^3$, defined at the river boundary, represent the approximate median of the 51 deltas dataset (0.6 kg/m$^3$ in Table 2.1) and one order of magnitude lower. This results in 56 models evaluating the Qav and Cs needed for form a delta in each of the four morphodynamic environments.

### *Analysis 3: Changes in basin conditions*

The effects of Cs, Dmm, and Dgrd on delta formation are explored in 14 varying morphodynamic environments that span the range of fluvial, wave, and tidal influence. In each of these 14 environments, two sediment concentrations are considered: Cs = 0.5 kg/m$^3$, and 5 kg/m$^3$. Three grain size distributions are considered in this study, with median Dmm = 31 μm, 0.13 mm, and 0.5 mm. For bathymetric gradient, Dgrd = 5x10$^{-5}$ m/m, 5x10$^{-4}$ m/m, and 5x10$^{-3}$ m/m are considered. Additionally, combinations of the smallest and largest bathymetric gradients (Dgrd = 5.0x10$^{-5}$ m/m and 5.0x10$^{-3}$ m/m) are tested with values with the largest sediment concentration (Cs = 5 kg/m$^3$) to determine if the combined effect of these parameters influences delta formation. The combination of Cs, Dmm, and Dgrd parameter changes for the 14 different combinations of fluvial, wave, and tidal influence results in an additional 97 models.

## 2.3.3. Normalized morphodynamic influence ratios

Of the 229 models run in this study, only 207 models are used for further analysis (not included in any calculations, statistics, or the sensitivity analysis). The 21 models not carried forward for further analysis are excluded due to errors in the modeling, ranging from early model termination to unusual or undiagnosed model behavior.

Normalized morphodynamic influence ratios ($nMIi$) are used to compare the proportion of fluvial discharge, wave height, and tidal amplitude in each model, where $i = [f, w, t]$. Each model has a normalized fluvial, wave, and tidal ratio based on Pf, Pw, and Pt, used in the boundary conditions. Normalized morphodynamic influence ratios are defined as the percentile of the influence divided by the sum of the percentiles for all three influences:

$$nMIi = Pi/(Pf + Pw + Pt) \qquad (2.1)$$

Quantifying the deltaic environment using normalized morphodynamic influence ratios based on percentiles accounts for variations in the model input rather than simulated outputs. Additionally, using percentiles based on data from deltas around the world allows for a comparison of the modeling environment to physical deltaic environments.

### 2.3.4. Analysis of sensitivity

We undertook two sensitivity analyses. The first sensitivity analysis uses all 207 models to evaluate the sensitivity of delta formation to changes in all parameters investigated in this study (Qav, Wa, Ti, Cs, Dgrd, and Dmm). The second analysis is done to determine the sensitivity of delta formation when primarily influenced by a single morphodynamic influence. The second sensitivity analysis uses three groups of models with varying degrees of fluvial, wave, and tidal influence: 1) fluvial influence group (nMIf $\geq$ 0. 5); 2) wave influence group (nMIw $\geq$ 0.4); 3) tidal influence group (nMIt $\geq$ 0.35). The normalized morphodynamic influence ratios defining each group were chosen so that each group has a similar number of models. The fluvial group is comprised of 73 models, the wave group is comprised of 69 models, and the tidal group is comprised of 71 models.

The sensitivity analyses are preformed using a Distance-Based Generalized Sensitivity Analysis (DGSA) approach (Fenwick et al., 2014; Scheidt et al., 2018). Results from a DGSA indicate 1) the main effects, defined as the effects of individual input parameters on the response, and 2) interactions, defined as the effects of interactions between input parameters on the response. The response of interest is whether a delta forms or does not form. The input parameters of interest are Qav, Wa, Ti, Cs, Dgrd, and Dmm.

Delta formation occurs in a model if the following three criteria are met at the end of the simulation: 1) sediment has deposited along the initial beach shoreline, 2) the area of accumulated sediment is greater than 5 $km^2$, equivalent to the smallest delta included in this study, and 3) there is at least one active channel extending from the initial channel to the ocean. The shoreline boundary is mapped using the Open Angle Method (Shaw et al., 2008), with an open angle of 135 degrees to accommodate wider tidal channels. The area of accumulated sediment is calculated by mapping the shoreline boundary between the deposited sediment and determining the number of land pixels within the boundary. Land pixels within the boundary are defined as pixels where the elevation of the sediment is higher than 0 m. The channel network within a delta is mapped using Rivamap (Isikdogan et al., 2017). An active channel is defined herein as a channel that intersects the shoreline and connects back into the main stem of the delta.

To compute the sensitivity of the response to changes in the input parameters, models are first sorted into two classes (Scheidt et al., 2018); those that formed a delta and those that did not. The sensitivity of the response to changes in a parameter is quantified based on the distance between the prior frequency distribution and the frequency distribution of a parameter for each class (Scheidt et al., 2018). A hypothesis test with a 95% confidence level ($p < 0.05$) is used to determine if the response is sensitive to each input parameter. The null hypothesis is that the input parameter has no influence on the response (Scheidt et al., 2018). An influential, or critical parameter, rejects the null hypothesis while a non-influential, or insensitive parameter, fails to reject the null hypothesis.

DGSA is also used to assess the effect of two-way parameter interactions. An interaction occurs when the effect of a parameter on the response changes as another parameter is varied. Sensitivity of the response to interactions is calculated by further dividing each class into low and high value bins based on a second parameter. For example, the interaction of discharge with sediment concentration would sort the discharge values in each class into low and high bins based on whether the sediment concentration in the model is low or high. The threshold value for low and high bins is unique to each parameter and is computed using evenly spaced quantile values (Fenwick et al., 2014). A global sensitivity measure is calculated based on the distance between the frequency distributions for each bin and the class frequency distribution. A critical interaction will occur when there is distance between the binned frequency distribution and the response class frequency distribution. The same hypothesis test used to determine the sensitivity of the main effects is also used to determine the sensitivity of the interactions.

## 2.4. Results

### 2.4.1. Modeled delta formation and morphology

The Mississippi, Ganges-Brahmaputra, and Sao Francisco deltas are classic examples of fluvial, tidal, and wave deltas (Figure 2.3A, B, C). Examples of the generic modeled deltas from this study (Figure 2.3D, E, F) visually reproduce the morphological characteristics expected in fluvial, wave, and tidal environments. One of the fluvial models (Figure 2.3D) created a delta plain that progrades into the basin and has an area

of 779 km$^2$. The modeled tidal delta (Figure 2.3E) has a larger area, at 854 km$^2$ and increased channelization (Figure 2.3E) compared to the fluvial delta. Many of these channels have bifurcations and exhibit a funnel shape where the channel widens near the river mouth. The shape of both the fluvial and tidal deltas is semi-circular but the tidal delta has a more rugged shoreline. The delta plain in the wave delta model (Figure 2.3F) does not stretch as far into the ocean and has an area of 330 km$^2$. The shoreline in the wave model is smooth and the delta exhibits a cuspate shape.

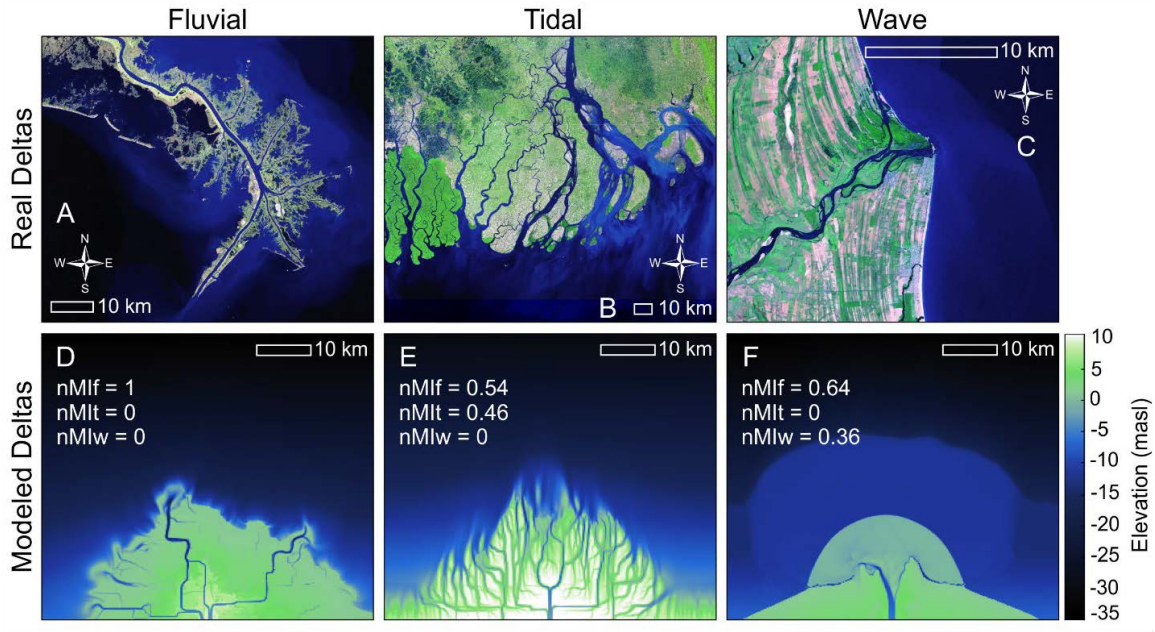


**Figure 2.3. The A) Mississippi, B) Ganges-Brahmaputra, and C) Sao Francisco deltas as examples of actual fluvial, tidal, and wave dominated deltas, respectively. The second row shows examples of modeled D) fluvial, E) tidal, and F) wave influenced deltas.**

Of the 207 models that ran without significant error and that were carried forward for analysis, 73 have an nMlf greater than 0.5, indicating that more than 50% of the influences are fluvial. Twenty-seven models have an nMlw greater than 0.5, and 37 have an nMlt greater than 0.5. A total of 70 models do not have a single morphodynamic influence greater than 0.5, with 42 of those models having equal fluvial, wave, and tidal normalized morphodynamic influences. Of the 207 models, 171 form a delta (83%) and 36 (17%) do not form a delta. The successful models cover much of the Galloway diagram (Figure 2.4A). Of the 36 models that do not form a delta (Figure 2.4A, grey dots), 38.8% are fluvial (nMlf $\geq$ 0.5), 19.4% are wave (nMlw $\geq$ 0.40), and 13.9% are tidal (nMlt $\geq$ 0.35). There are 13 occurrences where a model that did form a delta occupies

the same space on the Galloway ternary diagram as a model that did not form a delta (Figure 2.4A).

When models that do not include wave or tidal influence fail to form a delta (located at the top of the ternary diagram in Figure 2.4A), the failure results from a change in fluvial discharge or sediment concentration (Figure 2.4B, C). Delta formation commenced at Qav = 1000 $m^3/s$ (Pf = 0.375) when Cs = 0.5 $kg/m^3$ (Appendix A Figure A4). However, when Cs = 0.05 $kg/m^3$, delta formation did not occur until Qav reached 2000 $m^3/s$ (Pf = 0.5).

Models that have only two influences, i.e., models located along the axes of the ternary diagram, form a delta when fluvial influence is greater than 40% (nMIf > 0.4). Below this 40% threshold, some models form a delta while others do not. This can be explained by variations in Cs, Dmm, and Dgrd (Appendix A Figure A5). In models with Wa = 2. 5 m (Pw = 0.9), delta formation occurred when Qav reached 2000 $m^3/s$ (Pf = 0.5) regardless of the Cs value (Appendix A Figure A5). Delta formation commenced at the lowest discharge, Qav = 500 $m^3/s$ (Pf = 0.25), when Ti = 3.6 m (Pt = 0.9) and Cs = 0.5 $kg/m^3$ (Appendix A Figure A5). When Cs was decreased to Cs = 0.05 $kg/m^3$, delta formation occurred at Qav = 1000 $m^3/s$ (Pf = 0.375).

Models with equal wave and tidal influence (nMIw = nMIt) also follow the 40% fluvial influence threshold. With Pw and Pt = 0.9, delta formation did not occur until Pf = 0.75 with Cs = 0.05 $kg/m^3$. Some sediment did deposit along the shoreline when Pf = 0.375 and Pf = 0.5, but these landforms do not meet the criteria of being a delta. Interestingly, when Cs was decreased to Cs = 0.05 $kg/m^3$, delta formation began at Qav = 500 $m^3/s$ (Pf = 0.25) (Appendix 3 Figure A3.1).

For models with a mixture of fluvial, wave, and tidal influence that are not equal, the 40% fluvial threshold was no longer observed. A combination of low tidal influence ($nMIt \leq 0.2$) and high wave influence ($nMIw \geq 0.4$), shows some models not forming with a fluvial influence between 40-50%.

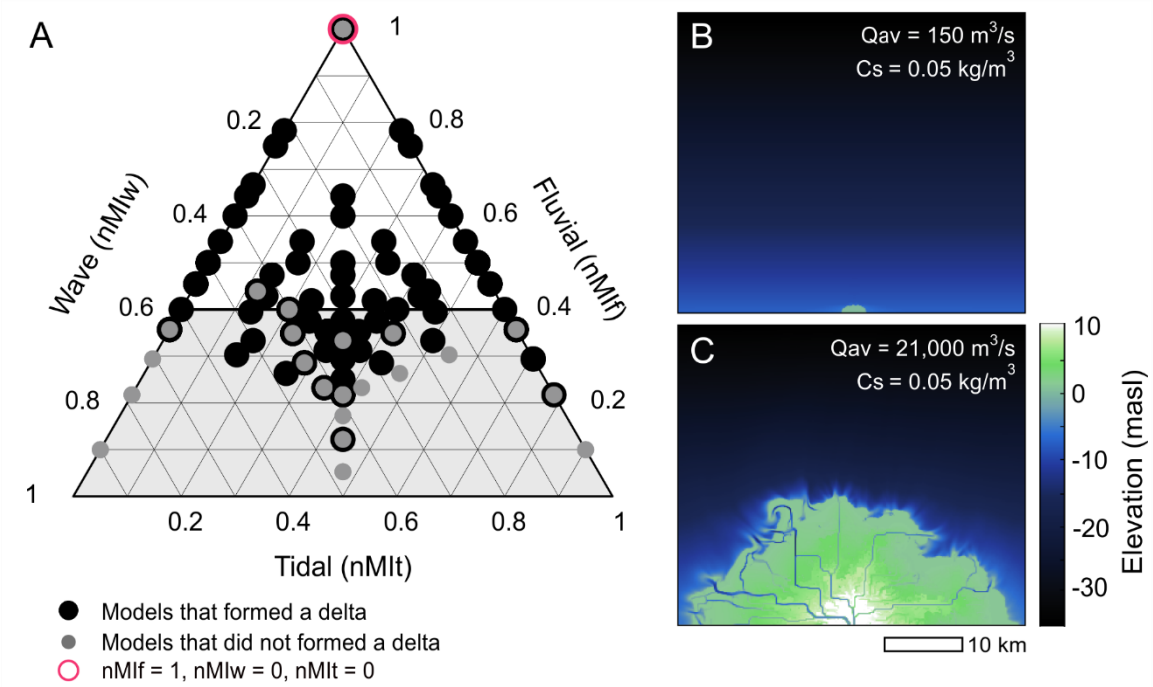


**Figure 2.4.** **A) Galloway ternary diagram populated with delta models that form and do not form deltas. An example of a model that B) does not form a delta (nMlf = 1, Qav = 150 $m^3/s$) and C) does form a delta (nMlf = 1, Qav = 150 $m^3/s$).**

## 2.4.2. Sensitivity of delta formation

When considering all models, regardless of the dominant influence, delta formation is most sensitive to changes in Qav and Dgrd (red bars in Figure 2.5A). Ti and Dmm are both insensitive parameters (blue bars in Figure 2.5A). Each parameter has at least one critical or important interaction with another parameter, except Ti, which is insensitive in all cases (red squares in Figure 2.5B). Dgrd has the greatest number of critical interactions, interacting with Qav, Ti, and Cs (Figure 2.5B; Row 5). Wa has critical interactions with Qav and Ti (Figure 2.5B; Row 2). (Figure 2.5B; Row 1). Although Ti is an insensitive parameter (Figure 2.5B; Row 3), the critical interaction between Wa and Ti (Figure 2.5B; Row 2, Column 3) indicates that delta formation is sensitive wave action for certain tidal ranges. Additionally, delta formation is more sensitive to Dgrd at certain values of Ti (Figure 2.5B; Row 5, Column 3). There is a critical two-way interaction between Cs and Dgrd (Figure 2.5B; Row 4, Column 5 and Row 5, Column 4), indicating that delta formation is sensitive to Cs for certain bathymetric slopes and is also sensitive to Dgrd at certain sediment concentrations. Dmm also has a critical interaction with Cs (Figure 2.5B; Row 6, Column 4). There is a one-way interaction between Qav and Dmm

(Figure 2.5B; Row 1, Column 6), suggesting more sensitivity of delta formation to Qav for certain Dmm.

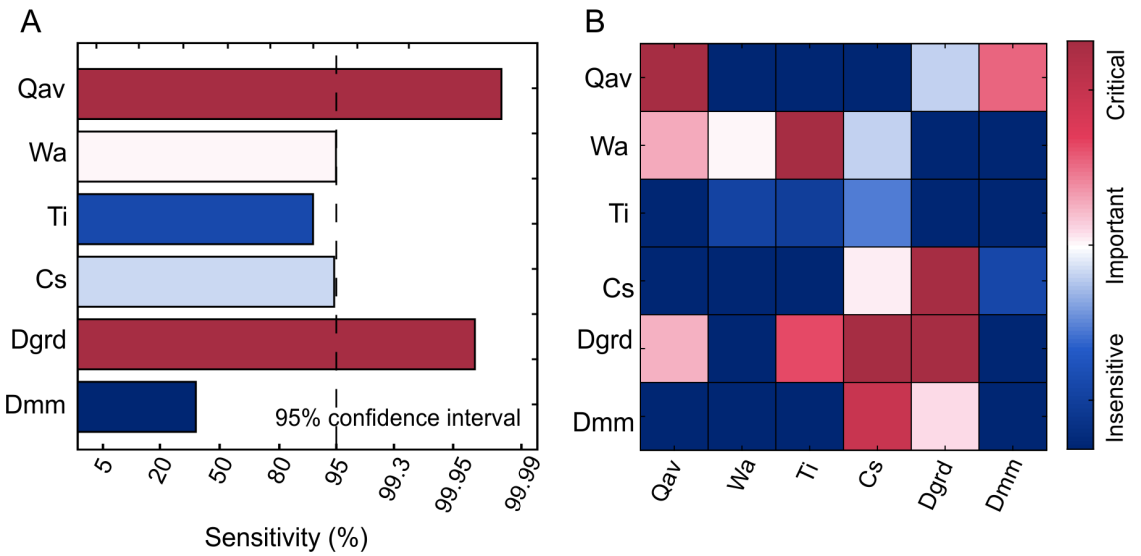


**Figure 2.5. A) Main effects and B) interactions of eight parameters: fluvial discharge (Qav), wave height (Wa), tidal range (Ti), sediment concentration (Cs), bathymetric gradient (Dgrd), and median grain size (Dmm) on delta formation. The diagonal of the interaction matrix in B is the same as the main effects shown in A.**

Results from the DGSA on whether a delta will form or indicate that parameter sensitivity depends on the dominant morphodynamic influence: fluvial, wave or tidal (Figure 2.6). Each environment has one to two critical parameters, one or two important parameters, and up to three insensitive parameters. The parameter most critical to delta formation in the fluvial environment is Qav, followed by Wa (Figure 2.6B). Cs is also important in fluvial environments but is not critical. In wave environments, Dgrd is the only parameter critical to delta formation, with Cs also being important (Figure 2.6C). The Wa and Ti parameters are insensitive for models with a high wave influence. In tidal environments, Qav and Wa are critical, while Ti and Dgrd are important (Figure 2.6D). Cs is insensitive in tidal environments. Dmm is insensitive in all three environments, indicating changes in this parameter within the range of Dmm values use in this study (1.25 μm, 0.125 mm, and 0.5 mm) does not produce a significant change in the ability of a delta to form.

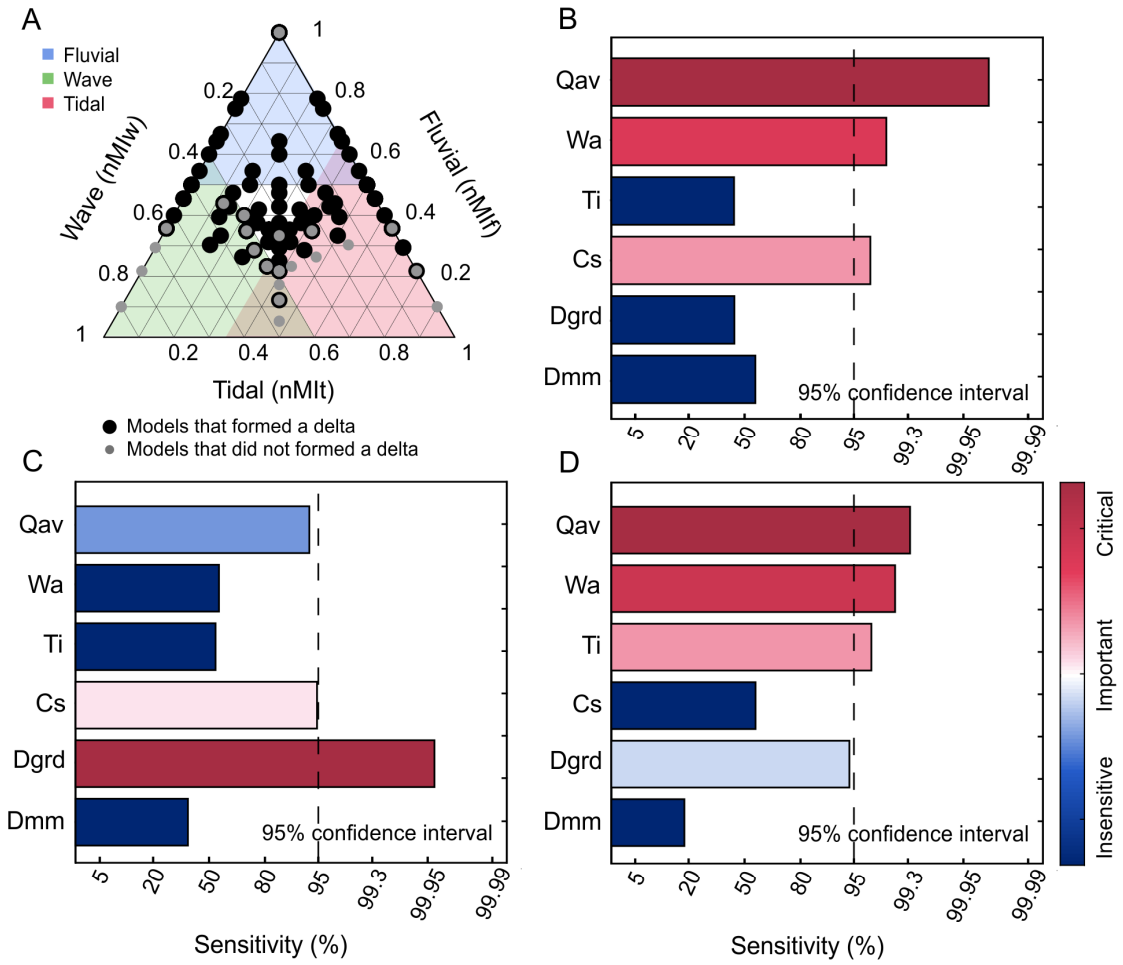


**Figure 2.6.** **Sensitivity of delta formation to six parameters for three groups of models with varying degrees of fluvial, wave, and tidal influence: B) fluvial influence group (nMlf ≥ 0. 5); C) wave influence group (nMlw ≥ 0.4); D) tidal influence group (nMlt ≥ 0.35). Parameters include fluvial discharge (Qav), wave height (Wa), tidal range (Ti), sediment concentration (Cs), bathymetric gradient (Dgrd), and median grain size (Dmm).**

## 2.5. Discussion

The ternary diagram proposed by Galloway (1975) was used to describe how the morphology of a delta changes relative to the proportion of fluvial, wave, and tidal influence. Recent research has focused on quantifying delta morphology and basin characteristics, giving us a better idea of the proportion of morphodynamic influence that will result in certain geomorphic features (Syvitski and Saito, 2007; Caldwell et al., 2019; Nienhuis et al., 2020). Global data show that deltas can form when the average fluvial discharge is as low as 1.0 $m^3/s$, suggesting that there is no lower limit of fluvial discharge

required for a delta to form. Although large coastal deltas tend to have higher fluvial discharge than smaller deltas, the distribution of wave height and tidal range in large deltas exist across the same range of wave height and tidal range seen in smaller deltas. This indicates that the presence of increased marine morphodynamic influence (waves and tides) does not necessarily inhibit delta formation. The numerical morphodynamic models in this study used a combination of fluvial, wave, and tidal influence to create deltas that exhibit the expected geomorphic characteristics observed in fluvial, wave, and tidal influenced deltaic environments, allowing the ternary parameter space to be filled more completely.

All modeled parameter combinations result in some sediment deposition; however, some combinations do not result in delta formation even though the model forcings were within the range fluvial discharge, wave height, and tidal amplitude exhibited in deltas around the world. Out of 207 models that ran successfully, 171 models (83%) produce a deltaic landform. Of the 171 models, 59 are fluvial, 55 are wave, and 59 are tidal. Of the models that do not form a delta, 14 models have over 50% fluvial influence (nMIf = 0.5), seven models have over 50% wave influence (nMIw = 0.5), and five models have over 50% tidal influence (nMIt = 0.5), indicating that the location of the model on the ternary diagram does not determine if the model will form a delta.

Some models that do not form a delta share the same proportion of morphodynamic influences as a model that does form a delta, occupying the same space on the Galloway ternary diagram. This implies that delta formation is more complicated than simply balancing constructive and destructive influences and that basin conditions as well as interactions between parameters should be considered. The models in this study clearly show that changing bathymetric gradient (Dgrd) and sediment concentration (Cs) can have a significant effect on delta formation. The only parameter that did not impact the formation of coastal deltas in any environment was median grain size (Dmm). However, our results show that Qav does interact critically with Dmm when considering all modeled environments. Dmm also interacts with Cs and Dgrd, suggesting that the role Dmm plays in delta formation is complex.

Delta formation, overall, is most sensitive to changes in Qav and Dgrd. Models are predominately insensitive to changes in Dmm and Ti. Therefore, we propose that fluvial discharge and waves are the primary constructive and destructive influences

acting on delta formation, respectively. Although tides impact mouth bar configuration and ultimately the morphology of a delta, tides alone do not critically impact the ability of a delta to form in most environments. However, interactions between tides and other morphodynamic influences do have a significant impact on delta formation. We show that tidal action can decrease the amount of fluvial discharge required to commence delta formation, indicating that tidal interactions with fluvial discharge and waves have a constructive effect on delta formation. The exact effect tides have on reducing erosion in highly wave influenced deltaic environments requires further research, especially when accounting for interactions with changes in Cs and Dgrd. Untangling these complex interactions may provide valuable insight into which factors control sediment deposition in the most destructive coastal environments. This information can not be undervalued considering that sea level rise and more frequent extreme weather events may intensify marine influences, tipping the current morphodynamic balance in deltas toward increased waves and tides (Nienhuis et al., 2020). Knowing that delta formation in wave environments is sensitive to changes in bathymetric gradient may help inform future coastal engineering efforts that impact the sea floor (i.e., sea floor excavation).

Our sensitivity analyses suggest that only considering the impact of fluvial and marine influences on delta formation may oversimplify these multifaceted systems. Fluvial, wave, and tidal environments are most sensitive to different parameter combinations and interactions, implying that the role these mechanisms play in facilitating sediment deposition changes based on the morphodynamics of the system. All models in this study are sensitive to changes in fluvial discharge, signaling that the creation of new deltaic land may be most sensitive to prolonged periods of drought and anthropogenic structures (i.e. dams and water diversions) that decrease water entering the delta (Day et al., 2016). Being able to anticipate how sediment deposition in coastal deltas may change will be increasingly important as future changes are expected to influence all aspects of the hydrologic cycle interacting with the rivers feeding deltas and the marine environments deltas form in.

Over the past 8.5 ky, deltas have experienced variability in fluvial and marine influence on a variety of temporal scales ranging from hours to decades. For instance, reductions in fluvial discharge during periods of drought can supress delta building, while seasonal monsoons and extreme weather events can result in flooding and large influxes of fluvial sediment to the delta. The models in this study only consider steady

boundary conditions that represent average fluvial and marine conditions over the recent past and do not account for extreme weather events, seasonality variability, or changes in the long-term averages over the Holocene. It does not appear that this variability is necessary to form deltas. It may be that variability in basin characteristics through time gives deltas their unique character and shape, but that the variability is not necessary for formation. It is also possible that the inclusion of seasonal variability would enhance delta formation in these models when fluvial discharge is low, considering the large grid size used in the modeling. Also, flooding events can account for a significant portion of a delta's yearly sediment budget (Syvitski et al., 2022). Incorporating temporal variations in fluvial and marine conditions would require high performance computing facilities and may only be useful when trying to model the evolution of a specific delta.

We show that models with a greater fluvial discharge and incoming sediment concentration are more likely to form a delta than models with a lower discharge, regardless of whether other waves and tides are present. Furthermore, deltas are more likely to form when fluvial discharge makes up over 50% of the morphodynamic influence. Previous global datasets found a link between sediment discharge and the likelihood of delta formation, but concluded that sediment concentration did not impact delta formation (Caldwell et al., 2019). This study shows that delta formation is sensitive to changes in sediment concentration (Cs), especially in fluvial and wave environments. When waves and tides are not present, delta formation only occurs when Qav > 1,000 $m^3/s$ and Cs > 0.5 $kg/m^3$. The Qav threshold increases to 1,850 $m^3/s$ when Cs decreases by one order of magnitude, to 0.05 $kg/m^3$. Deltas are formed in all models where the Qav > 2,000 $m^3/s$, Cs > 0.05 $kg/m^3$, and the fluvial influence comprises over 50% of the total morphodynamic influence (i.e., nMIf > 0.5). In all cases where the model did not form a delta, one of these conditions is not met. It should be noted that the fluvial discharge values discussed here are a product of the model set-up (the boundary conditions and the grid size) and should not be taken as exact values in which a delta will or will not form. It is more important to note how the likelihood of delta formation changes as discharge, marine influence, and basin conditions change. Hydraulic geometry relations indicate that the width of a river channel is proportional to the water discharge moving through the channel. Since the channel width is limited by the cell size in the model (a channel can not be smaller than one cell wide, 200 m), the smallest fluvial discharge needed to produce a delta is also limited. Sensitivity analysis showed

that models within this study do not produce a delta if the fluvial discharge is less than 500 $m^3/s$. Fourteen of the 51 deltas in this study have a mean annual discharge less than 500 $m^3/s$. The Squamish Delta has a mean annual discharge of 230 $m^3/s$ and has a river width that varies between approximately 175 m at the thinnest section to 400 m widest according to satellite imagery. Although the large cell size does not account for channel width variations less than 200 m, it is likely that the impact of the cell size on the ability of a delta to form in the modeling domain is minimal since most models have fluvial discharge greater than 1500 $m^3/s$. The increase in wave height, resulting in a higher proportion of the morphodynamic influences being wave generated, reduced the ability of a delta to form. This result is consistent with previous research (Wright, 1977), indicating that wave action results in a faster water velocity, ultimately inhibiting the deposition of sediment and formation of deltaic land. When high wave action is present, more fluvial discharge is required to produce a delta than in fluvial or tidal environments. Interestingly, changes in sediment concentration did not influence the discharge needed for delta formation to commence when wave action was present in the models, even though wave influenced environments are sensitive to changes in incoming sediment concentration and bathymetric gradient. Wave deltas were less likely to form when bathymetric gradient was high (Dgrd = 0.005 m/m), unless sediment concentration was also high. Caldwell et al. (2019) indicate that the interaction between Dgrd and Cs may be explained by accommodation space (i.e., a deeper basin would require more incoming sediment to fill the accommodation space and create a delta). The significance of this interaction in wave environments may be most pronounced where erosion is increased. Almost all wave models formed a delta when the bathymetric gradient was low, regardless of sediment concentration, except when tidal range was also high.

Previous research proposed that the ability of wave and tidal action to change fluvial constructive processes is largely unknown (Caldwell et al., 2019). However, it was hypothesized that waves, and possibly tides, suppress delta formation (Caldwell et al., 2019). Although it is well established that tidal action influences delta morphology (Galloway, 1975), the models in this study show that tides alone do not affect the ability of a delta to form, except in tidal environments. However, these environments are more susceptible to changes in fluvial discharge and wave influence. In the absence of waves, delta formation occurs at a lower fluvial discharge when tides are present compared to models absent of waves and tides. This suggests that tidal action increases the ability

for a delta to form in the absence of waves or when wave influence is small compared to the fluvial and tidal influence. One physical explanation is that tidal modulation of the water level allows for sediment deposition at higher elevations, which may reinforce island structures and create more resilient landforms.

When both wave and tidal action are high, sediment deposition begins when Qav = 500 $m^3$/s, which is the same discharge that tidal environments without wave action begin to form deltas. Delta formation in most environments (except tidal environments) is insensitive to tides along with the interaction between tides and waves. However, asymmetry in the sensitivity of delta formation to the interaction between waves and tides indicates that wave action has a more powerful effect on delta formation for certain values of tidal influence, specifically when tidal influence is low. At higher tidal ranges, wave action appears to have less of a destructive effect. The importance of these interactions for sediment deposition in destructive environments clearly merits additional research, especially considering predictions suggesting that many global deltas will experience a decrease in fluvial influence and sediment concentration while also undergoing increases in marine influence in the future (Nienhuis et al., 2020). Furthermore, since delta formation in wave environments is sensitive to sediment concentration and bathymetric gradient, there may be important three- or four-way interactions taking place that are not explored in this study.

Although the sensitivity analysis does not indicate a relation between parameters, there may be interactions between Dmm and Dgrd when considering steep mountainous terrain in basins such as the Copper Delta, Alaska. Caldwell and Edmonds (2014) indicate that a coarser sediment supply is more easily retained near the shoreline, and Caldwell et al. (2019) suggest that this mechanism may be responsible for increasing the likelihood of delta formation. In a delta with a steeper bathymetric gradient, a coarse median grade size may be required to accumulate enough sediment nearshore to form deltaic landforms. It is possible that Dmm was not sensitive in this study because the maximum grain size used was not coarse enough to influence the modeling outcome.

## 2.6. Conclusion

Data from 51 large coastal deltas around the world were used to inform numerical models simulating the formation of coastal deltas under various combinations of morphodynamic (fluvial discharge (Qav), wave height (Wa), tidal range (Ti)) and basin conditions (sediment concentration (Cs), bathymetric gradient (Dgrd), median grain size (Dmm)). Data for the 51 deltas show that deltas around the world exist across a wide range of morphodynamic and basin characteristics. The ability of a large delta to form across the entire range of wave height and tidal amplitude indicates that the presence of marine influences does not necessarily inhibit sediment deposition. The numerical models we created support this finding. Models that have high wave and tidal influence can form deltas in environments where there is adequate fluvial discharge suppling sediment. All models form deltas when the Qav > 2,000 $m^3/s$, Cs > 0.05 $kg/m^3$, and the fluvial discharge comprises over 50% of the morphodynamic influence. When one or more of these conditions are not met, there is a greater likelihood that a delta will not form. Differences in Cs and Dgrd were found to impact whether models with the same balance of morphodynamic influences either form a delta or do not. We suggest that although the classic Galloway ternary diagram is a useful tool to compare delta morphology, it does not explain why some combinations of fluvial, wave, and tidal influences result in delta formation while others do not.

## 2.7. Data availability

All data used in this study were previously published. See Appendix A for a complete description of the datasets used. Supplemental data in Appendix B provides a spreadsheet outlining the parameters used in each of the 229 models.

A version of this chapter has been submitted for publication. Upon publication of the journal article, example models and the source code for model processing will be available at https://github.com/aspenmanderson/delta_modeling. These resources are also available upon request.

# Chapter 3.

# Sensitivity of groundwater flux and subsurface permeability to morphodynamic and geomorphic characteristics of coastal deltas

## 3.1. Abstract

The amount of fresh water moving through over 2,000 coastal deltas worldwide is controlled by the complex subsurface structures within a delta. Morphodynamic influences produced by the feeding river, waves, and tides, in addition to transgressive and regressive sea levels, have resulted in deltaic aquifers that are highly heterogeneous and often discontinuous. We use 171 unique two-dimensional morphodynamic models to explore the range of subsurface permeability, hydraulic gradient, and groundwater flux within three end-member delta types (fluvial, wave, and tidal). We quantify the connectiveness of the subsurface permeability and estimate the horizontal heterogeneity and anisotropy that exists within deltaic permeability. We use a distance-based generalized sensitivity analysis to investigate the impact morphodynamic influences (fluvial, wave, and tidal), basin conditions (sediment concentration, bathymetric gradient), and geomorphic characteristics (number of channels, shape of the delta plain, delta from rugosity) have on the subsurface permeability, hydraulic gradient, and connectivity. We find that the median permeability in deltaic landforms is $4.0 \times 10^{-12}$ $m^2$ (relating to a hydraulic conductivity of $2.1 \times 10^{-5}$ m/s), the average hydraulic gradient is $3.9 \times 10^{-4}$, and the mean specific discharge is $1.3 \times 10^{-8}$ m/s. High permeability bodies are highly connected and are associated with the current and previous channelization. Subsurface permeability, hydraulic gradient, and the connectiveness of high permeability areas are sensitive to morphodynamic influences (fluvial, wave, tidal) and the geomorphic characteristics (number of channels, shoreline rugosity) within a delta. Since morphodynamic influences and geomorphic characteristics are easily identified by looking at the surface of the delta, we suggest that the deltaic subsurface can be characterized by identifying features on the delta surface.

## 3.2. Introduction

Coastal deltas form where rivers debouch into the ocean and deposit sediment eroded from headwater systems. Historically, humans have inhabited deltas because of their vast, complex ecosystem services that include fertile soil for productive agriculture, abundant nutrients sustaining aquaculture, safe harbours and landing points, and ample surface water provisions (Nicholls et al., 2018). Nearly all ecosystem services that make human life possible on deltas, in addition to those sustained through offshore submarine groundwater discharge, are directly affected by water flowing through the delta (Costanza et al., 1997; Kolker et al., 2013). While the amount of surface water entering a delta is directly dependent on the fluvial discharge of the feeding river, quantification of the fresh deltaic water in the shallow subsurface is complex and requires quantification of the groundwater flux.

Coastal groundwater systems are often categorized as either recharge-limited or topography-limited (Haitjema and Mitchell-Bruker, 2005). Because of the low-lying nature of deltas and the tendency for deltas to be located in humid regions, most deltaic groundwater systems are topography-limited (Gleeson et al., 2011), meaning that the volumetric flux of groundwater traveling through the subsurface of a delta is controlled by the topography, permeability, and the permeable area of the delta. Michael et al. (2013) showed that topography-limited systems are vulnerable to changes caused by sea level rise and suggested that subsurface permeability and coastal setting are important factors to consider. The spatial quantification of the subsurface permeability and groundwater flow through the delta has been thoroughly studied in a handful of deltas, including the Ganges-Brahmaputra (Michael and Voss, 2009; Khan et al., 2016; Michael and Khan, 2016), Mekong (Minderhoud et al., 2015; Van Pham et al., 2019), Red River (Tran et al., 2012; Larsen et al., 2017), Nile (van Engelen et al., 2019), Po (Mollema et al., 2013; Antonellini et al., 2015), and Rhine-Meuse (Post et al., 2003; de Louw et al., 2010; Oude Essink et al., 2010; Delsman et al., 2014). However, considering that there are likely over 2,000 coastal deltas estimated to exist around the world (Syvitski et al., 2022), more generalized research is needed to inform the expected permeability distribution in these systems and how thousands of years geomorphic evolution have shaped the subsurface.

Kolker et al. (2013) suggested that water in the Mississippi Delta flows from the surface water network through the deltaic subsurface as via paleochannels and other buried sand bodies that were identified with seismic imaging. This link between horizontal subsurface groundwater flow in deltas and the presence of permeable flow pathways through paleochannels was further confirmed using numerical morphodynamic and groundwater modeling (Hariharan et al., 2021; Xu et al., 2021). Steel et al. (2022) also used a physical delta model to characterize the connectivity of sand bodies within the delta and suggested that groundwater flow in a delta may be controlled by the lower permeability sediments rather than the connective sand bodies. The formation of channels within a delta, as well as the deposition of both high and low permeability sediments in a deltaic environment is largely controlled by the morphodynamic influences within the receiving deltaic basin.

It is well-documented that the morphology of a delta is dependent on three primary morphodynamic influences controlling the deposition of sediment: 1) the fluvial discharge of the sediment-bearing river, 2) waves, and 3) tides. Historically, the morphology of a delta has been described qualitatively, comparing characteristics of the delta plain and river network to distinguish end-member morphologies (Figure 3.1; Galloway, 1975). Fluvial deltas, like the Mississippi, are elongated and typically only have a few distributary channels. Wave deltas, like the Sao Francisco, have a smooth shoreline with one main channel cutting the delta plain. Tidal deltas, like the Mekong, have an abundance of sinuous tidal channels that are wider at the mouth and are separated by narrow inland structures. Other basin conditions, including regional bathymetry (Caldwell et al., 2019), the amount and particle size of sediment entering a delta (Syvitski et al., 2010; Caldwell and Edmonds, 2014; Rossi et al., 2016), and antecedent stratigraphy (Geleynse et al., 2011) explain geomorphic differences in deltas with similar proportions of each morphodynamic influence. Recently, geomorphic characteristics of deltas have been quantified, including the shape of the delta plain, elongation and skewness of the plain, the number of distributary channels, shoreline rugosity, channel sinuosity, and channel shape (Wright and Coleman, 1973; Syvitski and Saito, 2007; Caldwell and Edmonds, 2014). Research linking surface features in a delta, such as the river network, to the subsurface permeability have only considered fluvial deltaic environments (Kolker et al., 2013; Hariharan et al., 2021; Xu et al., 2021; Steel et al., 2022a).

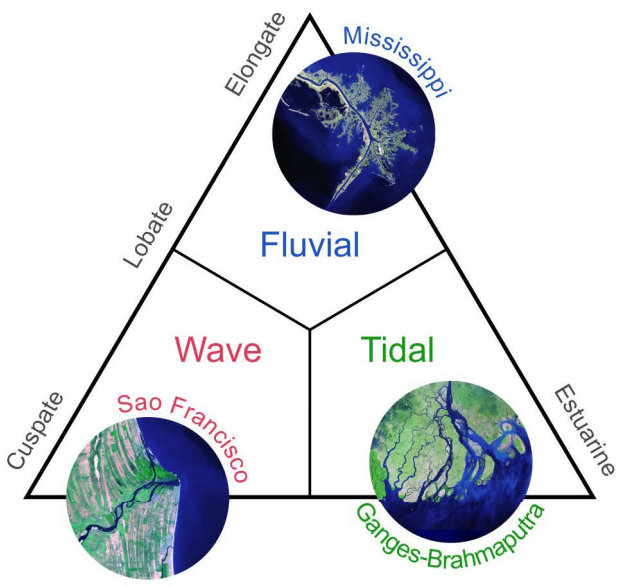


**Figure 3.1. Ternary diagram typically used to classify delta morphology (after Galloway, 1975).**

We explore how the morphodynamic influences, basin conditions, and geomorphic characteristics of a delta impact the groundwater flux (or specific discharge) through the delta. We use 171 unique two-dimensional models to characterize the geomorphic characteristics (number of channels, shape of the delta plain, delta from rugosity) and hydrogeologic conditions (permeability and hydraulic gradient) for the three end-member delta types: fluvial, wave, and tidal. We investigate the range of permeability and hydraulic gradient in each delta type to estimate the groundwater specific discharge through the deltas. We further look at delta permeability by investigating the horizontal heterogeneity and anisotropy as well as the connectivity of high permeability bodies. We use a distance-based generalized sensitivity analysis to investigate the sensitivity of permeability, hydraulic gradient, and connectivity of the high permeability bodies to changes in the morphodynamic influences, basin conditions, and geomorphic characteristics.

## 3.3. Methods

### 3.3.1. Numerical modeling

We use 171 unique models to simulate the formation of the top Holocene layer in modern coastal deltas (Chapter 2). The model domain is shown in Appendix C Figure

C1. Each model mimics a sediment carrying stream debouching into an ocean basin. Morphodynamic changes within the models include varying proportions of fluvial, wave, and tidal influences that are assigned at the stream and ocean boundaries. The models are categorized as a fluvial, wave, or tidal by the proportion of the morphodynamic influences present. In fluvial models, more than 50% of the influence is derived from the fluvial discharge (Qav) of the incoming stream (Chapter 2). In wave models, more than 40% of the influences are generated through wave action (Wa) at the northern basin boundary. In tidal models, more than 35% of the influences are generated through tidal modulation of the water level at the northern boundary (Ti). Of the 171 models, 59 are fluvial, 55 are wave, and 59 are tidal. The remaining 35 models have a combination of influences that does not allow for categorization in any of the end-member groups.

Basin conditions that vary within the models include the concentration of sediment entering the model through the stream boundary (Cs), the initial slope of the model representing regional bathymetric gradient (Dgrd), and the median grain size of sediment (Dmm) entering the model (Chapter 2). Sediment grain size entering the models ranges from $2x10^{-3}$ mm to 2 mm, representing six grain sizes between clay and coarse sand (Appendix C Table C1).

The morphodynamic modeling domain is 80 km x 100 km resulting in a 8,000 $km^2$ domain with grid cells that are 200 m x 200 m in size. Other delta modeling used studies using Delft3D have used a much smaller domain. The domain in Caldwell and Edmonds (2014) was 7500 m x 5625 m with grid cells of 25 m x 25 m while the domain in Broaddus et al. (2022) was 9 km x 21 km with grid cells 25 m x 25 m. Similarly, the set of models produced by Hariharan et al. (2021) and used by Xu et al. (2021) to investigate subsurface structure in a delta had a domain size of 20 km x 10 km with a grid size of 50 m x 50 m. Although the domain used in this modeling is significantly larger than what has been used in previous studies, we choose a larger domain to produce deltas on a similar scale to some of the world's largest deltas (Chapter 2). To accommodate the large domain size, a larger cell size is required to reduce computational time and produce reasonable runtimes. The increased cell size means that features smaller than 200 m are not distinguished within the model. This limits the spatial resolution of the geomorphic characteristics and hydrogeologic properties that are investigated. For instance, all river channels within the model are at least 200 m wide (one grid cell).

The morphodynamic models are 2D and use a depth-averaged approach to solving the flow and sediment transport equations (Deltares, 2012). We used depth-averaged flow to reduce model runtimes and because we are not expecting the horizontal flow field to have significant variation in the vertical direction (which can arise from wind forcing, bed stress, Coriolis force, and bed topography). Even though salinity is included in the model, analysis of initial modeling results showed that no saline water exists within the area of sediment deposition; this suggests that vertical variations in fluid density will not significantly impact the horizontal flow field within the morphodynamic models. Using a 2D depth-averaged approach has been used in several other delta modeling studies (Caldwell and Edmonds, 2014; Broaddus et al., 2022). Additionally, using depth-averaged morphodynamic models is applicable for deltaic environments with marine influences including waves and tides.

The vertical structure of sediment deposition is not recorded in the morphodynamic models. This means that any sediment contained within a cell is assumed to be “well-mixed”, producing vertically homogenous sediment deposits within the model. This limitation means that a vertical sediment structure can not be discerned. As such, this study is only concerned with horizontal heterogeneity that arises from sediment deposition within a delta. Since the cell size within the models is 200 m x 200 m, horizontal heterogeneity that varies within 200 m is neglected; this approach assumes that each grid cell is homogeneous and isotropic. Since deltas exhibit variability within a 200 m spatial scale, the large cell size is a limitation of this work. The effect of the model cell size on the model results is discussed in more detail in the Discussion section.

### 3.3.2. Calculation of geomorphic characteristics

#### *Shape of the delta plain*

Delta shape (Sh) is a metric describing the elongation of the delta into the receiving basin. The shape of a delta is found by first determining the extent of the delta plain contained within the shoreline. The shoreline is defined using the Open Angle Method with an open angle of 45 degrees (Shaw et al., 2008). The Open Angle Method allows for a definition of the shoreline across each river intersecting the shoreline by defining the angle that spans the view into open water; a small open-angle will define a

shoreline that closely follows that land-water interface while a large open-angle will produce a shoreline that is smoother (Shaw et al., 2008). Several open angles were tested; an angle of 45 degrees was chosen for this study because it can accommodate the widest river mouths produced in the models while still preventing over smoothing of the shoreline. Shape is calculated by dividing the maximum delta width (between the eastern and western boundaries) and dividing it by two times the maximum delta length (between the southern and northern boundaries) (Caldwell and Edmonds, 2014):

$$Sh = \frac{width}{2*length} \qquad (3.1)$$

Deltas with an elongated delta plain will have a smaller Sh, whereas deltas that stretch along the shoreline and do not protrude into the basin will have a larger Sh.

### *Rugosity of the shoreline*

Shoreline rugosity (Sr) is a sinuosity measurement calculated by dividing the length of the mapped shoreline by the length of a smoothed shoreline (Caldwell and Edmonds, 2014). The smoothed shoreline is calculated using a Gaussian filter on the mapped shoreline. A smoothing window of 30 pixels is used as it reduces the sinuosity of the mapped shoreline while still following the overall curve of the delta plain.

### *Channel network*

The channel network is mapped using Rivamap (Isikdogan et al., 2017), which identifies individual river segments using a multiscale singularity index to extract curvilinear structures from the elevation map of the delta. The number of channels (Cn) is calculated by identifying all the river segments that are longer than one-tenth the length of the delta plain. This minimum length ensures that single cells or small depressions in the elevation map are not identified as a river.

## 3.3.3. Hydrogeologic conditions

### *Hydraulic conductivity and permeability*

Hydraulic conductivity (K) of the sediment deposited in the delta is calculated using the Hazen method (Hazen, 1911) by first finding the K of each individual cell (200 m x 200 m) within the model domain,

$$K_{ij} = C{d_{10}}^2 \qquad (3.2)$$

where $K_{ij}$ is the hydraulic conductivity at a cell with index [i, j], C is a shape factor, and $d_{10}$ is the grain size at which ten percent of the sediment is finer than. A shape factor of 40 is used in this study, representing the bottom of the range for very fine, poorly sorted sand (Hazen, 1911). This value is selected because the range of sediment sizes that deposit in the delta model is between silt and medium sand. Using a C of 40 results in K values that are within the range expected within a coastal delta ($1x10^{-4}$ to $1x10^{-8}$ m/s). In each model cell, the $d_{10}$ is determined using a linear interpolation with 1000 values to calculate the cumulative density function representing the percent finer of the sediment deposited in that cell. Although other interpolation methods were considered (spline, cubic), a linear interpolation was deemed most relevant by visual inspection of the percent finer graphs. K is calculated using a geometric mean of $K_{ij}$ contained within the shoreline, providing a single value of hydraulic conductivity for the entire delta.

Permeability ($k_{ij}$) for each cell in the delta plain is computed as a function of $K_{ij}$, dynamic viscosity ($\mu$), density of the pore water ($\rho$), and gravitational constant (g):

$$k_{ij} = K_{ij} \frac{\mu}{\rho g} \qquad (3.3)$$

where $\mu = 1.8x10^{-3}$ kg/ms, $\rho = 1000$ kg/m$^3$, and g = 9.81 m/s$^2$ is used. The values for fluid density and viscosity assume fresh groundwater. Analysis of the salinity concentration in each model in the area of sediment deposition confirms this assumption. Permeability is calculated to provide an intrinsic property for the sediment alone, rather than K which depends on the fluid properties. The permeability k is calculated using a geometric mean of $k_{ij}$; this provides a single value of permeability for the entire delta and is used to compare the different delta types.

The percent of area within each delta that has high permeability, medium permeability, and low permeability is calculated. High permeability is defined as $k_{ij} > 2.7x10^{-10}$ m$^2$ ($K_{ij} > 5x10^{-5}$ m/s), medium permeability has $2.7x10^{-10} \geq k_{ij} > 1.1x10^{-11}$ m$^2$ ($5x10^{-5} \geq K_{ij} > 2x10^{-6}$ m/s), and low permeability has $10.9 \geq k_{ij} > 5.5x10^{-15}$ m$^2$ ($2x10^{-6} \geq K_{ij} > 1x10^{-9}$ m/s). These values correspond to the distinction between permeabilities expected in medium sand, fine sand, and silt environments (Domenico and Schwartz, 1990).

The heterogeneity of the permeability within each delta is further analysed using semivariograms. The semivariogram $\gamma(\mathrm{b})$ describes the averaged squared difference between $k_{ij}$ at two points separated by a lag distance (b). The Experimental (Semi-) Variogram program (Schwanghart, 2021) is used to compute the semivariogram for each delta permeability map using 10,000 randomly selected data pairs. The semivariograms are computed for angles 0, 30, 60, 90, 120, and 150 degrees, with the angle measured from the southern model boundary. The maximum b used is half the delta plain length, measured in the direction of interest. The sill of a semivariogram indicates the degree of heterogeneity while the range describes the scale of heterogeneity (Schwanghart, 2021). Differences between the semivariogram sill in each direction describe the degree of anisotropy. Although variogram based approaches are widely used to quantify heterogeneity and anisotropy, we do note they are often insufficient to capture the complexity of geologic structures with curvilinear features, such as the complex channel network seen in deltas (Scheidt et al., 2018). As such, the semivariograms produced herein are more categorical and only used to compare the three delta types rather than quantifying accurate values of heterogeneity and anisotropy.

### *Connectivity of high permeability bodies*

A high permeability body is defined as any cluster of model cells that have $\mathrm{k_{ij}}$ greater than the 75$^{th}$ percentile of the $k_{ij}$ within the model. The connectivity of the high permeability bodies (Co) is calculated by dividing the area of the largest high permeability body (Ahp) by the sum of the area of all high permeability bodies (Steel et al., 2022a):

$$Co = \frac{Ahp}{\sum Ahp} \qquad (3.4)$$

The 75$^{th}$ percentile is used to define Co because it aligns with qualitative analysis of the high permeability zones in each delta are. We tested this method using the 90$^{th}$ percentile but found that the results were skewed by grid cells with anomalously high permeability—only a few grid cells in the tidal and fluvial deltas met this criterion. Results from the 75$^{th}$ and 90$^{th}$ percentile were similar in the wave delta.

### *Hydraulic gradient*

The slope of the delta plain, referred to herein as the topographic gradient of the delta (dE/dl), is calculated as an average topographic gradient between the initial channel and the shoreline. Elevation at the initial channel (Ec) is calculated as an average of the elevation in the ten model pixels on both side of the channel. This removes any influence that the topographical depression in the channel would have on the slope. A gradient is calculated for every pixel (n) along the shoreline by subtracting the elevation at the shoreline ($\mathrm{Es_n}$) from Ec. An average slope is computed for each delta model by calculating the mean of the gradients:

$$\frac{dE}{dl} = \frac{1}{2}\sum_{i=1}^{n} \frac{Ec - Es_n}{2} \qquad (3.5)$$

The regional hydraulic gradient (dh/dl) is assumed to be equivalent to dE/dl. This is a reasonable assumption in a deltaic environment due to the gently sloping nature of the topography. Note, however, that local hydraulic gradients could be much greater in a real delta where groundwater pumping takes place. Furthermore, since we are only simulating the top Holocene sedimentation in modern deltas, we are interested in the shallow unconfined aquifer systems and not the deeper, confined, or semi-confined aquifer systems that exist as part of the transgressive and regressive nature of deltaic geologic history.

### *Specific discharge*

Specific discharge (or the groundwater flux; q) in each delta model is computed by multiplying K (the geometric mean of the delta) by dh/dl:

$$q = \mathrm{K}\left(\frac{dh}{dl}\right) \qquad (3.6)$$

Using the geometric mean of hydraulic conductivity provides one representative q value for the entire delta and does not consider the complexity and spatial variability of the hydraulic conductivity within each delta. Additionally, we are only considering the horizontal groundwater flux through the delta since K only varies horizontally and is vertically uniform. A value of q computed in this manner does not consider any recharge limitations that may exist and assumes that the system is topography-limited rather than recharge-limited. These simplifications mean that the computed values for q are likely

not comparable to q in real deltas and therefore are only used as a tool to understand how differences in the average K and dh/dl may impact groundwater flow within the shallow subsurface in the three delta types.

### 3.3.4. Analysis of sensitivity

We undertake three sensitivity analyses to determine how the morphodynamic influences, basin conditions, and geomorphic characteristics impact: 1) k, 2) dh/dl, and 3) Co. The sensitivity analyses are preformed using a Distance-Based Generalized Sensitivity Analysis (DGSA) (Fenwick et al., 2014; Scheidt et al., 2018). To compute the sensitivity of the response (k, dh/dl, Co) to changes in the input parameters (Qav, Wa, Ti, Cs, Dgrd, Dmm, Cn, Sh, Sr), models are sorted into a high and low class based on the response (Scheidt et al., 2018). The sensitivity of the response to changes in an input parameter is quantified based on the distance between the prior frequency distribution and the frequency distribution computed for each class (Scheidt et al., 2018). A hypothesis test with a 95% confidence level ($p < 0.05$) is used to test the null hypothesis that the input parameter has no influence on the response (Scheidt et al., 2018). An influential, or critical parameter, rejects the null hypothesis while a non-influential, or insensitive parameter, fails to reject the null hypothesis.

## 3.4. Results

### 3.4.1. Modeled delta morphology

Chapter 2 showed that the models used in this study can reproduce the geomorphologic characteristics expected in a fluvial, wave, and tidal influence delta (Figure 3.2A-C). The fluvial delta has an average of 11 channels, with only a few of these reaching from the delta apex to the shoreline (Figure 3.2A). The channels that do not connect to the delta apex are remnants of previous channelization that was deactivated, likely due to sediment backfilling or avulsion. The tidal delta exhibits the highest Cn, with an average of 13 channels, while the wave delta exhibits the least, having an average of two channels (Figure 3.2D). The distributary network in the tidal delta occurs throughout the delta plain, with many characteristic tidal channels that are wider at the shoreline and decrease in width inland (Figure 3.2C). In the wave delta, there is one main channel that cuts through the delta plain (Figure 3.2B). This main

channel bifurcates near the channel outlet where a subaqueous mouth bar has formed (Wright and Coleman, 1973). Note that some of the channels in the fluvial and tidal deltas exhibit a blocky shape where the channel changes direction at a 90-degree angle; this is likely a result of computational error. Each of the three delta types can have as few as only one channel (Figure 3.2D). For fluvial and tidal deltas, this happens more frequently in models that have a lower Qav, resulting in a smaller delta that experiences less avulsions and tidal reworking.

Delta models primarily influenced by fluvial influences have the smallest average Sh (1.4), indicating that the delta plain is elongated into the receiving basin (Figure 3.2E). Interestingly, the tidal deltas have the highest average Sh (2.3). Historically, wave deltas have been considered to have the highest Sh. However, due to the increased reworking of sediment from tides, many of the tidal deltas build sediment evenly across the southern boundary, resulting in a wider delta. In nature, many tidal deltas form in drowned valleys where the width of the delta is confined by the shape of the basin (Syvitski et al., 2022). This may explain why wave deltas are typically thought of as the widest deltas even if tidal reworking has the potential for lateral sediment transport. Additionally, the morphodynamic models only simulate waves that are perpendicular to the initial shoreline; this is often not the case in nature where wave incidence can be oblique to the river mouth, resulting in littoral drift that redirects sediment adjacent to the coastline (Wright, 1977). The average Sh for wave deltas is 1.9. Elongation of wave deltas into the receiving basin increases as Qav increases. The wave delta has the smoothest shoreline, with Sr = 1.1. Wave deltas also have the smallest range of values, $1.3 > Sr > 1.1$. The tidal delta has the most rugged shoreline, with Sr = 1.2, as well as the widest range of shoreline rugosity values, $1.6 > Sr > 1.1$. Some of the smaller values for Sr in the tidal deltas can be explained by models that have some wave influence, reducing the overall tidal reworking and creating a smoother shoreline.

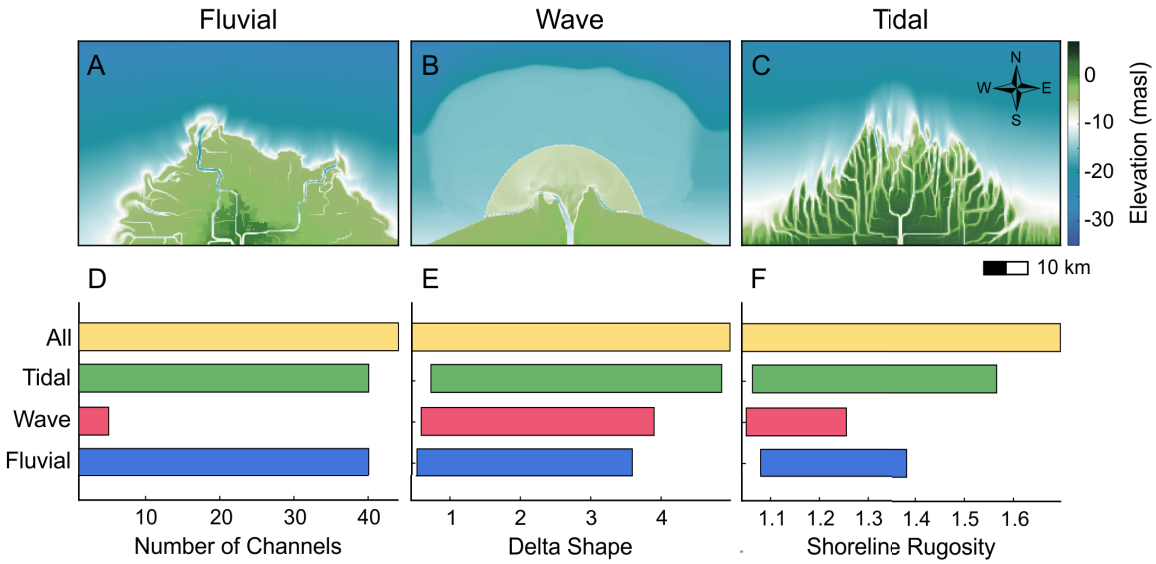


**Figure 3.2. Examples of a modeled A) fluvial, B) wave, and C) tidal delta. Range of D) the number of channels in the delta (Cn), E) the delta shape (Sh), and F) the shoreline rugosity (Sr) for the three delta types as well as all delta models.**

### 3.4.2. Permeability

The k within the delta models ranges from $3x10^{-14}$ $m^2$ to $9.4x10^{-11}$ $m^2$ (Figure 3.3A). The tidal deltas have the lowest k ($1.3x10^{-12}$ $m^2$), followed by the fluvial ($2.7x10^{-12}$ $m^2$) and the wave deltas ($1.0x10^{-11}$ $m^2$) (Figure 3.3A). The median k of the wave delta occurs near the top of the interquartile range, indicating that the distribution of k is negatively skewed. The percent of high, medium, and low permeability area in each delta type (Figure 3.3B, C, D, E) indicates that, on average, wave deltas are comprised of 68% high permeability, 29% medium permeability, and 3% low permeability sediment. The fluvial deltas have 41% high and 33% low permeability material, with only 26% medium permeability. The tidal deltas have mostly medium permeability, comprising 53% of the delta material. Low permeability material makes up 33% of the tidal deltas and 14% is high permeability.

The spatial permeability maps (Figure 3.3F, G, H) indicate that the higher permeability areas in the fluvial and tidal deltas occur in the middle of the delta and align with the distributary channel network. The higher permeability areas within the fluvial delta have $k \geq 2x10^{-11}$ $m^2$, with lower permeability material ($k < 5x10^{-13}$ $m^2$) along the shoreline. Most of the permeability within the tidal delta falls within $2x10^{-13}$ to $7x10^{-12}$ $m^2$.

The tidal delta has less low permeability material along the shoreline compared to the fluvial delta and has a few locations within the main channels where $k \geq 3x10^{-10}$ $m^2$. These higher permeability areas develop due to tidal influence of the river network. Modulation of the fluvial outflow results in lower water velocities and retention of course-grained material within the river network.

Less than 10% of the permeability in the wave delta is $< 1x10^{-12}$ $m^2$ (Figure 3.3G). The regions with the greatest permeability in the wave delta ($k \geq 2.3x10^{-11}$ $m^2$) occur along the sides of the main channel, where the delta has built levees. Within the levees, some linear high permeability structures appear; it is possible that these are swash bar features, indicative of wave influence. The part of the delta plain located adjacent to the levees is characterized by a smooth shoreline and medium permeability ($k < 2x10^{-11}$ $m^2$). This part of the delta plain exhibits minor variation in k because most of the sediment that deposits adjacent to the levees is fine sand. Smaller grain sizes are unable to deposit within the delta plain because increased wave action leads to higher water velocities, inhibiting the deposition of fine-grained material. However, the wave action in these models is not powerful enough to carry the coarse-grained sediment in bedload transport away from the river mouth.

Results from the semivariograms (Appendix C Figure C2) show that wave deltas have the greatest median sill in all directions (Appendix C Figure C3A), which implies that wave deltas have more variance in the horizontal permeability than fluvial and tidal deltas. This suggests that overall, wave deltas have higher horizontal heterogeneity than tidal and fluvial deltas. Heterogeneity is greatest across the width of the delta (between the eastern and western boundaries) compared to along the length of the delta (between the southern and northern boundaries) for all three delta types. The increased heterogeneity across the delta width is because channelization creates high permeability features that are primarily oriented from the delta apex to the shoreline (between the southern and northern boundaries). Because there are larger differences in the range between the length and the width in the fluvial and tidal deltas, these deltas have a higher degree of anisotropy (within the horizontal plane, not vertical) compared to the wave deltas.

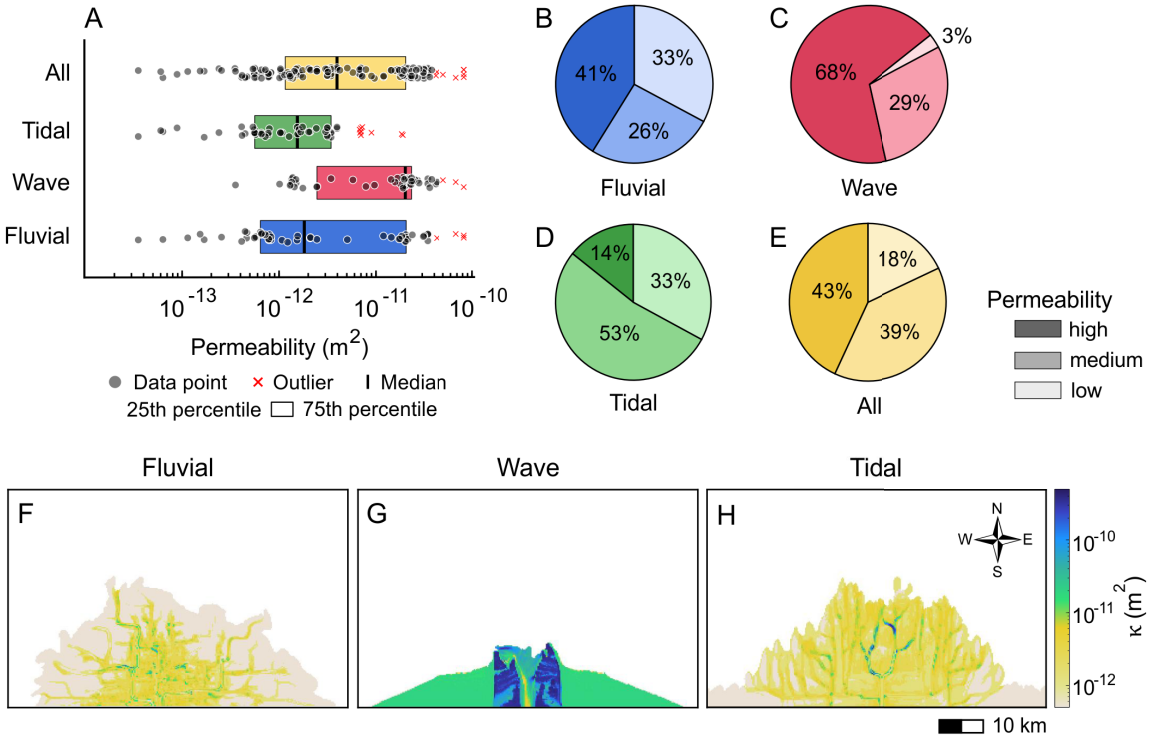


**Figure 3.3.** **A) The geometric mean of the permeability (k) across the entire delta (all model cells) and B-E) the portion of high, medium, and low permeability material in fluvial, wave, tidal, and all delta models. Spatial permeability map of a F) fluvial, G) wave, and H) tidal model.**

### 3.4.3. Connectivity of high permeable bodies

The maximum number of connective bodies in each of the delta type is 76 for fluvial deltas, 27 for wave deltas, and 62 for tidal deltas. The median connectivity (Co) in all the delta types is 0.99, indicating that most of the high permeability bodies are connected (Figure 3.4A). Wave deltas have the largest interquartile range for connectivity (Co = 0.75 to 1.0), implying that the connective bodies within wave deltas can be more discontinuous than in fluvial and tidal deltas. This results from the connective bodies that exist within the delta levees being separated by lower permeability material within the channel. In wave delta models that have large Qav, the high-water velocity in the channel is too great for fine-grained sediments to deposit, resulting in higher permeability within the channel and higher connectivity between the levees. When Qav is small compared to Wa, lower water velocities that result from the convergence of fluvial discharge and wave actions reduce the transport competence of the river and allow for finer sediments to settle within the channel, separating the high

permeability bodies. In general, the high permeability bodies within the wave delta are larger than those in the fluvial or tidal deltas and are contained within the channel levees rather than spread throughout the delta. The median size of a connective body in a wave delta is 74% of the total delta area, compared to 32% of the total delta area in both the fluvial and tidal deltas.

The percent of the channel network that contains a high permeability body is 45% in fluvial deltas, 35% in tidal, and 22% in wave (Figure 3.4C). The high permeability bodies within the fluvial delta correspond to the active distributary channels as well as in previously channelized areas, located in the middle of the delta plain (Figure 3.4D). The high permeability bodies in the wave delta are less contained within the channel network than in fluvial and tidal deltas because the high permeability bodies exist adjacent to the channel where levees are constructed (Figure 3.4E). Although most of the high permeability bodies in the tidal delta align with the tidal network, some of the tidal channels that exist outside of the active delta (channels that form near the southern boundary) do not contain high permeability material (Figure 3.4F).

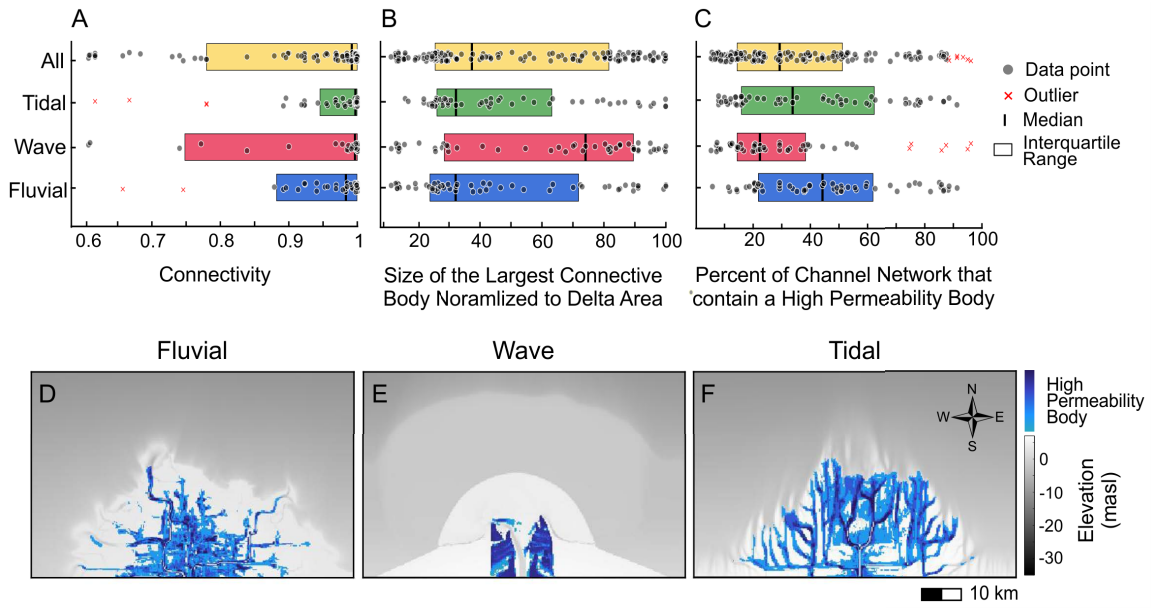


**Figure 3.4. A) The connectivity of high permeability bodies (Co), B) size of the largest permeable body normalized by delta area, and C) percent of the channel network that contains a high permeability body in fluvial, wave, tidal, and all delta models. Maps of the high permeability bodies for a D) fluvial, E) wave, and F) tidal model.**

### 3.4.4. Hydrogeologic properties

The median dh/dl in the delta models is $2.9 \times 10^{-4}$ m/m (Figure 3.5A). The dh/dl is largest in the tidal delta, with a median gradient of $1.4 \times 10^{-3}$ m/m. The increased dh/dl in the tidal delta results from an increase in accommodation space during flood tides, allowing sediment deposition at higher elevations. The median dh/dl in the fluvial and wave deltas are $2.9 \times 10^{-4}$ m/m and $1.4 \times 10^{-4}$ m/m, respectively.

Although there is variation in dh/dl between the different delta types, there is slight variation between the medians of q (Figure 3.5B). Wave deltas have the greatest median q ($1.4 \times 10^{-8}$ m/s), while tidal deltas have the lowest q ($7.2 \times 10^{-9}$ m/s). Although tidal deltas have the largest dh/dl, the lower K results in a smaller q compared to the wave and fluvial deltas. Similarly, although the wave delta has the smallest dh/dl, the increased K results in a larger q in the wave delta models.

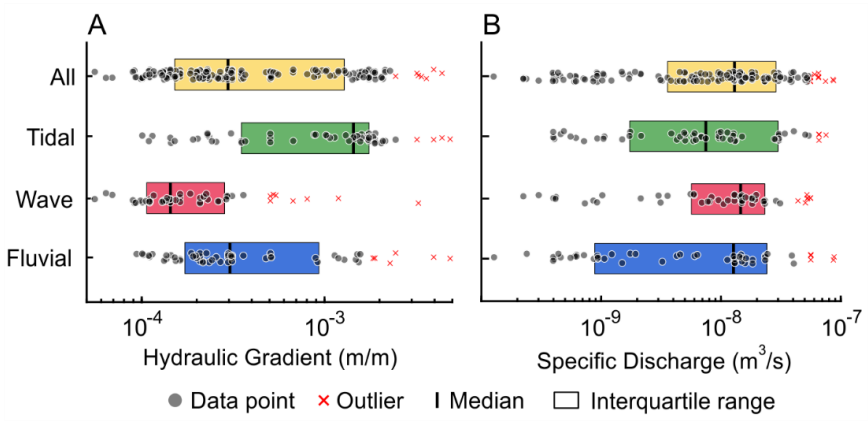


**Figure 3.5. The A) average hydraulic gradient (dh/dl) and B) specific discharge (q) in fluvial, wave, tidal, and all delta models.**

### 3.4.5. Sensitivity analysis

Permeability is most sensitive to changes in the Ti and Wa, as well as Cs and Cn (Figure 3.6A). The sensitivity of k to changes in Ti and Wa is explained by the ability of the delta to retain coarse-grained material within the delta. Deltas with high Wa prohibit the deposition of fine-grained material and retain coarse-grained material within the channel levees. In comparison, larger Ti results in more sediment of medium permeability that deposits around the channel network, which is extensive throughout the delta plain. The distinction between morphodynamic influences within wave and tidal

deltas is reflected in the number of channels within a delta, making k also sensitive to changes in Cn. The sensitivity of k to Cs indicates that the grain size that is deposited in the delta is dependent on the amount of sediment coming into the basin. However, k is insensitive to changes in Dmm.

The dh/dl within a delta is also sensitive to changes in the Ti, in addition to Cn and Sr (Figure 3.6B). Gradient is highly sensitive to Ti because tides can deposit sediment at higher elevations when the water level rises. Once again, an increased Cn is indicative of tidal influence, resulting in dh/dl being sensitive to Cn. The dh/dl is also sensitive to changes in Sr, which is better able to distinguish fluvial deltas from tidal deltas.

Co is most sensitive to changes in Qav, Wa, and Ti; it is not sensitive to any of the geomorphic characteristics (Figure 3.6C). The sensitivity of Co to Qav and Wa may be explained by the relative proportion of fluvial and wave power. When fluvial and wave power are similar, the convergence of fluvial discharge and wave action results in lower water velocity, allowing fine sediment to settle and create a barrier between the two high permeability levees. When either fluvial or wave power dominates within the channel, the water velocity remains high and prohibits the deposition of fine sediment within the channel.

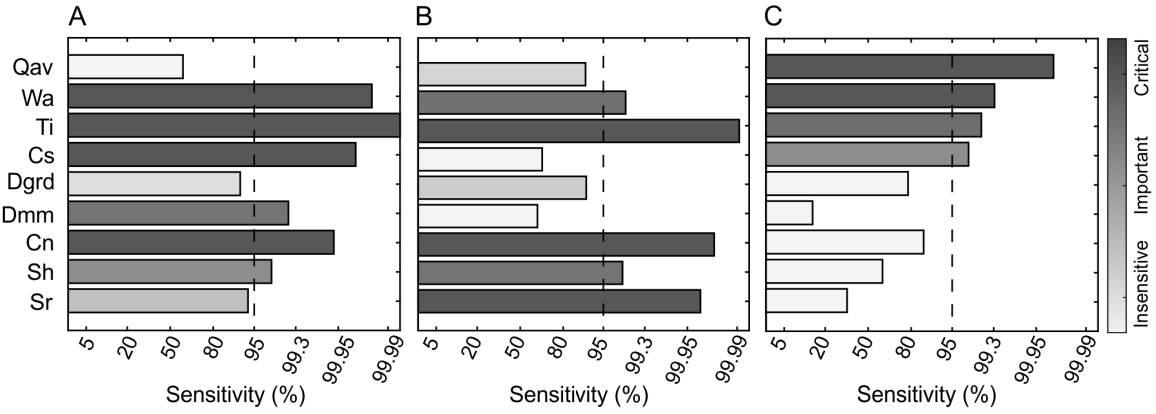


**Figure 3.6. Sensitivity of A) permeability (k), B) hydraulic gradient (dh/dl), and C) connectivity of high permeability bodies (Co) to changes in fluvial discharge (Qav), wave height (Wa), tidal amplitude (Ti), incoming sediment concentration (Cs), bathymetric gradient (Dgrd), incoming median grain size (Dmm), the number of distributary channels (Cn), delta shape (Sh), and shoreline rugosity (Sr).**

## 3.5. Discussion

Most of the previous groundwater modeling studies focusing on coastal deltas have used 1D or 2D models that evaluate vertical groundwater flow through a column or along a longitudinal cross section of the delta (Bridger and Allen, 2006; Delsman et al., 2014; Larsen et al., 2017; Van Pham et al., 2019). The lack of lateral heterogeneity and anisotropy within deltas results in a limited understanding of how permeability structures vary across the delta plain and how this influence horizontal groundwater flow through a delta. We focus on quantifying and characterizing the horizontal spatial variability in the deltaic subsurface that arises because of varying morphodynamic influences. Our findings that deltaic permeability and hydraulic gradient are sensitive to changes in morphodynamic influences, as well as variations in the channel network and shoreline rugosity, are promising because they suggest that some knowledge of the subsurface properties of a delta can be inferred by simply identifying if the delta is fluvial, wave, or tidal. The quantification of permeability, hydraulic gradient, connectivity of permeable bodies, and the location of high permeability bodies for three end-member delta types provides a general understanding of what the hydrogeologic system in a delta might look like spatially without having to conduct costly field campaigns. Our results also support previous work that has linked permeable bodies and preferential pathways to current and previous channelization (Kolker et al., 2013; Xu et al., 2021; Steel et al., 2022a).

The permeability maps generated herein are limited by the cell size within the modeling domain, the steady-state boundary conditions, and homogeneity in the vertical direction. To reduced runtimes of the morphodynamic models, a cell size of 200 m x 200 m is used; this approach assumes that each grid cell is homogeneous and isotropic, neglecting horizontal heterogeneity that varies within 200 m. Since deltas exhibit variability within a 200 m spatial scale, the large cell size is a limitation of this work. Overbank deposits and high permeability features caused by small channels (less than 200 m wide) are two features that are not reflected in the permeability maps due to the model set-up. Of these two features, overbank deposits are more likely to have an impact on groundwater flow through a delta since these deposits typically have low permeability and may act as a barrier to horizontal groundwater exchange between the permeable channels/paleochannels and the surrounding sediment. Using a smaller cell size may allow for overbank deposits to be more distinguishable within the permeability

maps by adding more low permeability material around the channel networks. The formation of overbank deposits requires flooding that is often associated with extreme weather events or seasonal high flows; the steady state boundary conditions used means that this variability required to form overbank deposits was not accounted for. Although overbank deposits are features in many deltas, Michael and Voss (2009) noted the absence of overbank deposits in the Bengal Basin and attributed this to the mobile nature of the channels in the tidal environment. The results of this study would benefit from the inclusion of seasonal variability within the boundary conditions and from a smaller spatial resolution that can account for variability at smaller spatial scales.

The vertical structure of sediment deposition is not recorded in these models. This means that any sediment contained within a cell is assumed to be “well-mixed”, producing vertically homogenous sediment deposits within the model. This limitation means that a vertical sediment structure can not be discerned. Channel stacking patterns are important when considering vertical connectivity of fluvial sediment deposition within deltas around the world (Steel et al., 2022b; Xu et al., 2022). Further, the ability for channels to erode through marine confining layers and create vertical discontinuities is critical to account when evaluating regional-scale subsurface structure in a delta (Van Pham et al., 2019). Improvements to this work may include the use of 3D modeling or implementation of the stratigraphy module in Delft3D (Deltares, 2013), allowing for the preservation of sedimentation records vertically throughout the model simulation.

### 3.5.1. Permeability and morphodynamics

We estimate that overall permeability in deltaic landforms has a median value of $4.0x10^{-12}$ $m^2$, relating to a hydraulic conductivity value of $2.14x10^{-5}$ m/s. Across all delta models, 42% of permeabilities represent medium sand ($k > 2.7x10^{-10}$ $m^2$, $K > 5x10^{-5}$ m/s), 40% fine sand ($2.7x10^{-10} \geq k > 1.1x10^{-11}$ $m^2$0, $5x10^{-5} \geq K > 2x10^{-6}$ m/s), and 18% silt ($1.1x10^{-11} \geq k > 5.5x10^{-15}$ $m^2$, $2x10^{-5} \geq K > 1x10^{-9}$ m/s). These values are consistent with the permeability values that deltaic groundwater flow and solute transport modeling studies have used (Table 1). The percent of sand and fine sediment in the Mississippi Delta reported by (Williamson et al., 1990) closely resembles the proportion of high, medium, and low conductivity area for fluvial deltas herein (Table 3.1, Row 1). Most deltas that have in-depth groundwater studies are tidal (Table 3.1), which may reflect an

overall lower permeability, considering our finding that tidal deltas have the lowest average permeability and the greatest proportion of medium and low permeability compared to the overall delta size.

Many groundwater modeling studies report the existence of clays and peat layers (Michael and Voss, 2009; Minderhoud et al., 2015; Larsen et al., 2017; van Engelen et al., 2019; Van Pham et al., 2019). However, lower permeabilities that would be representative of clays ($k < 5.5x10^{-15}$ $m^2$, $K < 1x10^{-9}$ m/s) were not present in any of our delta models. Analysis of sediment profiles within the delta (Supplemental Information Figure C4) indicates that clays and some silts do not deposit within the delta plain due to increased water velocity. Clays and silts are found in the subsurface of deltas around in the world due to deposition of fine-grained sediment during marine transgression and seasonal inundation. Clay and silt units deposited during periods of sea level rise often make up the aquitard structures in coastal deltas and can be barriers to vertical groundwater flow. The results of this study would benefit from including temporal variation in the boundary conditions and simulating seasonal flooding events that lead to deposition of more fine-grained material within the delta. Additionally, simulating the impact of sea level change and including the vertical variability in the sediment deposits would likely increase the preservation of fine-grained sediments within the subsurface and would allow for analysis of subsurface permeability vertically.

Permeability representative of coarse-grained sands ($k > 1.1x10^{-9}$ $m^2$, $K > 6x10^{-3}$ m/s) are also not present in the delta modeling even though grain sizes up to 2 mm are included in the incoming sediment within the models. Analysis of the sediment distributions indicate that the coarsest-grained material does deposit within the river channels in the tidal and fluvial deltas, and in the levees in the wave deltas (Figure B4). However, the proportion of finer-grained sands that also deposit within these model cells is greater, resulting in a hydraulic conductivity that is more representative of the fine-grained sand material.

**Table 3.1. Horizontal hydraulic conductivity values used in deltaic groundwater modeling studies. Note that the delta type reflects the dominant morphodyanmic influence controlling the geomorphic characteristics in the delta (Nienhuis et al., 2020). **Values from the Holocene layer only.**

| Delta | Delta Type | Horizontal Hydraulic Conductivity (m/s) | Study |
|---|---|---|---|
| **Mississippi** | Fluvial | 56% sand, 42% fines: $3.7 \times 10^{-4}$ m/s ** | Williamson et al., 1990 |
| **Nile** | Fluvial | Holocene fluvial clay: $2.3 \times 10^{-6}$ m/s<br>Quaternary sand: $8.7 \times 10^{-4}$ m/s<br>Quaternary marine clay: $1.2 \times 10^{-9}$ m/d<br>Quaternary clayey sands: $8.7 \times 10^{-4}$ m/s | Van Engelen et al., 2019 |
| **Po** | Wave | Sand: $5.0 \times 10^{-6}$ m/s<br>Silt: $1.0 \times 10^{-6}$ m/s<br>Clay: $5.0 \times 10^{-8}$ m/s | Antonellini et al., 2008 |
| **Ganges-Brahmaputra** | Tidal | Gravel: $6.0 \times 10^{-3}$ m/s<br>Coarse sand: $1.1 \times 10^{-3}$ m/s<br>Medium sand: $5.8 \times 10^{-4}$ m/s<br>Fine sand: $3.0 \times 10^{-4}$ m/s<br>Silt: $4.6 \times 10^{-6}$ m/s<br>Sandy Clay: $1.0 \times 10^{-6}$ m/s<br>Clay: $7.0 \times 10^{-10}$ m/s | Michael and Voss, 2009 |
| **Fraser** | Tidal | Fine to medium sand: 2 $4 \times 10^{-4}$ m/s<br>Silt: 3 $1 \times 10^{-10}$ m/s | Bridger and Allen, 2006 |
| **Red River** | Tidal | Sand: $5.7 \times 10^{-5}$<br>Gravel-Sand: $3.4 \times 10^{-4}$ m/s<br>Clay: $1 \times 10^{-6}$ – $1 \times 10^{-11}$ | Larsen et al., 2017 |
| **Mekong** | Tidal | Fine sand: $8.0 \times 10^{-5}$ m/s **<br>Sandy clay, peat: $4.0 \times 10^{-7}$ m/s **<br>Fine sand: $2.0 \times 10^{-4}$ m/s **<br>Sandy clay, peat: $1.0 \times 10^{-8}$ m/s ** | Minderhoud et al., 2015<br><br>Van Pham et al., 2019 |

The permeability averages reported in this study are not sensitive to changes in the median incoming sediment grain size within the model, suggesting that deltaic permeability is not controlled by the grain-size of sediment being delivered to the delta. This is especially true in wave deltas where wave action increases the water velocity and inhibits the deposition of fine-grained sediments within the delta plain and carries the small particle sizes offshore. Much of the fine-grained sediments found in real deltas around the world is a product of sea level variation that changes a near-shore environment into an offshore environment. Here we only consider the sediment deposition that occurs within the deltaic basin during delta formation (when sea level regression slows). Therefore, permeability within the delta is dictated by the presence of

the morphodynamic influences. This likely results from the natural sorting abilities of the morphodynamic influences within the delta; high water velocities arising from increased fluvial discharge, waves, and tides prohibit the deposition of small grain sizes. However, these influences promote bedload transport of the larger grain-size material. The places that experience lower water velocities, specifically outside the influence of the fluvial discharge and in the absence of waves and tides, allows for more deposition of fine-grained sediments, that then results in lower permeability. The resulting permeability distributions appear differently in each delta type based on which influences are present within the model and the strength of those influences throughout the receiving basin.

Semivariograms produced herein are used to understand differences within heterogeneity and anisotropy within fluvial, wave, and tidal deltas. Although variogram based approaches are widely used to quantify heterogeneity and anisotropy, they are often insufficient to capture curvilinear features (Scheidt et al., 2018), like the channel network within a delta. As such, we use the semivariograms categorically and only as a tool to compare the three delta types rather than quantify accurate values of heterogeneity and anisotropy. Results from the semivariograms suggest that overall, wave deltas have higher horizontal heterogeneity than tidal and fluvial deltas. This is likely because there is a larger difference in permeability between the delta plain and the channel levees in the wave delta compared to the permeability difference between the delta plain and channel network in the fluvial and tidal deltas. It is possible that this increased heterogeneity stems from the increased water velocity in a wave delta that prohibits fine-grained sediment from depositing within the levees. All three delta types are more heterogeneous across the width of the delta (between the eastern and western boundaries) compared to along the length of the delta (between the southern and northern boundaries). Because there are larger differences in the permeability maps between the length and the width in the fluvial and tidal deltas, these deltas have a higher degree of anisotropy (within the horizontal plane) compared to the wave deltas.

### 3.5.2. Groundwater flow

We found that despite the variation in the average permeability in the three delta types, specific discharge remains relatively similar across the deltas due to variations in the hydraulic gradient. The increased permeability in the wave deltas is offset by a smaller hydraulic gradient due to low topographic relief. On the other hand, the

increased hydraulic gradient in the tidal deltas stemming from a larger topographic relief is counteracted by overall lower permeability. Although variations in the specific discharge of the three deltas types is small, delta type is important when considering barriers to groundwater flow. Steel et al. (2022) state that the low permeability material may be more of a barrier to groundwater flow through the delta than the permeable pathways; this conclusion was made by physically modeling the formation of a delta within a basin that is void of waves and tides. The permeability maps in this study confirm that fluvial deltas have an accumulation of low permeability material along the shoreline that blocks some of the permeable pathways from extending from the delta apex to the shoreline. This may also be relevant for wave and tidal deltas that have an accumulation of fine-grained sediment adjacent to the delta plain or offshore in the subaqueous delta.

Our models show a close link between the high permeability bodies within a delta and the location of the channel network, which is consistent with other generic delta modeling studies that have estimated permeability or hydraulic conductivity changes laterally (Hariharan et al., 2021; Xu et al., 2021; Steel et al., 2022a). The high permeability material within fluvial and tidal deltas is associated with current and paleochannelization, and is primarily located within the channels. Furthermore, the high permeability bodies are highly connective and extensive throughout the delta. The high connectivity of permeable bodies horizontally was also found by Xu et al. (2021) and Steel et al. (2022) with the numerical and physical modeling of a fluvial delta. Modeling the formation of delta using numerical morphodynamic models can preserve the high permeability features that are created due to previous channelization which is not visually apparent on the delta surface due to avulsions. This is particularly important when considering permeability structures in fluvial deltas, as more of the high permeability corresponds to channels that have been backfilled.

The high permeability features in the wave delta are not directly located within the channels but rather are present in the delta levees. Many wave delta models exhibit lower permeability within the channel network; this may be explained by lower water velocities resulting from the convergence of fluvial discharge and wave actions within the channel when fluvial and wave power are similar. When either fluvial or wave influence dominates within the channel, the water velocity remains high and prohibits the deposition of fine sediment within the channel, resulting in one large connective body.

The blob-like high permeability bodies located within the channel levees in the wave-delta are less likely to be connected compared to the high permeability bodies that follow the channel network in the fluvial and tidal deltas. Although many real-world deltas do not have detailed spatially varying permeability maps, similarities can be drawn between the modeled deltas and known characteristics of real world. High permeability swash bar features are known to form in wave deltas and are apparent in the Sao Francisco and Senegal deltas (Wright, 1977) and may explain the high permeability linear features contained within the delta levees.

The balance of the morphodynamic influences shaping deltas has been subject to change in the recent past and will continue to change in the future. The effects of this are already evident, with river damning restricting the amount of discharge and sediment entering deltas globally (Giosan et al., 2014; Nienhuis et al., 2020). As sea level rises, it is also likely that wave and tidal action will increase, shifting the balance toward marine dominance in many global deltas (Nienhuis et al., 2020). Increased extreme weather events combined with rising sea levels not only threatens to inundate deltaic lands but will likely result in the deposition of more fine-grained surface material intermixed with highly erosive episodes. The shallower elevation and hydraulic gradient in wave deltas make these landforms more susceptible to inundation as well as groundwater salinization through marine encroachment. Additionally, the high connectivity of the deltaic subsurface may allow for faster salinization of the subsurface through permeable pathways.

## 3.6. Conclusion

Quantitative evaluation of groundwater supply in coastal deltas requires the estimation of large-scale hydrogeologic characteristics that control groundwater flow. This study evaluated the horizonal permeability in fluvial, wave, and tidal deltas. The sensitivity analysis suggests that permeability, hydraulic gradient, and the connectiveness of high permeable bodies can be characterized through the identification of morphodynamic influences (fluvial, wave, tidal) and geomorphic characteristics (number of channels, shoreline rugosity) withing a delta. Using numerical morphodynamic modeling of delta formation in 171 unique models, we found that:

1. The overall permeability in deltaic landforms has a median value of $4.0 \times 10^{-12}$ $m^2$, relating to a hydraulic conductivity value of $2.14 \times 10^{-5}$ m/s. The average hydraulic gradient is $3.9 \times 10^{-4}$. Wave deltas are the most permeable but have the smallest hydraulic gradient while tidal are the least permeable and have the highest hydraulic gradient.

2. The high permeability bodies are associated with current and previous channelization in a delta and are highly connected horizontally in the shallow subsurface. This high connectivity potentially allows for salinization through permeable pathways as sea level rises. The channel network is most evenly distributed in tidal deltas, resulting in high permeability bodies located throughout the entire delta plain. High permeability bodies in wave deltas are only located in the channel levees and are not pervasive throughout the entire delta.

3. Wave deltas may be most susceptible to inundation and groundwater salinization through marine encroachment due to the smaller hydraulic gradient and increased permeability.

## 3.7. Data availability

Supplemental data in Appendix D provides a spreadsheet outlining parameters for the 229 models created in Chapter 2 along with the geomorphic and hydrogeologic parameters calculated for each delta model in Chapter 3.

A version of this chapter has been submitted for publication. Upon publication of the journal article, example models and the source code for model processing will be available at https://github.com/aspenmanderson/delta_permeability. These resources are also available upon request.

# Chapter 4.

# The impact of delta morphology on groundwater freshening and salinization in large coastal deltas

## 4.1. Abstract

Large population centers built upon coastal deltas often rely upon groundwater to meet freshwater demands; groundwater pumping of deltaic aquifers can degrade groundwater quality and may further intensify land subsidence that threatens to sink coastal deltas. We explore how interactions between delta morphology, climate, and population impacts the vulnerability of coastal deltas to groundwater salinization. Numerical groundwater flow and solute transport modeling is used to determine the percent of groundwater volume impacted by salinity in three end-member delta types: fluvial, wave, and tidal. We investigate the effect of recharge on groundwater salinity using recharge representative of an arid (dry) climate and recharge representative of a tropical (wet) climate. We reduce the recharge within the model during the last 500 years of the simulation to determine how groundwater pumping and climate change impacts fresh groundwater resources. We classify 55 deltas around the world by their dominant morphodyanmic influence and recharge entering the delta; this allows us to pair each real delta to one of the generic numerical models. We use the numerical modeling results to determine which types of deltas are most vulnerable to groundwater salinization in the future and how this may impact fresh groundwater availability in coastal deltas around the world. We estimate that the volume of saline water in the shallow subsurface within deltas around the world varies between 36% and 89% of the total groundwater volume, depending on the delta type and the amount of recharge the delta receives. The number and location of channels in a delta plays an important role in determining the fresh groundwater volume. The freshwater lens is often deepest surrounding the river networks or in high permeability channel levees. We find that although deltas located in a wet climates have greater freshwater volume in the shallow subsurface, these deltas are most impacted by groundwater abstraction, simulated by a reduction in recharge. Wave deltas are particularly susceptible to groundwater salinity in the shallow subsurface and have the highest salinization rates under pumping

conditions. Wave deltas are most sensitive because of the increased hydraulic conductivity within the delta, low hydraulic gradient, and fewer river channels.

## 4.2. Introduction

Over 330 million people around the world live on a coastal delta (Ericson et al., 2006; Edmonds et al., 2020), with four out of eight of the world's largest mega cities being built upon coastal deltas. Coastal population centers often rely upon groundwater to meet domestic, agricultural, and industrial water demands because fresh groundwater is typically more abundant and of higher quality than surface waters (Post and Abarca, 2010; van Weert and van der Gun, 2012; Custodio and Bruggeman, 2013). Deltas are also some of the largest providers of submarine groundwater discharge, providing necessary freshwater and nutrients to estuaries and offshore environments (Zhou et al., 2019). Anthropogenic activities associated with urbanization and climate change in coastal deltas (i.e. excessive groundwater abstraction, coastal engineering, and urban loading) have stressed fresh groundwater resources in regions already vulnerable to water quality degradation from seawater intrusion and interactions with saline paleowater, as seen in polders located in the Netherlands and Bangladesh (Oude Essink, 1996; Custodio, 2002; Vandenbohede et al., 2008; Wada et al., 2010; Custodio and Bruggeman, 2013). Coastal aquifers co-located with large population centers are more vulnerable to groundwater abstraction than sea level rise, suggesting that efforts to adapt to sea level rise at the expense of better water management are misguided (Ferguson and Gleeson, 2012; Mabrouk et al., 2018).

To meet current and future freshwater demands in coastal deltas, it is critical to quantify the fresh groundwater resources that exist in the subsurface (Barlow and Reichard, 2010). Subsurface salinization is the biggest limitation to freshwater resources in coastal areas, making it imperative to understand how much salinity exists, how it is distributed, and how it might be impacted by anthropogenic activities. The present subsurface fresh-salt water distribution is a product of geomorphic evolution over thousands of years (Stanley and Warne, 1994). Vertical groundwater flow in deltas is complex, as transgressive and regressive sea level regimes have resulted in the formation of aquifer/aquitard structures that are highly heterogeneous and often discontinuous across the delta plain (Michael and Khan, 2016; Larsen et al., 2017). The resulting semi-confined leaky aquifers experience both groundwater freshening and

salinization over geologic timescales as sea level varies, resulting in complex mixing patterns between paleowater and fresh recharge (Post and Abarca, 2010; Delsman et al., 2016; Kim et al., 2017; Larsen et al., 2017; Van Pham et al., 2019). Several studies suggest that freshening of deeper salinity primarily occurs through vertical groundwater flow and is dictated by the supply of freshwater to the ground surface, and subsequent freshwater available within shallow, unconfined aquifer systems (Delsman et al., 2014; Van Pham et al., 2019; van Engelen, 2020).

The formation of deltaic land and shallow coastal groundwater system have closely linked feedbacks—changes that occur on the land surface affect groundwater flow and solute transport. The formation of Holocene aquifers through the subsurface is shown to be directly influenced by delta morphodynamics that control sediment deposition within the delta (Chapter 3; Kolker et al., 2013; Hariharan et al., 2021; Xu et al., 2021, 2022; Steel et al., 2022). The relative strength of fluvial, wave, and tidal morphodynamic influences controls the geomorphic characteristics of a delta, including the shape of the delta plain and the number of channels; historically, these characteristics are used to categorized deltas into one of the three end-member archetypes: fluvial, wave, and tidal influenced deltas (Galloway, 1975). Although wave deltas have increased subsurface permeability compared to tidal and fluvial deltas, the absence of strong wave action results in increased channelization and connectivity of high permeability bodies in fluvial and tidal deltas (Chapter 3). These differences in channelization and subsurface permeability making it crucial to account for delta morphology when considering groundwater flow through the delta plain.

Globally, coastlines average one delta for every 300 km of shoreline (Caldwell and Edmonds 2014). Of the thousands of deltas that exist worldwide, a detailed understanding of the groundwater system is only available in a handful of locations. Consequently, generic modeling has been increasingly used to understand the link between delta morphology and groundwater flow. Several recent studies have shown that channelization impacts the subsurface structure of a delta by creating permeable pathways for solute transport (Kolker et al., 2013; Xu et al., 2021, 2022; Steel et al., 2022). Although generic modeling of coastal systems allows a deeper understanding of the interactions between surface and groundwater, the influence of waves and tides has not yet been considered in coupled morphodynamic-groundwater models. Additionally, many groundwater modeling case studies have only focused on tidal deltas, including

the Rhine-Meuse (Oude Essink et al., 2010; Delsman et al., 2016), Ganges-Brahmaputra (Michael and Voss, 2009; Khan et al., 2016), Mekong (Minderhoud et al., 2017, 2020; Van Pham et al., 2019), Fraser (Bridger and Allen, 2006), and Red River (Larsen et al., 2017). Because of the diversity in the climate and the unique anthropogenic influences within each delta, it is difficult to decern how morphology impacts groundwater freshening and salinization in coastal deltas.

We determine the susceptibility of shallow deltaic aquifers to groundwater salinity and the vulnerability of large coastal deltas around the world to future groundwater salinization using numerical modeling along with previously published information on morphodynamics, climate, population, and groundwater salinity within deltas. We use the numerical modeling code iMOD-WQ to model the formation of coastal groundwater throughout the Holocene and determine the percent of groundwater impacted by salinity in three end-member delta types: fluvial, wave, and tidal. We account for variations in climate by estimating the distributed recharge for each delta type under dry and wet climate conditions using the United States Environmental Protection Agency's (EPA) Hydrologic Evaluation of Landfill Preformation (HELP) model forced by a stochastically generated weather series (United States Environmental Protection Agency, 1984). We simulate pumping during the last 500 years of the simulation by reducing the recharge within the model to determine how fresh groundwater resources may be impacted by salinization. The numerical modeling results are used to understand the vulnerability of 55 of the largest and most populated deltas to loss of fresh groundwater through induced lateral salinization.

## 4.3. Methods

### 4.3.1. Numerical modeling

The conceptual model used in this study proposes that groundwater freshening in the shallow subsurface occurred during modern delta building throughout the Holocene. This assumes that as sea level rise stagnated 8 thousand years ago (kya), and that sediment deposition occurred along the shoreline where a sediment-bearing river debouched into the ocean (Stanley and Warne, 1994). Additionally, it is assumed that freshwater lenses began to form in the permeable material as freshwater entered the subsurface and the saline water was flushed from the delta subsurface. The primary

salinity flushing mechanisms we consider are: 1) fresh surface water delivered to the delta through the river network and 2) diffuse recharge from precipitation.

We investigate the role that delta morphology plays in groundwater freshening and salinization throughout the Holocene using generic deltaic landforms representative of three end-member delta types: 1) fluvial, 2) wave, and 3) tidal. The generic deltaic landforms for each delta type investigated were created through morphodynamic modeling (Chapter 2, Deltares, 2013) (Figure 4.1A, B, C). The morphodynamic modeling domain is 80 km x 100 km resulting in an 8,000 $km^2$ domain, with grid cells that are 200 m x 200 m in size; this domain was chosen to produce deltas on a similar scale to the world's largest deltas (Chapter 2). The impact of the cell size on the modeling results is discussed further in section 4.5.3.

The morphodynamic balance of fluvial, wave, and tidal influence was varied by changing the fluvial discharge, wave height, and tidal amplitude within each model. The representative fluvial delta has 100% fluvial influence, the wave delta has 50% fluvial and 50% wave influence, and the tidal delta has 50% fluvial and 50% tidal influence. These simulated deltas were chosen to represent the three delta types because they depict the geomorphic characteristics expected in a fluvial, wave, and tidal influenced delta (Chapter 2). These three deltas also have the same initial gradient and sediment properties. The wave delta has a smooth, cuspate shoreline with one primary channel in the middle while the tidal delta has an abundance of channels that are wider at the mouth and narrow inland. The fluvial delta protrudes farther into the receiving basin than the wave delta and has fewer channels than the tidal delta with a less rugged shoreline.

The morphodynamic models, do not record the vertical structure of sediment deposition. This means that any sediment contained within a cell is assumed to be "well-mixed", producing vertically homogenous sediment deposits within the model. As such, groundwater modeling in this study is only concerned with groundwater flow and salinity variations that are produced by horizontal heterogeneity within the deltas. Furthermore, the morphodynamic models in this study only generate the sediment deposits representing modern delta formation that has occurred in the past 8500 years. This neglects the older vertically layered aquifer/aquitard structure and restricts the analysis to only looking at groundwater flow within the shallow subsurface.

### *Domain*

The initial groundwater flow and solute transport model, created in iMOD-WQ, is shaped around the delta plain of each delta (Figure 4.1D, E, F): the fluvial delta is 840 $km^2$, the wave delta is 360 $km^2$, and the tidal delta is 900 $km^2$. The groundwater model uses the same domain as the morphodynamic models used to create the generic deltaic landforms for each delta type. This means that the groundwater models are composed of 200 m x 200 m cells in the horizontal direction with each grid cell being homogeneous and isotropic. Although a large cell size is often used to simulate deep groundwater systems, it is not as well suited for capturing the small-scale flows that may be most important to water table dynamics and deltaic systems that have interactions with surface water features. Hydraulic conductivities within deltas can vary within a 200 m spatial scale, making the cell size a limitation of this study. However, the large cell size is necessary to reduce simulation runtimes and for integration of the morphodynamic modeling results into the groundwater model. The large cell size also allows for the modeling domains to be representative of the spatial scale seen in large coastal deltas around the world.

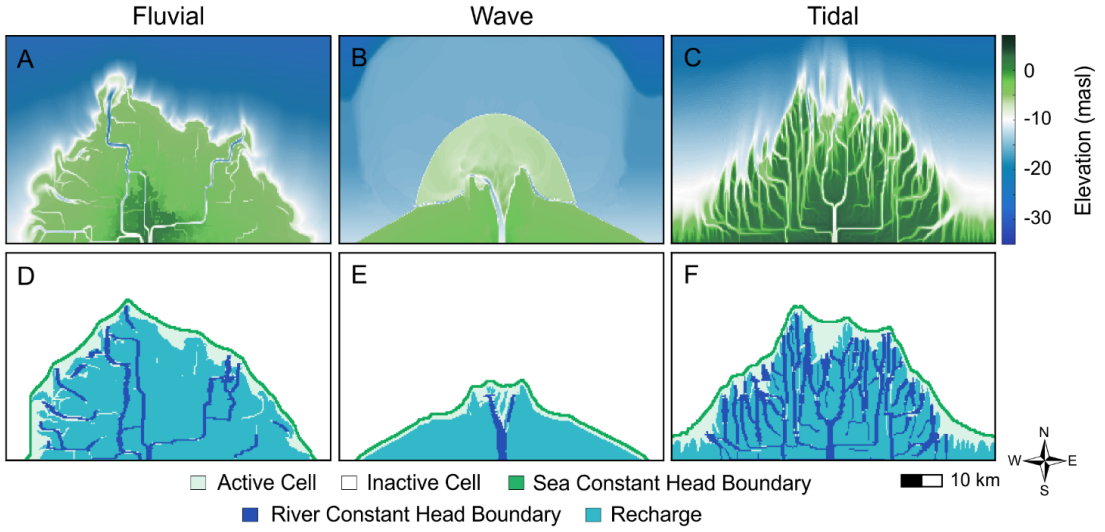


**Figure 4.1. Simulated deltas and the corresponding modeling domains for the A and D) fluvial, B and E) wave, and C and F) tidal deltas.**

The average thickness of unconsolidated aquifer material in 31 of the world's largest deltas ranges from 60 m to 440 m, with an median thickness of 210 m (Zamrsky et al., 2018). Literature on Holocene sediment in deltas around the world suggest that the upper Holocene sediment can vary between approximately 10 to 400 m in thickness

(Table 4.1). We used a total model thickness of 120 m, with the vertical direction being discretized into 10 layers. Layers 1 and 2 are 5 m thick, layers 3 through 9 are 10 m thick, and layer 10 is 40 m thick (Layer 1 is the top layer in the model).

The top of Layer 1 is based on the simulated ground surface elevation in the morphodynamic model. To remove small depressions in the ground surface elevation profile created through channelization, we smoothed the simulated elevation profile using a median filter with a width of 15 cells. The resulting smoothed elevation profile for each delta accurately depicts the delta plain and preserves the elevation change from the delta apex to the shoreline. The maximum elevation at the delta apex is 9.5 m, 5.4 m, and 11 m in the fluvial, wave, and tidal deltas, respectively.

Each model is run for a total of 8 ky. There are 15 stress periods throughout the simulation. Five stress periods are within the first 1 ky of the simulation (at 25, 50, 100, 500, and 1000 years) to capture the initial changes within the model. This is followed by a stress period every 1 ky for the next 6.5 ky of simulation (at 2, 3, 4, 5, 6, and 7 ky). The first 7.5ky of simulation employ fixed and unvarying boundary conditions. Between 7.5 and 8 ky, the recharge boundary condition is decreased to reflect changes in the water budget resulting from anthropogenic influences.

**Table 4.1. Reported thicknesses of shallow aquifers in selected coastal deltas.**

| | Delta Type | Thickness | Description | Citation |
|---|---|---|---|---|
| **Fraser** | Tidal | 165 m | Confined or semi-confined (depending on overlying silts) topset sheet sands | Bridger and Allen, 2006 |
| **Ganges** | Tidal | 20 to 100 m | Holocene confined aquifer; fine to medium sand and peat | Ravenscroft and Mcarthur, 2004 |
| **Mississippi** | Fluvial | Mean of 170 m, maximum of 372 m | Holocene and Upper Pleistocene alluvial aquifer; sands and fine sediments | Williamson et al., 1990 |
| **Red River** | Tidal | 11 to 46 m | Holocene aquifer; sand, clay sand, sandy clay | Trafford et al., 1996 |
| **Vistula** | Wave | 20 m | Holocene aquifer; fluvial, lake and marine sands | Jaworska-Szulc, 2009 |
| **Waipaoa** | Fluvial | 40 to 80 m | Four shallow Quaternary aquifers; pumice, sand, and gravel | Golder Associates, 2014 |
| **Yangtze** | Tidal | 0.5 to 5 m<br>11 m | Unconfined<br>Holocene aquifer; silt and clay | Li et al., 2006<br>Cao et al., 2013 |

### *Layer properties*

The sediment distributions generated by each morphodynamic delta model were used to create spatially varying hydraulic conductivity maps for the three deltas (Chapter 3). The overall heterogeneity and the distribution of high hydraulic conductivity areas is sensitive to the portion of fluvial, wave, and tidal influence within each morphodynamic delta model (Chapter 3). The hydraulic conductivity in each model only varies spatially in the horizontal direction, meaning that no vertical heterogeneity is considered.

During initial numerical modeling, we determined that the hydraulic heads in the fluvial model with high recharge values are strongly influenced by low permeability material that exist inland of the shoreline (Figure E1). The low permeability material resulted in hydraulic head values that are substantially above the ground surface (up to 100 m above the top of the model). In a real delta, a build-up of hydraulic head would result in ground flooding and overland flow. However, since we are using a groundwater

model, the increased hydraulic head in the model results in abnormally fast groundwater freshening within the delta. The fluvial models used in this study were built from parameters gathered for deltas around the world (Chapter 2). Unfortunately, data regarding the incoming median grain size and grain size distribution of sediment arriving in the delta is limited; only 19 deltas in the dataset have this information. As such, the same median grain size and grain size distribution were used for all delta types. When evaluating the incoming grain size of only fluvial deltas in the dataset, the median grain is considerably larger. Since fluvial deltas do not have the natural sorting properties that exist within tidal and wave deltas, a higher median grain size would change the permeability within the fluvial model. We found that increasing the hydraulic conductivity in fluvial models by one order of magnitude (the median hydraulic conductivity in the fluvial model increase from $3.9x10^{-6}$ m/s to $3.9x10^{-5}$ m/s) produced more realistic hydraulic head values that generally followed the topography of the delta and were not unreasonably high. As such, results in this paper were generated from the model with increased hydraulic conductivity. Final hydraulic conductivity profiles used in the groundwater modeling are given in Figure E1.

Hydraulic conductivity with the delta models varies between $1x10^{-6}$ m/s and $5x10^{-3}$ m/s, which is within range of hydraulic conductivity values reported in deltas around the world (Chapter 3). The median hydraulic conductivity within the delta plain in the fluvial, wave, and tidal models is $3.9x10^{-5}$ m/s, $1.9x10^{-4}$ m/s, and $8.3x10^{-6}$ m/s, respectively (Appendix E Figure E1). The vertical to horizontal anisotropy ratio in K is 0.1, the longitudinal dispersity is 10 m, and the transverse dispersity is 1 m for all deltas (Table 4.2). The specific storage is $1x10^{-5}$ $m^{-1}$ and the effective porosity is 0.35; specific storage has little effect on the salinization process because pressure equilibrates faster than salinity (Michael et al., 2013).

**Table 4.2. iMOD-WQ domain, discretization, hydraulic properties and transport properties used in the fluvial, wave, and tidal models.**

| | Fluvial | Wave | Tidal |
|---|---|---|---|
| **Delta/domain area ($km^2$)** | 840 | 360 | 900 |
| **Horizontal discretization (m)** | 200 x 200 | 200 x 200 | 200 x 200 |
| **Vertical discretization (m)** | | | |
| **Layers 1-2** | 5 | 5 | 5 |
| **Layers 2-9** | 10 | 10 | 10 |
| **Layer 10** | 40 | 40 | 40 |
| **Maximum elevation of Layer 1 (m asl)** | 8.5 | 4.4 | 11 |
| **Median horizontal hydraulic conductivity; Kx = Ky (m/s)** | $4x10^{-5}$ | $2x10^{-4}$ | $8x10^{-6}$ |
| **Ratio of vertical to horizontal anisotropy (m)** | 0.1 | 0.1 | 0.1 |
| **Specific storage ($m^{-1}$)** | $1x10^{-5}$ | $1x10^{-5}$ | $1x10^{-5}$ |
| **Effective porosity** | 0.35 | 0.35 | 0.35 |
| **Longitudinal/transverse dispersivity (m)** | 10/1 | 10/1 | 10/1 |

### *Initial conditions*

The initial hydraulic head in each model layer is specified as 1 m below the top model layer, which is the smoothed elevation profile for each delta model (Appendix E Figure E2). The highest initial head is 7.5 meters above sea level (m asl) for the fluvial delta, 3.4 m asl for the wave delta, and 11 m asl for the tidal delta. The initial head at the sea boundary is 0 m asl.

The initial concentration of salinity in the model is 35,000 mg/L, representing an entirely saline subsurface. Saline water in the model has a density of 1025 $kg/m^3$ while freshwater in the model has a density of 1000 $kg/m^3$. The only cells that are not saline at the beginning of the simulation are the cells representing the river network. The initial concentration in the river network cells is 0 mg/L, representing fresh water. Delsman et al. (2014) found that assuming the subsurface was entirely saline at the beginning of delta formation (6.5 kya) resulted in modeled salinity distributions that are similar to present-day salinity measured in the Rhine-Meuse Delta.

### *River and sea boundaries*

The models consist of a constant head boundary representing the river water level within the top layer of the model and a constant head boundary representing the ocean water level along the northern edge of the model (Figure 4.1D, E, F). The river pixels in the model are mapped using Rivamap which identifies individual river segments by extracting curvilinear structures from the elevation map using a multiscale singularity index (Chapter 3, Isikdogan et al., 2017). To simulate the river network, all river pixels in

the top model layer are assigned as a constant head boundary with the head equal to the initial head in the model and a specified inflow concentration of 0 mg/L, representing fresh water. Defining the constant head values in the river network equivalent to the initial head assumes that the hydraulic gradient is approximately equivalent to the gradient off the ground surface elevation (Chapter 3). We chose a constant specified head boundary condition to represent the river network instead of a river boundary (which requires the estimation of a conductance value on the bottom of the riverbed) because we simulated the hydraulic conductivity of the materials underlying the river network using the sediment transport modeling. Channels within the delta originating from the feeder river are not distinguished from channels originating from tidal influence; both types of channels are assigned a constant head with a concentration equal to that of fresh water (0 mg/L).

The sea boundary is represented with a constant head boundary condition of 0 m asl and a specified inflow concentration of 35,000 mg/L. The location of the sea boundary condition is determined using the Open Angle Method with an open angle of 160 degrees for the fluvial models and 140 degrees for the tidal and wave models (Shaw et al., 2008). Although several open angles were tested, 160 and 140 degrees were chosen because they capture the shape of the delta plain without including the sinuosity shown in deltas that have a rugged shoreline (Chapter 3).

Zero flux boundaries are assigned across the bottom of the model, the southern edge of the model (the land-ward side of the delta), and on the outside of the sea boundary (Figure 4.1D, E, F). We assume that groundwater fluxes out the bottom layer of the model are impeded by aquitard structures that often underlie the permeability Holocene material, justifying the zero-flux boundary. In reality, the shallow subsurface within a delta does interact with deeper groundwater systems. Interactions between shallow aquifers and deeper subsurface groundwater has been explored in several case-studies (Delsman et al., 2014; Van Pham et al., 2019; van Engelen, 2020) and is outside the scope of this paper. The implication of assuming a zero-flux boundary on the bottom of the model is discussed further in section 4.5.3. Although it is likely that there is some continental inflow to the groundwater system in deltas, it is difficult to quantify how much groundwater flowing through a delta originates as continental groundwater and how much is supplied from surface recharge or the river network. As such, for simplicity we use a zero-flux boundary along the southern border of the model, signifying no

continental inflow to the delta. It is possible that inclusion of continental groundwater may increase the freshwater volume within the model and move the fresh-saline water interface closer to the shoreline.

### *Recharge*

We investigate the effect of recharge on groundwater salinity using four recharge scenarios: 1) no recharge, 2) recharge representative of an arid climate, 3) recharge representative of a temperate climate, and 4) recharge representative of a tropical climate. For each climate type, we simulate the diffuse recharge for each of three material types, representing low, medium, and high hydraulic conductivity deltaic sediments. We use the 1D water balance code Hydrologic Evaluation of Landfill Preformation (HELP) developed by United States Environmental Protection Agency's (EPA) (United States Environmental Protection Agency, 1984).

The water balance is simulated for three vertical percolation columns with varying hydraulic conductivity (K), low medium and high, representing the range of values in the delta models. Each percolation column consists of a single layer with homogenous material. The base of the column represents the approximate depth of the water table, which is defined as the difference between the ground surface and the water level within the morphodynamic models. A thickness of 1.2 m is used as average of the unsaturated zone in the fluvial (0.9 m), wave (0.8 m), and tidal (2 m) delta models. The low permeability material is assigned a saturated hydraulic conductivity of $3x10^{-7}$ m/s, the medium permeability material $3x10^{-5}$ m/s, and the high permeability material $2x10^{-4}$ m/s (Appendix E Table 3E). Other soil properties were assigned based on values in the HELP material database for each approximate grain size (Appendix E Table 3E).

Runoff is calculated in HELP using the Soil Conservation Service Curve-Number (Mishra and Singh, 2003). A slope of 0.03% is applied to the top of each percolation column, representing the median topographic gradient for all delta types (Chapter 3); initial results suggest that the small change in slope that exists between delta types does not impact the runoff estimation within the HELP models, justifying the use of a single slope for all delta types. For simulating evapotranspiration, vegetation is represented as a "good stand of grass" with a specified evaporative zone depth and maximum leaf area index (Appendix E Table E1). This vegetation type is appropriate because many deltas around the world are agricultural hubs, even those located in arid climates. Additional

parameters needed for evapotranspiration include growing season start and end day, average wind speed and quarterly humidity (Appendix E Table E1).

The HELP model requires a daily climate series as input. Daily data representative of each climate type are generated using the stochastic weather generator WGEN (Richardson and Wright, 1984). The weather series is generated using precipitation and temperature climate normals, climate statistics, incoming solar radiation, wind speed, and relative humidity. Weather Generator includes a database of meteorologic stations with calculated climate statistics. We used climate information from three real deltas (the Mekong, Po, and Nile) to force the HELP models. Although the climate information in the HELP models is representative of real deltas, the properties of the vertical percolation columns (hydraulic conductivity, slope of the model top, vegetation type, etc.) are the same in each model and represent properties of the modeled deltas rather than conditions found in these three real deltas.

We use the Damascus Airport weather station to represent the arid climate conditions in the Nile Delta, the Venezia/b Tesser weather station to represent the temperate climate conditions in the Po Delta, and the Saigon (HoChiMin) weather station to represent the tropical climate conditions in the Mekong Delta (Appendix E Table 1E). The Damascus Airport station is 470 km from Nile Delta shoreline and has the same climate classification as the Nile Delta—arid, hot desert (Peel et al., 2007). The Venezia/b Tesser weather station is used to represent the temperate climate conditions as it is the station closest to the Po Delta, Italy. The climate in the Po River basin is described as a temperate, warm summer climate (Peel et al., 2007). The Saigon (HoChiMin) weather station is used to for the tropical climate conditions because it is located closest to the Mekong Delta, Vietnam, which is characterized by a tropical savannah climate (Peel et al., 2007). Using the climate normals (Appendix E Table 2E) and evapotranspiration parameters (Appendix E Table 3E) for each weather station, WGEN is run for a 100-year simulation period to generate daily time series representative of the current climatic conditions at each station. The stochastic weather data for each climate type are used as forcing data in the HELP water balance modeling.

The HELP models are run for 100 years, allowing the model to spin-up to a pseudo-steady state moisture content. Outputs of the HELP models include summaries for all simulated water balance components in addition to daily water balance

components including rainfall, runoff, evapotranspiration, evaporative zone water content, and percolation of water through the column. The average annual percolation of water through the column is used to assign recharge values in the iMOD-WQ model for each of the three representative climates. We assign annual average recharge values derived from the low conductivity column to cells with $K < 2x10^{-6}$ m/s. Recharge values derived from the medium conductivity column are assigned to cells with $2x10^{-6}$ m/s $\leq K < 5x10^{-5}$ m/s. Recharge values derived the high conductivity (loamy sand) column are assigned to cells with $K \geq 5x10^{-5}$ m/s.

Results of the HELP recharge modeling indicate that deltas in an arid climate would receive 5, 13, and 18 mm/yr for low, medium, and high hydraulic conductivity areas, respectively; deltas in the temperate climate receive 240, 250, and 294.4 mm/yr; and deltas in the tropical climate receive 270, 270, and 350 mm/yr. Initial groundwater modeling results showed no difference in the groundwater head or concentration between the models run with recharge representing temperate and tropical climates; therefore, results in this study only focus on the arid climate (labeled as the dry climate) and the tropical climate (labeled as the wet climate). Spatially distributed recharge based on hydraulic conductivity in the three deltas indicates that the wave delta receives the most recharge while the fluvial and tidal deltas receive less recharge (Figure 4.2).

In the last 500 years of the simulation (between years 7500 and 8000), the recharge in each delta model is reduced by 25%, 50%, 75%, and 100% to determine how sensitive the groundwater system is to changes in freshwater entering the delta. We use a distributed recharge reduction as a proxy for groundwater abstraction. At the beginning of groundwater development, pumped water is derived from a depletion in groundwater storage. Over time, pumped water is increasingly obtained from capture of groundwater recharge or discharge. Considering the long simulation times within the study, reducing recharge to the groundwater system approximates distributed groundwater pumping that captures incoming recharge.

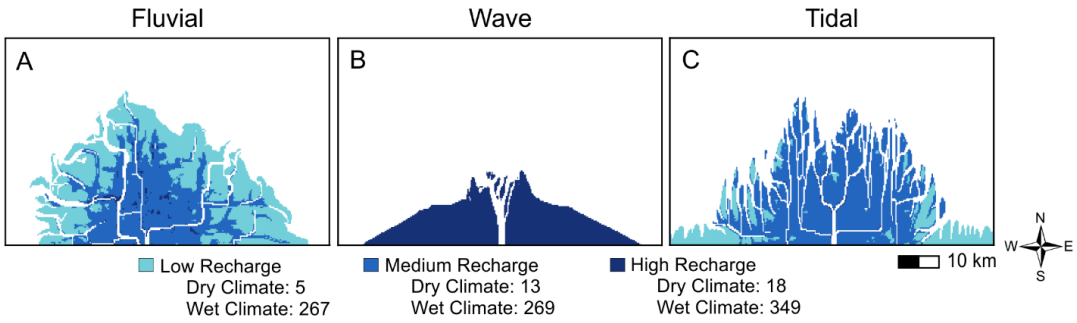


**Figure 4.2. Recharge applied to the A) fluvial, B) wave, and C) tidal delta. Model cells where $K < 2x10^{-6}$ m/s are assigned a low recharge value, model cells where $2x10^{-6}$ m/s $\leq K < 5x10^{-5}$ m/s have a medium recharge value, and model cells where $K \geq 5x10^{-5}$ m/s have a high recharge value.**

### 4.3.2. Vulnerability analysis

We use the numerical modeling results of generic deltas to understand the vulnerability of the world's largest and most populated deltas to salinization of the shallow groundwater system through lateral intrusion. Although we do not specifically model any real deltas, we pair each of the real deltas to one of the generic models using delta morphology and climate information. This allows us to understand how characteristics of each real delta impacts the potential for lateral saline intrusion that results in a loss of freshwater availability.

We define vulnerability (V) as a measure of the physical susceptibility (S) of the shallow deltaic aquifer to saline conditions in the presence of a hazard threat (H), which is any stressor (natural or anthropogenic) that may act to contaminate the freshwater resource through salinization (Simpson et al., 2014):

$$V = SH \qquad (4.1)$$

This definition of vulnerability is part of a risk framework that has been used in several coastal groundwater applications (Holding and Allen, 2016; Klassen and Allen, 2017). We chose this definition of vulnerability because it allows for the integration of our model results with hazards specific to groundwater quality in coastal hydrogeological settings.

Using several previously published datasets, we compile the following information for 60 deltas around the world for use in the vulnerability calculation: 1)

average annual groundwater recharge (Döll and Fiedler, 2008), 2) sediment discharge produced by river, waves, and tides (Nienhuis et al., 2020), and 3) population living within the delta (Edmonds et al., 2020). Although not necessary for the vulnerability calculation, we also note if previous research has found the presence of groundwater salinity near the ground surface originating from previous marine transgressions (Larsen et al., 2017; van Engelen, 2020) (Appendix F).

### *Susceptibility*

To quantify S for deltas around the world, we categorize the global deltas into six groups that correspond with one the groundwater models: 1) dry fluvial, 2) wet fluvial, 3) dry wave, 4) wet wave, 5) dry tidal, and 6) wet tidal. A delta is classified as dry if the delta receives less than 100 mm/yr of recharge, and the delta is classified as wet if the delta receives more than 100 mm/yr of recharge. The primarily morphodynamic influence within each delta (Figure 4.1) is based on the amount of sediment discharge produced by the river ($\mathrm{Q_{fluvial}}$) as well a parameterization of the ability for waves and tides to move sediment within the delta (Nienhuis et al., 2020). Potential for waves to move sediment away from the river mouth ($\mathrm{Q_{wave}}$) is calculated by convolving the angular distribution of wave energy with an approximation of longshore sediment transport (Nienhuis et al., 2020). The potential for tides to move sediment within the delta ($\mathrm{Q_{tide}}$) is a function of the tidal angular frequency and the tidal prism, which is a product of the tidal range amplitude and the distance of tidal influence into the channel (Nienhuis et al., 2020). Using a normalized three-way ratio, we compute the proportion of fluvial, wave, and tidal influence ($\mathrm{R_i}$, where $\mathrm{i} = [\mathrm{fluvial}, \mathrm{wave}, \mathrm{tide}]$) within each of the deltas:

$$R_i = {Q_i}\Big/{(Q_{fluvial} + Q_{wave} + Q_{tide})} \qquad (4.2)$$

In this equation, $\mathrm{i} = [\mathrm{river}, \mathrm{wave}, \mathrm{tide}]$. Fluvial deltas have $\mathrm{R_{fluvial}}$ > 0.5, wave deltas have $\mathrm{R_{wave}}$ > 0.5, and tidal deltas have $\mathrm{R_{tide}}$ > 0.5 (Figure 4.3). Although most of the deltas in this study (82%) have > 5% secondary morphodynamic influences, we classify each delta into one of the three end-member types for simplicity. Four deltas in the dataset do not have a single morphodynamic influence >50% and are therefore classified as a mixed delta; these deltas are not included in vulnerability analysis as they do not directly correspond to one of the groundwater models. The only delta in the dataset that does

not have the sediment discharge information available is the Barka Delta, Sudan; this delta is also not included in the vulnerability analysis. Although a total of 60 deltas are included in the dataset, only 55 are used in the vulnerability analysis.

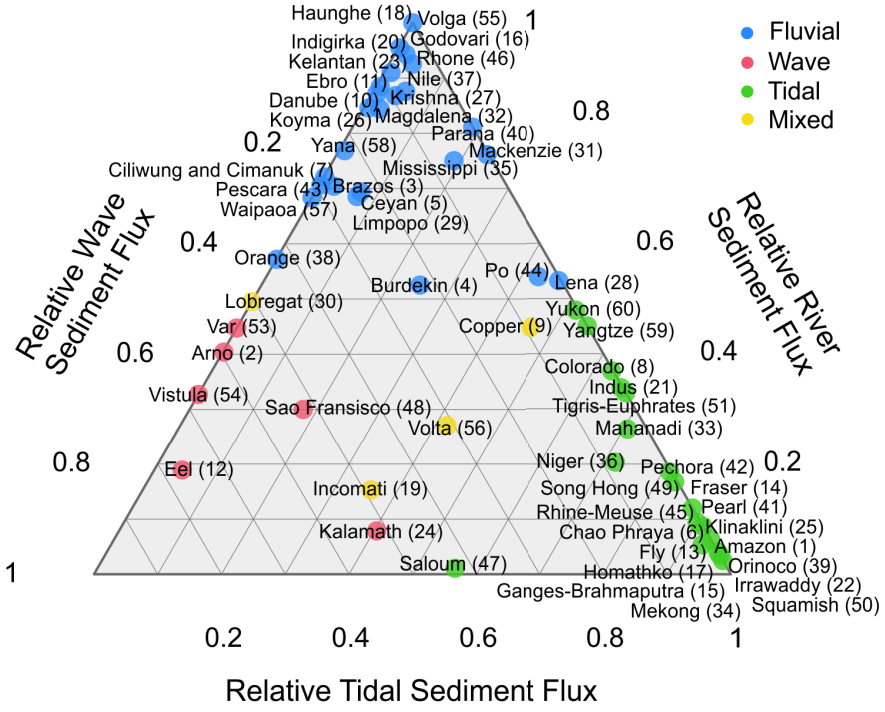


**Figure 4.3. A) The Galloway ternary Diagram populated with 60 of the world's largest and most populous deltas (Galloway, 1975; Nienhuis et al., 2020). The number assigned to each delta corresponds to the data listed in Appendix E.**

We calculate S for each of the 55 global deltas using the results from the numerical groundwater model assigned to the delta. Susceptibility is the volume of groundwater within the delta model that is saline (Vs) after 7500 years divided by the total groundwater volume within the model (Vt). A model cell is defined as saline if the concentration of salinity (Cs) > 300 mg/L.

$$S = {}^{Vs_{7500}}/_{Vt} \qquad (4.3)$$

Susceptibility values vary between 0 and 1, with 0 representing no susceptibility (a completely fresh subsurface) and 1 representing high susceptibility (a completely saline subsurface).

### *Hazard*

We define H as any stressor (natural or anthropogenic) that may act to contaminate the shallow subsurface through salinization. Many stressors have the potential to perpetuate salinization in the shallow subsurface; these include, but are not limited to, groundwater pumping within the shallow or deep aquifer systems, decreased recharge due to climate change or city building, decreased groundwater flow entering the delta due to pumping upstream, decreased surface water within the delta due to damming or water diversions upstream, upwelling of deeper salinity due to natural or anthropogenically induced ground subsidence, storm surge, and sea level rise relative to ground surface. Quantifying the impact any one of these stressors has on the groundwater system in 60 deltas is a significant undertaking. Although there are many mechanisms that can lead to groundwater salinization, we are most interested in evaluating the impact of groundwater pumping and are therefore not considering any of the other stressors.

Determining the impacts of groundwater pumping in coastal deltas is difficult because groundwater extraction information (including pumping location for each well, screen depth, pumping rate) is often not readily available. van Engelen et al. (2022) attempted to quantify groundwater abstraction in 15 deltas using the PCRaster Global Water Balance model, which computes daily groundwater extraction rates based on water demand and surface water availability but found that considerable differences can exist between the simulated total abstraction rates and regional datasets. To determine the potential for future salinization due to groundwater pumping, we use population in combination with the numerical modeling results as a proxy for the potential of future salinization to occur.

Population data for each delta are collected using the methods in Edmonds et al. (2020); we extracted Gridded Population of the World data (GPWv4; Socioeconomic Data and Applications Center, 2020) by identifying the delta polygon that corresponds to each of the 60 deltas in this study. Seven deltas that did not have population information in the dataset; so we acquired population data using census information. We calculated a normalized population (Pn) for each delta by dividing the population of each individual delta (P) divided by the sum of the population in all 60 deltas:

$$Pn = {}^{P}/_{\sum_{n=60}^{i} P_i} \qquad (4.4)$$

We assume that the degree of stress placed on the shallow subsurface and subsequent salinization is proportional to the population within the delta; a delta with no population will not pose any hazard to the groundwater system whereas a delta with a large population will pose abundant hazard to the groundwater system. To determine how stressors within a delta contribute to salinization of the shallow subsurface, we reduce the recharge within the numerical models associated with each delta. In the last 500 years of the simulation (between years 7500 and 8000), recharge is reduced by 25% if $0 < P \leq 50{,}000$ (17 deltas), by 50% if $50{,}000 < P \leq 500{,}000$ (9 deltas), by 75% if $500{,}000 < P \leq 10$ million (12 deltas), by 100% if $P > 10$ million (8 deltas). Recharge is not reduced in the model if $P = 0$ (9 deltas). Using the numerical modeling results for each delta, we calculate the change in saline volume (Vc) as the difference between the volume of salinity at year 7500 ($Vs_{7500}$) and 8000 ($Vs_{8000}$) divided by Vt:

$$Vc = {}^{(Vs_{8000} - Vs_{7500})}/_{Vt} \qquad (4.5)$$

Hazard (H) is defined as the change in saline volume within the delta between 7500 and 8000 due to the reduction in recharge multiplied by $Pn$:

$$H = Vc * Pn \qquad (4.6)$$

where both Vc and Pn vary between 0 and 1, resulting in hazard values that also varies between 0 and 1.

No hazard (H = 0) represents a delta with no population living on the delta plain or no change within the saline volume due to decreasing recharge within the associated numerical model. A delta has a high hazard if the delta is highly populated and there is a large change in salinity in the associated delta model. A value of H = 1 is only achieved if the delta with the highest population (Pn = 1) has a 100% change of saline volume (Vc = 1).

## 4.4. Results

### 4.4.1. Numerical modeling

#### *Climate effects on salinization*

In general, the wave delta has the largest proportion of saline groundwater compared to the fluvial and tidal deltas (Figure 4.4). There is little difference in the proportion and spatial distribution of groundwater salinity in dry climate models compared to the models that did not receive any recharge. Increasing the groundwater recharge in the wet climate models (Figure 4.4B, E, I) results in less groundwater salinity compared to the dry climate models (Figure 4.4C, F, J).

When no recharge is applied to the models, the percent of groundwater that is saline in the shallow subsurface after the 7500-year simulation is 71% for the fluvial delta, 89% for the wave delta, and 65% for the tidal delta. In the dry climate models, the percent of saline water in the subsurface is 71%, 89%, and 65% for the fluvial, wave, and tidal deltas, respectively. In general, most of the salinity exists in the deeper model layers while freshwater accumulates near the surface, creating a freshwater lens that sits atop deeper groundwater salinity. Although the tidal delta has the largest amount of freshwater in the subsurface compared to the fluvial and wave deltas, the average depth of the fresh-saline water interface is greatest in the fluvial delta. The average depth of the fresh-saline water interface in the dry fluvial model is 23 m, with the deepest part of the interface near the delta apex in the fluvial delta and the wave delta (Figure 4.4A, B, respectively). A shallow freshwater lens develops inland of the shoreline where the river network supplies freshwater to the subsurface and the subsurface permeability is higher (Figure 4.4A). The average depth of the interface in the dry wave delta is 7.6 m, with the deepest part of the freshwater lens corresponding to the location of the main channel stem (Figure 4.4B). The fresh-saline interface in the dry tidal delta has an average depth of 23 m and the freshwater lens is more extensive across the entire delta compared to the fluvial and wave deltas (Figure 4.4C). However, the depth of the interface in the tidal delta is more spatially variable, with the interface being deepest where there are more channels that correspond with areas of increased hydraulic conductivity.

In the wet climate models, the percent of saline water in the subsurface is 36%, 47%, and 37% for the fluvial, wave, and tidal deltas, respectively. The fluvial delta has

approximately the same percent of saline water as the tidal delta in the wet climate models, whereas in the dry climate models, the tidal delta has 6.3% less volume of saline water than the fluvial delta. In these wet climate models, the freshwater lens is greater than 80 meters below sea level (mbsl) throughout most of the delta (Figure 4.4D, E, F). The fluvial model has a small anomaly in the middle of the delta plain where the freshwater lens does not exist and there is salinity at the ground surface (Figure 4.4D). This location corresponds to a depression in the top of the model, which is also evident in the initial water level (Appendix E Figure E2). In the wave delta, the high permeability levees surrounding the main channel stem are the only place where the freshwater lens is shallower in the wet climate model (Figure 4.4E) compared to the dry climate model (Figure 4.4B). The freshwater lens in the levees has a thickness of 20 to 40 m inland but is nonexistent near the shoreline. Out of the three delta types, the fresh-saline water interface is most variable in the tidal delta (Figure 4.4F). While the freshwater lens is deepest under the channels in the dry climate tidal model (Figure 4.4C), the lens is shallowest under the rivers in the wet climate tidal model (Figure 4.4F). This is due to the function of the boundaries applied to the river channels in each climate. In the dry climate, rivers in the tidal delta supply fresh water to the subsurface. In the wet climate, water enters the model through recharge applied to the islands and groundwater flows to the river network and the sea boundary, resulting in more salinity undercutting the river network.

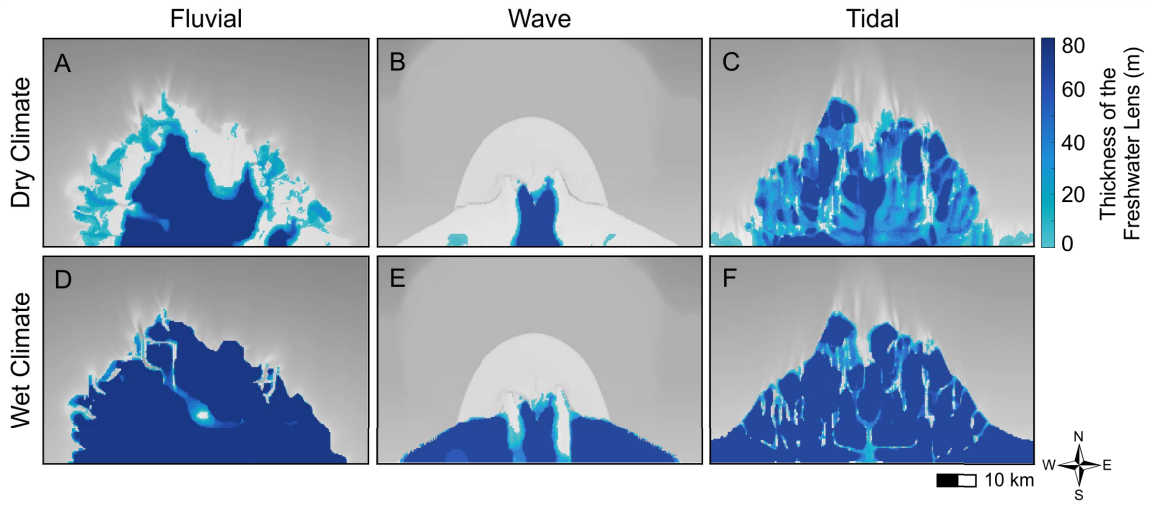


**Figure 4.4. Thickness of the freshwater lens for A-C) dry climate models and D-F) wet climate models in a fluvial (first column), wave (second column) and tidal (third column) delta.**

### *Distributed recharge reduction—groundwater pumping*

Recharge reduction within the last 500 years of the simulation (7500-8000 years) results in an overall salinization in the subsurface in all wet and dry climate models except the 25% and 50% recharge reduction in the dry climate tidal models. In the dry climate models with 100% recharge reduction, there is a 4.4%, 18%, and 1.6% increase in total groundwater salinity in the fluvial, wave, and tidal deltas, respectively. In the wet climate models with 100% recharge reduction, these deltas experience a total groundwater salinity increase of 74%, 27%, and 49% in the fluvial, wave, and tidal deltas, respectively.

In general, salinization occurs within deeper model layers while freshening primarily occurs within the top model layers. Although there is a higher percentage of salinity increase in the wet climate models, the increase in salinity in the dry climate models is more spatially distributed compared to the more focused salinization that occurs in the wet climate models. Increases in salinity in the dry climate fluvial model occur along the shoreline within the deeper model layers (Figure 4.5A). The increase in salinity in the wet climate model, which also occurs along the shoreline, but is mostly focused on the western half of the delta (Figure 4.5D). Freshening in the fluvial deltas occurs within the top model layers in the dry climate model inland of the salinization. In the wet climate fluvial model, freshening occurs inland of the depression in the model elevation while salinization occurs toward the shore. In the dry climate wave model, salinization occurs throughout much of the delta plain, with some freshening directly adjacent to where the freshwater lens exists (Figure 4.5B). In the wet climate wave model, salinization occurs along the shoreline and adjacent to the freshening along the channel network. Less salinization takes place inland and within the middle of the delta plain. Salinization in both the dry and wet tidal models is spatially variable (Figure 4.5C, F). In the dry climate tidal model, most of the salinization occurs on the eastern and western edges of the delta plain, with a thin strip of salinization that occurs along the shoreline. In the wet climate tidal model, salinization along the shoreline is slightly more pronounced. Salinization also occurs inland along some of the main channels in the top layers of the model.

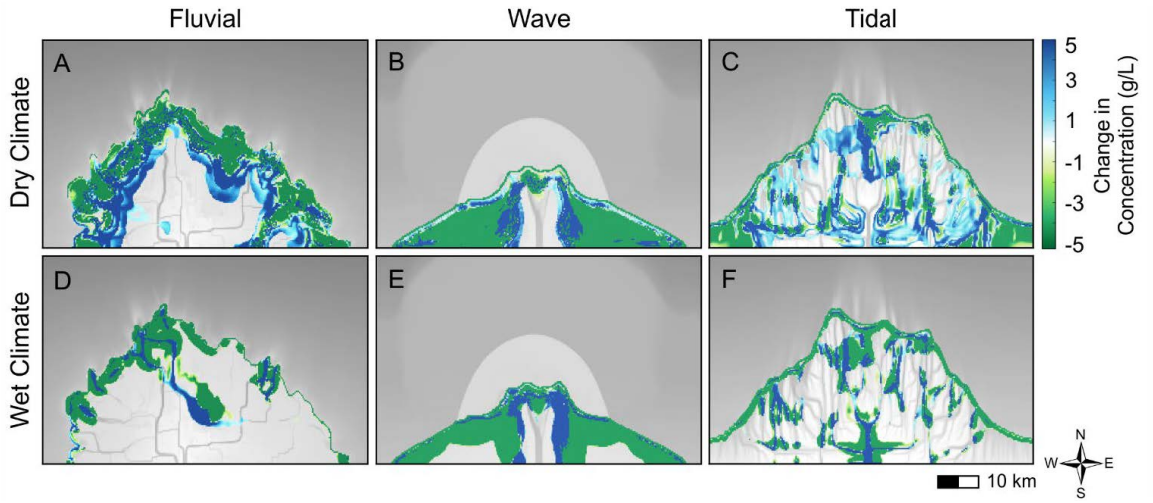


**Figure 4.5. Change in the concentration of groundwater salinity for A-C) dry climate models and D-F) wet climate models for the 100% recharge reduction scenario.**

The greatest change in saline volume occurs in the wet wave models, where salinized volume increases by 6%, 13%, and 24% in the 50%, 75%, 100% recharge reduction scenarios, respectively. The wet fluvial delta experiences 5.2% increased in saline volume while the wet tidal delta experiences 3.2% increase in saline volume with a 100% reduction in recharge. The other wet climate models have less than a 3.0% change in saline volume due to the reduction in recharge. The dry wave delta also exhibits an overall increase in saline volume, but the change is less than 0.1% regardless of the recharge reduction. The dry climate fluvial models, as well as the dry climate tidal models with a 25% and 50% recharge reduction, experience a decrease in salinized volume between 7500-8000 years. These models continue to increase in freshwater volume because the majority of freshwater entering the subsurface is supplied from the river network, which is unaffected by a decrease in recharge in the dry climates.

In the dry climate models, there is less than a 1 m change in the average depth of the fresh-salt water interface when recharge is reduced. However, there is significant decrease in the depth of the interface in most wet climate models that have a recharge reduction greater than 50%. Figure 4.6 illustrates the results for a 100% reduction in recharge for both the dry and wet models. The wet climate fluvial, wave, and tidal models with a 100% reduction in recharge undergo an average of 7.5 m, 35 m, and 2.3 m decrease in the depth of the freshwater interface, respectively. In the wet fluvial model, most of the reduction in the depth of the fresh-salt water interface occurs along

the western half of the delta near the shoreline (Figure 4.6D). Deepening of the interface occurs on the inland side of the depression in the surface of the model while the shore-side of the depression experiences a reduction in the depth of the interface. Most of the reduction in the depth of the interface in the wave model occurs in the lower permeability material in the delta plain, on the outside of the subaqueous levees (Figure 4.6E). The high permeable material in the subaqueous levees allows for deepening of the interface in the wave delta by up to 40 m. Reduction in the depth of the fresh-salt water interface in the tidal delta occurs along the outside of the islands within the delta, adjacent to the river network (Figure 4.6F). The tidal delta is the only delta where the freshwater lens thins near the delta apex. This increase in salinization occurs as freshwater continues to enter the subsurface from the river network, pushing salinity that underlies the rivers into the lower permeability material adjacent to the rivers.

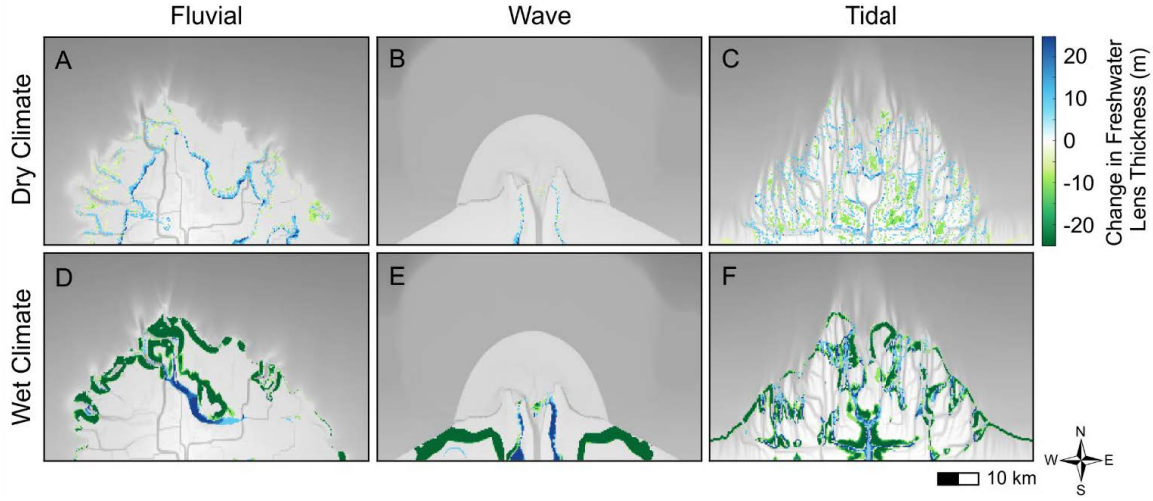


**Figure 4.6. Change in the depth of the fresh-saline water interface for A-C) dry climate models and D-F) wet climate models for the 100% recharge reduction scenario.**

### *The role of rivers vs. recharge*

The amount of water entering/exiting the model through the river boundaries shows that the role of the river network can change depending on the amount of recharge applied to the model (Figure 4.7). In all three delta types with a dry climate, the constant head river boundary supplies most of water entering the subsurface and therefore is responsible for most of the groundwater freshening occurring within these models. The decrease in recharge in the dry climate models has very little effect on the

total amount of freshwater entering the subsurface, explaining why the decreased recharge does not greatly impact the freshwater volumes in the dry climate models.

In the wet climate models, recharge supplies a significant portion of the water entering the models, especially when recharge reduction is 50% or less. In some models where recharge is high, the constant head boundary representing the river network acts as a sink, removing water from the river network; this occurs in fluvial models with less than 50% recharge reduction and tidal models with less than 75% recharge reduction. The river network in the wave model is always a freshwater source, suppling more than 50% of the water entering the model in all scenarios, except the wet climate model which does not have any reduction in recharge.

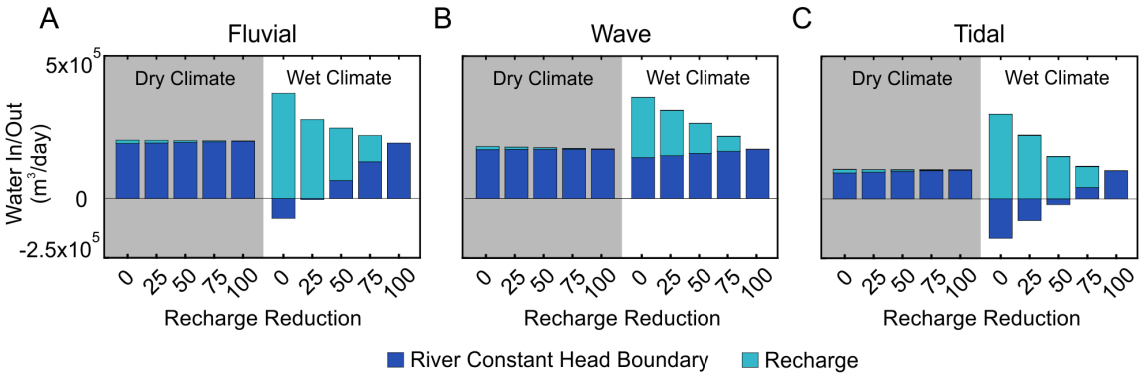


**Figure 4.7. Water budget for A) fluvial, B) wave, and C) tidal delta models with no recharge, recharge representing a dry climate, and recharge representing a wet climate after 7500 years. The water budget for models incorporating a decrease in recharge are taken at 8000 years.**

## 4.4.2. Vulnerability analysis

Out of the 60 real deltas in this study, 43% of the deltas are fluvial (26 deltas), 10% are wave (6 deltas), 38% are tidal (23 deltas), and 8% are mixed (5 deltas) (Figure 4.3). The low number of wave deltas included is due to the increased destructive morphodynamic influences (i.e., waves) which result in smaller deltas. The four mixed deltas that are not included in the vulnerability analysis of this study include the Copper, Llobregat, Volta, and Incomati deltas. The Barka Delta is also not included in the vulnerability analysis since information on the delta morphodynamics is not available.

Deltas that receive the most recharge include the Amazon (510 mm/yr), the Niger (420 mm/yr), the Fraser (400 mm/yr), and the Rhine-Meuse (380 mm/yr) (Appendix E Figure E3). Seven of the top ten deltas receiving the most recharge are tidal and three are fluvial. The Klamath, Eel, and Vistula deltas are the wave deltas that have the most recharge, receiving approximately 240 mm/yr. Thirty four of the 60 deltas are classified as having a wet climate ($R \geq 100$ mm/yr) while 26 are classified as having a dry climate ($R < 100$ mm/yr). Notable deltas that receive very little recharge include the Nile ($R = 2.5$ mm/yr) and the Indus ($R = 3.7$ mm/yr) (Appendix E Figure E3).

There are 53 deltas that have people living on the delta plain or in a nearby population center (Figure 4.8). The 53 populated deltas have a combined population of 300 million people, with 80% of the population in coastal deltas living in tidal deltas (243 million people) and 19% of the population living in fluvial deltas (59 million people). Out of the ten deltas with the largest population, eight are tidal deltas located in wet climates (Appendix E Figure E3). Eight deltas in the study have a population greater than 10 million. The Nile and the Yangtze deltas have over 40 million people while the Ganges-Brahmaputra Delta has a population of over 111 million people. The Nile Delta is a dry fluvial delta and is the only delta with a large population that is not classified as a wet tidal delta. Several of the deltas that have very little population (less than 1000 people) are in remote northern regions of North America and Russia, including the Copper, Mackenzie, Lena, Pechora, Yana, Indigirka, Kolyma deltas (Figure 4.8). Half of the 60 deltas in this study have groundwater salinization influenced by previous marine transgressions (Figure 4.8). Thirteen of these 30 deltas with known groundwater salinity are fluvial (43%), 9 are tidal (30%), 1 is wave (3%), and 6 are mixed (20%).

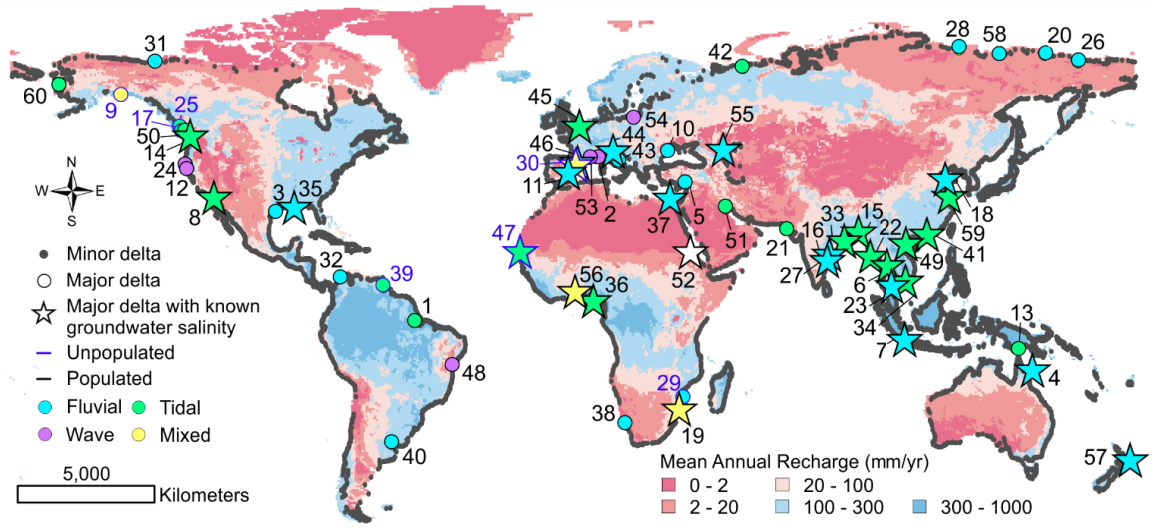


**Figure 4.8. Map of deltas around the world (Neinhuis et al., 2020) compared to deltas that have been the focus of a detailed groundwater modeling study. The number assigned to each delta corresponds to the deltas shown on Figure 4.3 and data in Appendix E. Deltas where a modeling study have been completed are classified as a fluvial, wave, or tidal deltas based on the morphodynamic influence within the delta and the defining geomorphic characteristics. The Barka Delta, Sudan (#52) is uncolored because it is missing morphodynamic information. Deltas with a blue outline are unpopulated and deltas with a black outline are populated. Global mean annual recharge is provided by Döll and Fiedler (2008).**

Susceptibility within the 55 deltas considered in the vulnerability analysis is based on the percent of saline volume that exists within the generic numerical model that corresponds to the delta's climate and morphology (Figure 4.9A). Susceptibility rankings from highest to lowest are: 1) dry fluvial deltas, 2) dry tidal deltas, 3) wet wave deltas, 4) wet tidal deltas, and 8) wet fluvial deltas. Numerical modeling results of the generic deltas suggests that the volume of saline water is highest in dry wave deltas. However, there are no dry wave deltas included in this study, making dry fluvial deltas the most susceptible to salinity within the shallow subsurface.

Hazard rankings are based on a combination of the population living within the delta in addition to salinization that occurs within the shallow subsurface when recharge is decreased in proportion to population size. Numerical modeling results suggest that wet wave deltas with populations greater than 500,000 people experience the greatest salinization due to recharge reduction; this is followed by wet fluvial and tidal deltas with populations greater than 10 million people. Nine out of the 10 deltas with the highest hazard rankings are wet tidal deltas (Figure 4.9B). The Mississippi Delta is the fluvial

delta with the highest hazard while the Vistal Delta is the wave delta with the highest hazard. In general, deltas with the lowest potential for salinization due to the recharge reduction are dry fluvial and tidal deltas. Similarly, these deltas also tend to have the lowest populations (Appendix D Figure D4), resulting in low hazard (Figure 4.9B). The only deltas that have very low hazard ($H < 0.2$) that are not a dry fluvial or tidal delta are unpopulated and include the Var Delta (wet wave), Orinoco Delta (wet tidal), and Arno (wet wave).

Vulnerability to groundwater salinization in the shallow subsurface due to groundwater abstraction and simulated by reducing recharge is greatest in the: 1) Vistula, 2) Ganges-Brahmaputra, 3) Yangtze, 4) Mekong, 5) Niger, 6) Pearl, 7) Song Hong, 8) Nile, 9) Irrawaddy, and 10) Mahanadi deltas (Figure 4.9C). Out of these ten deltas, seven are wet tidal deltas located in Southern Asia. Although wet tidal deltas are less susceptible to groundwater salinity, they are sensitive to changes in recharge. Additionally, these deltas make up 93% percent of the population in the 55 deltas in the vulnerability analysis, resulting in high vulnerability. The Vistula Delta has the highest vulnerability of all deltas included. The population within the Visual Delta is small compared to many of the other deltas in this study (265,000 people); however, the wet wave deltas have increased susceptibility in addition to a greater change in saline volume due to recharge. The Nile Delta is the fluvial delta with the highest hazard. Although the population of the Nile Delta is over 44 million people, dry fluvial deltas experience a slight freshening of the subsurface with reduction in recharge, resulting in low hazard. Susceptibility of dry fluvial deltas is the highest of any delta type in the study, explaining the high vulnerability of the Nile Delta. The thirteen deltas with no vulnerability are also the deltas that have zero population living within the delta. Even though these deltas do not have a high vulnerability, many do have high susceptibility since they are primarily fluvial and tidal deltas located in a dry climate.

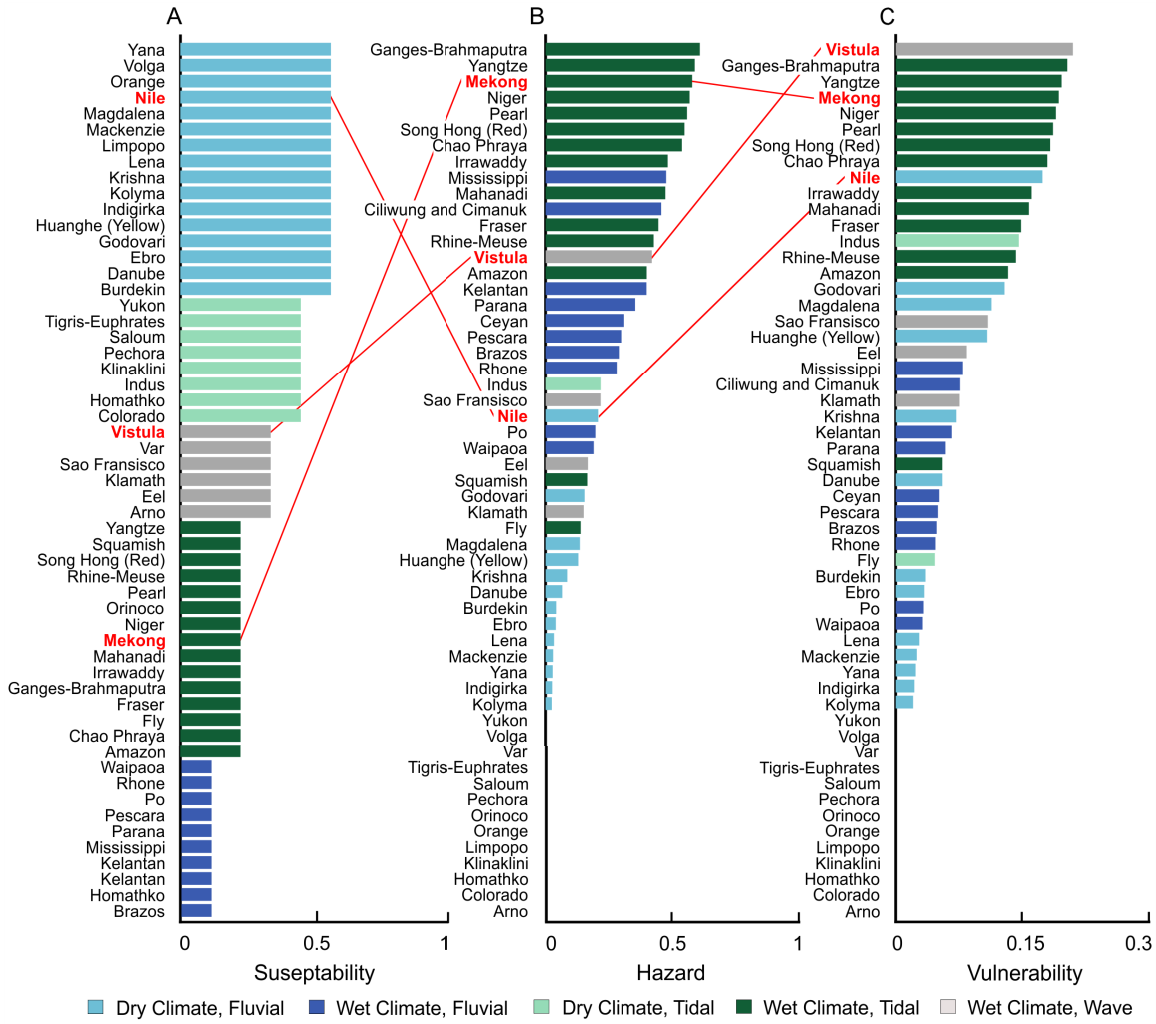


**Figure 4.9.** **A) Susceptibility, B) hazard, and C) vulnerability rankings for 60 of the largest and most populated coastal deltas around the world. The red text and lines track the susceptibility, hazard, and vulnerability of a fluvial (Nile), wave (Vistula), and tidal (Mekong) delta.**

## 4.5. Discussion

We estimate that the volume of saline water in the shallow subsurface within deltas around the world varies between 36% and 89%, depending on the morphodynamic influences and the amount of recharge the delta receives. Deltas that are most susceptible to salinity within the shallow subsurface are located within dry climates that receive less than 100 mm/yr of recharge. Deltas classified as wave or fluvial are especially susceptible. In particular, wave deltas have smaller overall hydraulic gradient and increased hydraulic conductivity (Chapter 3), making them more susceptible to salinity compared to fluvial and tidal deltas that receive similar recharge.

Additionally, wave deltas also experience the most salinization and reduction of the freshwater lens when freshwater entering the delta is reduced.

Out of the 55 deltas included in the vulnerability analysis, the Vistula Delta has the highest vulnerability. Although there are only 265,000 people living within the delta, there is a higher potential for salinization because of the wave influence. The groundwater resources in the Quaternary aquifers in Vistula Delta have been exploited for the municipal water demand since the mid 1900's; the city of Gdansk now relies entirely on groundwater resources (Szpakowski, 2007). Abstraction within the shallow deltaic subsurface resulted in a drawdown of the water table by up to 4 m with reported aquifer salinization (Szpakowski, 2007). One of the two main locations for groundwater extraction in Gdansk was terminated in 1993 due to salinization of the Quaternary aquifer (Szpakowski, 2007). Even though the population living within the Vistula Delta is small compared to many other deltas around the world, groundwater pumping has resulted in serious depletion and degradation of the of the freshwater resources, likely because of the high vulnerability of the delta.

There are no wave deltas located in dry climates included in this study because there are limited large wave deltas around the world, and none that exist within dry climates. Wave deltas have increased destructive morphodynamic influences that carry sediment away from the river mouth, inhibiting the growth of a delta in a strongly wave influenced environment. In dry climates, there is not enough fluvial discharge carrying sediment into the delta to produce a large delta in a wave environment. However, the majority of smaller deltas around the world are wave influenced (Nienhuis et al., 2020). Extrapolating the results of this study to smaller deltas, we suggest that the majority of the shallow subsurface in wave deltas located in a dry climate is likely saline and is not fit for human consumption without treatment.

Fluvial deltas located in dry climates are also highly susceptible to groundwater salinity in the shallow subsurface. The Nile Delta, the most populated fluvial delta in a dry climate, has a long history of groundwater salinity within the shallow subsurface (van Engelen et al., 2018; van Engelen, 2020). The 44 million people living on the Nile Delta rely on pumping of fresh groundwater in the shallow subsurface to meet the water needs and agricultural demand (van Engelen, 2020). Interestingly, groundwater modeling showed that 30 years of groundwater pumping in the Nile Delta did not strongly influence

groundwater salinity (van Engelen et al., 2019). Our results support this finding because we show that a < 1% change in salinity occurs in dry climate fluvial deltas when the amount of freshwater entering the delta is reduced by 100%. It is possible that a tipping point exists within dry deltas, where enough groundwater abstraction eventually leads to groundwater salinization. Mabrouk et al. (2018) showed that larger effects were observed after a 100-year pumping period in the Nile Delta. Current estimates of groundwater pumping in the Nile Delta are 2.6 $km^3$/yr (van Engelen, 2020). Assuming the delta has an area of 20 $km^2$,and receives a mean annual recharge of 2.5 mm/yr, recharge across the entire delta is estimated at $5x10^{-5}$ $km^3$/yr—resulting in a freshwater deficit.

Deltas located in a wet climates have greater freshwater volume in the shallow subsurface compared to deltas in dry climates. Coincidentally, the majority of deltas with the highest populations and groundwater demands are also located in wet climates, with many being tidal deltas found in Southern Asia. The Ganges-Brahmaputra, Mekong, and Song Hong deltas have populations > 10 million and have a long history of groundwater pumping. Groundwater pumping in the Mekong Delta is estimated to be 0.9 $km^3$/year (van Engelen, 2020), with average annual recharge totally 11 $km^3$/yr (assuming a delta area of 4,500 $km^2$). Our findings suggest that tidal deltas co-located with large population centers that are in a wet climates are highly vulnerable to groundwater stressors, indicating that the Mekong Delta is most likely not the only delta experiencing unintended consequences of groundwater abstraction in Southern Asia.

### 4.5.1. Impact of delta morphology on groundwater

Studies from around the world show that the average thickness of the Holocene aquifer ranges from approximately 10 to 400 m. In this research, we assume the maximum thickness of the Holocene material is 120 m, which results in the formation of a freshwater lens with an average thickness varying between 7.6 m and 72 m. In wet climates, the average thickness ranges from 62 to 72 m while dry climates see an average thickness of 7.6 to 23 m. The groundwater system in a delta is indirectly impacted by morphology through the permeability distribution, determining where freshwater will infiltrate into the subsurface and preferential pathways of transport through the delta (Chapter 3, Xu et al., 2022). Spatially, we find that the freshwater lens in the shallow subsurface in deltas is mostly located around the river network where

water is infiltrating into higher permeability material compared to the surrounding delta plain. Pockets of salinity are more often found where there is low permeability material that is not located near a channel. This is most evident in fluvial models, where small grain size material can deposit and there are fewer river networks cutting through the delta plain.

In addition to permeability, delta morphology impacts the number of river channels in a delta, with tidal deltas having an abundance of rivers while wave deltas generally only have one (Chapter 3). This study, in addition to Xu et al. (2022), highlights that the number and placement of rivers in a delta play an important role in determining the fresh groundwater volume in a delta. Additionally, we show that the role of the river network is dynamic and is highly sensitive to changes between water removal and supply. When recharge in a delta is high, freshwater moves from the delta plain and islands within the delta to the river network and the sea boundary, resulting in subsurface freshening. However, when recharge at the ground surface is limited, the main supply of freshwater to the subsurface is through the river network. Wave deltas, and fluvial deltas that do not have an abundance of rivers, are likely to have increased salinity in the subsurface away from the river network in dry climates. Understanding how delta morphology impacts the spatial distribution of groundwater salinity in a delta can aid in identifying locations that are most likely to hold freshwater and inform future planning of water resource development.

It is well understood from previous research that the aquifer/aquitard structure in a delta is often highly heterogeneous and discontinuous, allowing for interactions between the shallow subsurface and deeper aquifer systems (Michael and Khan, 2016; Larsen et al., 2017). It is likely that discontinuities in confining units result from channels eroding into marine or glaciomarine layers and depositing coarser-grained material that is highly connective within the delta. Deltas that have more channelization through increased fluvial and tidal influence are likely to have more connective pathways with the deeper subsurface, impacting contaminant transport between aquifer systems. Although more research is needed to determine the role delta morphology plays in the vertical connectivity of deltaic aquifers, the Ganges-Brahmaputra Delta has been shown to have vertical connectivity resulting in contaminant migration from the surface into deeper aquifer systems because of increased groundwater pumping at depth (Khan et al., 2016). Identifying deltas fluvial or tidal deltas with increased channelization at the

surface may provide a first approximation to determining which deltas are most vulnerable to salinization of the shallow groundwater resources through vertical groundwater flow of deeper groundwater salinity.

### 4.5.2. Future sustainability of coastal deltas

Given the high population density of deltas and the importance of deltas from an ecological perspective, recent reviews have summarized the current risk to deltas and evaluated the sustainability of these landscapes (Syvitski, 2008; Giosan et al., 2014; Ingebritsen and Galloway, 2014; Elliott et al., 2019). It is well understood that deltas are highly sensitive to land subsidence and global sea-level rise. Dewatering of aquifers due to over pumping of groundwater promotes coastal subsidence through the collapse of pore space within the porous media; this is generally considered irreversible because compaction in aquifer-aquitard systems is inelastic. In the Mekong Delta, 25 years of groundwater pumping has induced subsidence that caused the land surface to sink an average of approximately 18 cm, with some areas up to 30 cm (Minderhoud et al., 2017) and is responsible for 90% of the relative sea level rise expected by 2050 (Erban et al., 2014).

In additional to coastal subsidence, upstream water management and damming practices pose threats to delta sustainability and have resulted in a 50% decrease in freshwater and sediment being supplied to deltas through the river network compared to prehuman times (Syvitski and Saito, 2007; Syvitski, 2008; Giosan et al., 2014). Globally, it is estimated that there are 58,000 large dams, with the majority of these being built in the last 60 years (Mulligan et al., 2020). River dams impact deltas by removing the peak discharge events and reducing instantaneous sediment and water flux to the delta. Although it is uncertain how these temporal changes in flow may impact groundwater salinity within deltas, the impoundment sediment in dams has been shown to reduce deltaic area in large and medium sized deltas (Giosan et al., 2014). Water transfers and removal of water from a watershed feeding a coastal delta is expected to accelerate salinization of the upper subsurface; this is most likely to occur in dry climate zones where there is abundant domestic or agricultural demand. Water transfers out of the Colorado River basin used to meet domestic and agricultural water demand in the arid American Southwest has impacted the overall surface water supply in the Colorado Delta. Based on the results of this study, we hypothesis that water transfers, or a

reduction of surface water supplied to the delta, will mostly impact groundwater salinization in deltas that rely solely on the river network as a source of groundwater freshening (i.e., deltas in dry climates). In addition to the Colorado Delta, other deltas that have diminishing freshwater input and are located in a dry climate include the Tigris-Euphrates, Indus, and Nile (Day et al., 2019). To fully understand the dynamic relation between the river network and the shallow subsurface, integration of groundwater and surface water models is needed.

Since mitigating groundwater degradation is often costly, it is critical to note that countries around the world have different financial means to mitigate environmental hazards. Effective mitigation strategies to reduce subsidence and salinization from groundwater abstraction include using alternative water sources (piped water, high quality surface water, or desalinized water), relocating/distributing groundwater abstraction to areas that are less exploited or where subsidence is less harmful, and employing managed aquifer recharge/groundwater injection (Minderhoud et al., 2020). In The Netherlands, upconing of saline groundwater due to the low elevation of the polders results in groundwater salinity at the ground surface; salinity contamination of the agriculture land in these areas is mitigated by periodically flooding the fields with freshwater from the river network (Oude Essink et al., 2010). Although it is outside the scope of this study, a country's economic means to deal with environmental hazards occurring in major deltas ultimately affects the risk to coastal deltas (Tessler et al., 2015).

### 4.5.3. Limitation and implications of this study

Density-dependent groundwater modeling of large coastal areas over thousands of years requires significant computational time and data storage. Many simplifications and assumptions were made to achieve the models used in this study; these simplifications resulted in models that took between 2 and 15 days to run and required between 500 GB to 1 TB of memory for each model. This section outlines limitations within the modeling and the biggest simplifications that were made.

The groundwater models created in this study representing generic fluvial, wave, and tidal deltas were developed from numerical morphodynamic models that simulated sediment deposition in these three end-member deltaic environments (Chapter 2).

Considering that the morphodynamic modeling domain is 80 km x 100 km (chosen to represent the size of large coastal deltas throughout the world), the grid cell size needed to be large to reduce simulation runtimes. Since each grid cell is 200 m x 200 m, horizontal heterogeneity that varies within 200 m is neglected. The large cell size is a limitation because hydraulic conductivity within deltas can vary within a 200 m spatial scale. Overbank deposits and high permeability features caused by small channels (less than 200 m wide) are two features that are not reflected in the hydraulic conductivity in each model. Out of these two features, overbank deposits are more likely to have an impact on groundwater flow through a delta since these deposits typically have low permeability and may act as a barrier to horizontal groundwater exchange between the permeable channels/paleochannels and the surround sediments. A smaller cell size may have allowed for overbank deposits to be more distinguishable within the permeability maps by adding more low permeability material around the channel networks.

The morphodynamic and groundwater models use steady state boundary conditions to simplify the deltaic environments so that the longer timescale of delta formation can be simulated without leading to unreasonable runtimes. Although using steady state boundary conditions makes it feasible for us to investigate groundwater freshening and salinization that takes place within deltas over thousands of years, the models do not account for seasonal variability that greatly impacts the delta structure and the groundwater system. The morphodynamic models used to create the sediment distributions were created using steady state river and marine boundary conditions. In reality, temporal variability in annual rainfall and sediment delivery impact delta construction; seasonal flooding often provides the highest rates of sediment delivery and can result in delta building events (Davis and Fitzgerald, 2003). Seasonal high flows and extreme weather events also lead to the formation of overbank deposits and mud drapes and can act as a barrier to groundwater flow; these features were also not accounted for since the boundary conditions remain steady throughout the simulation. Within the groundwater models, the use of a constant head boundary condition for the river network may also underestimate the functionality of the river network in wet climates driven by seasonal flood or extreme weather events. The results of this study would benefit from the inclusion of seasonal variability within the boundary conditions and from a smaller spatial resolution that can account for variability of a small spatial scale.

Another limitation of this study is that the vertical structure of sediment deposition is not recorded in the morphodynamic models. This means that any sediment contained within a cell in the morphodynamic models is assumed to be “well-mixed”, producing vertically homogenous sediment deposits within the model. This simplification means that a vertical sediment structure impacting heterogeneity in the hydraulic conductivity vertically can not be discerned. Channel stacking patterns are important when considering vertical connectivity of fluvial sediment deposition within deltas around the world. Xu et al. (2022) found that vertical transport of groundwater contaminants is influenced by channel stacking patterns. The 2D planform models in this study only consider the lateral changes in hydraulic conductivity that are derived from channelization and do not capture any vertical variation. We hypothesize that including vertical heterogeneity in the hydraulic conductivity would make the systems more connected, which may lead to an underestimate of the salinization that occurs due to recharge reduction (i.e. pumping). Improvements to this work may include the use of 3D modeling or implementation of the stratigraphy module in Delft3D (Deltares, 2013), allowing for the preservation of sedimentation records vertically throughout the model simulation.

Many large coastal deltas around the world are a product of several marine transgressive and regressive periods that have created layered aquifer/aquitard structures. Our morphodynamic models only generate the sediment deposits representing from modern delta formation. This neglects the deeper vertically layered aquifer/aquitard structure and restricts the analysis to only looking at groundwater flow within the shallow subsurface. Additionally, the zero-flux boundary at the bottom of the groundwater models assumes that there are no interactions between the shallow and deep groundwater systems, which likely underestimates the volume of saline groundwater within the shallow subsurface because no upwelling of deeper salinity can occur. Although it would be a significant undertaking, modeling the formation of coastal deltas through several periods of marine transgression and regression would allow for a more representative deltaic subsurface. We hypothesis that the morphodynamic balance within a delta impacts the ability for channels to erode through marine confining units, ultimately controlling vertical groundwater flow between aquifer systems.

Feedbacks between the morphodynamic and groundwater systems are also not accounted for in the modeling. Using the output of the morphodynamic model at the end

of the simulation as an input into the groundwater model neglects the impacts groundwater can have on shaping delta morphology. We suspect that groundwater may impact sediment transport and deposition in deltas that have large areas of low permeability material that inhibit groundwater flow to the ocean and result in inundation; this was only seen in the fluvial models. To fully account for feedbacks between the surface and subsurface, integrated morphodynamic, surface water, and groundwater models are needed. The Community Surface Dynamics Modeling System (CSDMS) repository is making progress toward integration of models capable of simulating more complex systems (Community Surface Dynamics Modeling System, 2009). There is also potential for the integration of iMod with Delft3d since both softwares are developed under the umbrella of Deltares and use two of the most widely recognized codes for morphodynamic modeling and variable-density groundwater flow and solute transport models.

We used recharge reduction as a proxy for groundwater abstraction, but groundwater is actually pumped from the subsurface at specific locations, placing additional stress on certain parts of the aquifer. Including groundwater wells within a density-dependent flow model would greatly increase computation time and require detailed information about the location of wells and pumping rates. Unfortunately, compiling this kind of detailed information is a significant undertaking and data are not openly available for most coastal deltas. However, considering that the spatial and temporal changes that occur from groundwater pumping are critical to fully understand how groundwater pumping impacts salinity in the subsurface. Additionally, there are many stressors that have the potential to perpetuate salinization in the shallow subsurface. We do not consider the effects of storm surge, sea level rise, or upwelling of deeper salinity due to natural or anthropogenically induced ground subsidence. We also do not consider decreased surface water within the delta due to damming or water diversions upstream. These processes are important to gain precise estimates of the freshwater volume in coastal deltas and how this may change in the future.

In lieu of these limitations and simplifications, the groundwater models in this study provide important insights about how delta morphology can impact the amount and spatial distribution of freshwater within a delta and which types of deltas are most vulnerable to future groundwater salinization.

## 4.6. Conclusion

The interaction between delta morphology, climate, and population impacts the susceptibility of fresh groundwater in the subsurface and the vulnerability of coastal deltas to future groundwater quality degradation. We used numerical groundwater models to explore the impact morphology has on freshwater volumes in fluvial, wave, and tidal deltas. The numerical modeling results along with morphodynamic, recharge, and population data were used to investigate the vulnerability of 55 of the world's largest and most populated deltas to salinization of the shallow subsurface. We found that:

1. Wave deltas are more susceptible to groundwater salinity in the shallow subsurface than fluvial and tidal deltas. Wave deltas also have the highest salinization rates when groundwater is abstracted. These deltas are particularly sensitive because of the increased hydraulic conductivity within the delta, a low hydraulic gradient, and fewer river channels.

2. We estimate that the volume of saline water in the shallow subsurface within deltas around the world varies between 36% and 89% of the total groundwater volume, depending on the delta type and the amount of recharge the delta receives. Deltas receiving less recharge are more susceptible to groundwater salinity compared to deltas in wet climates that receive substainial recharge (more than 100 mm/yr).

3. Although deltas located in a wet climates (receiving more than than 100 mm/yr of recharge) have greater freshwater volume in the shallow subsurface, these deltas are most impacted by groundwater abstraction. Freshwater volumes of groundwater in wet climates can decrease by up to 24% in a wave delta and 5% in a fluvial delta within 500 years. Deltas located in dry climates are more resistant to decreases in groundwater recharge.

4. The number and location of delta channels in a delta play an important role in determining the fresh groundwater volume. In dry climates, rivers are responsible for most of the freshening that has occurred in the past 8 ky of modern delta formation. In wet climates, the role of the river network to supply or remove water from the shallow subsurface is highly sensitive to changes in groundwater removal and supply when channels are not abundant throughout the delta.

5. The freshwater lens that develops in the shallow subsurface is often deepest surrounding the river networks in fluvial and tidal deltas. In wave deltas, the freshwater lens is deepest adjacent to the river network in the subaerial levees. Salinity is most likely found in areas with low hydraulic conductivity that are not near a river channel.

## 4.7. Data availability

All data used in this study were previously published. Supplemental data in Appendix E provides a spreadsheet outlining the morphodynamic, geomorphic, and hydrogeologic characteristics of the 60 global deltas investigated in this study.

A version of this chapter is in preparation for publication. Upon publication of the journal article, example models and the source code for model processing will be available at https://github.com/aspenmanderson/delta_groundwater_modeling. These resources are also available upon request.

# Chapter 5.

# Conclusions, Contributions, and Recommendations

The research presented in this thesis demonstrates that there is a link between delta morphology and fresh groundwater resources in coastal deltas. Data from deltas around the world were used to inform numerical morphodynamic models that reproduced coastal delta formation under varying fluvial, wave, and tidal influences (Chapter 2). The deltas created in the morphodynamic models are used to create spatially varying permeability profiles for each delta and explore the connectivity of high permeability material within coastal deltas (Chapter 3). A distance-based generalized sensitivity analysis shows how morphodynamic influences and geomorphic characteristics impact the permeability, hydraulic gradient, and groundwater flow rate through a delta (Chapter 3). The permeability profiles of three-end member delta morphologies are used to develop density-dependent groundwater flow and solute transport models for representative fluvial, wave, and tidal deltas (Chapter 4). The vulnerability of shallow deltaic groundwater resources to salinization is calculated for 60 of the world's largest and most populated global deltas. The following sections highlight the main conclusions from Chapters 2-4 and the significant contributions of the research. Recommendations to build upon this work are also included.

## 5.1. Conclusions

**Chapter 2:** Controls on coastal delta formation under varying morphodynamic conditions and basin characteristics.

Data from 51 large coastal deltas around the world were used to inform numerical models simulating the formation of coastal deltas under various combinations of morphodynamic (fluvial discharge (Qav), wave height (Wa), tidal range (Ti)) and basin conditions (sediment concentration (Cs), bathymetric gradient (Dgrd), median grain size (Dmm)). Data for the 51 deltas show that large deltas can form across a wide range of wave height and tidal amplitude, indicating that the presence of marine influences does not inhibit sediment deposition. The numerical models created in this study support these observations; models that have high wave and tidal influence can form deltas in

environments where there is adequate fluvial discharge supplying sediment. All models form deltas when the Qav > 2,000 $m^3/s$, Cs > 0.05 $kg/m^3$, and the fluvial discharge comprises over 50% of the morphodynamic influence. When one or more of these conditions are not met, there is a greater likelihood that a delta will not form. Differences in Cs and Dgrd were found to impact whether models with the same balance of morphodynamic influences either form a delta or do not. I suggest that although the classic Galloway ternary diagram is a useful tool to compare delta morphology, it does not explain why some combinations of fluvial, wave, and tidal influences result in delta formation while others do not.

**Chapter 3:** Sensitivity of groundwater flux and subsurface permeability to morphodynamics and geomorphic characteristics of coastal deltas.

Quantitative evaluation of groundwater supply in coastal deltas requires the estimation of large-scale hydrogeologic characteristics that control groundwater flow. This study evaluated the horizonal permeability distribution in fluvial, wave, and tidal deltas. The sensitivity analysis suggests that permeability, hydraulic gradient, and the connectiveness of high permeability bodies can be characterized through the identification of morphodynamic influences (fluvial, waves, tides) and geomorphic characteristics (number of channels, shoreline rugosity) within a delta. Using numerical morphodynamic modeling of delta formation in 171 unique models, I found that:

1. The overall permeability in deltaic landforms has a median value of $4.0x10^{-12}$ $m^2$, relating to a hydraulic conductivity value of $2x10^{-5}$ m/s. The average hydraulic gradient is $4x10^{-4}$. Wave deltas are the most permeable and have the lowest hydraulic gradient while tidal are the least permeable and have the highest hydraulic gradient.

2. The high permeability bodies are associated with current and previous channelization in a delta and are highly connected horizontally. This high connectivity potentially allows for salinization of the subsurface through permeable pathways as sea level rises. The channel network is most evenly distributed in tidal deltas, resulting in high permeability bodies located throughout the entire delta plain. High permeability bodies in wave deltas are only located in the channel levees and are not pervasive throughout the entire delta.

3. Wave deltas may be most susceptible to inundation and groundwater salinization through marine encroachment due to the lower hydraulic gradient and increased permeability.

**Chapter 4:** Impact of delta morphology on vulnerability of large coastal deltas to groundwater salinization.

The interaction between delta morphology, climate, and population impacts the susceptibility of fresh groundwater in the subsurface and the vulnerability of coastal deltas to future groundwater quality degradation. I used numerical groundwater models to explore the impact morphology has on freshwater volumes in fluvial, wave, and tidal deltas. The numerical modeling results along with morphodynamic, recharge, and population data were used to investigate the vulnerability of 55 of the world's largest and most populated deltas to salinization of the shallow subsurface. I found that:

1. Wave deltas are more susceptible to groundwater salinity in the shallow subsurface than fluvial and tidal deltas. Wave deltas also have the highest salinization rates when groundwater is abstracted. These deltas are particularly sensitive because of the increased hydraulic conductivity within the delta, low hydraulic gradient, and fewer river channels.

2. I estimate that the volume of saline water in the shallow subsurface within deltas around the world varies between 36% and 89% of the total groundwater volume, depending on the delta type and the amount of recharge the delta receives. Deltas receiving less recharge are more susceptible to groundwater salinity compared to deltas in wet climates that receive substantial recharge (more than 100 mm/yr).

3. Although deltas located in a wet climates (receiving more than than 100 mm/yr of recharge) have greater freshwater volume in the shallow subsurface, these deltas are most impacted by groundwater abstraction. Freshwater volumes of groundwater in wet climates can decrease by up to 24% in a wave delta and 5% in a fluvial delta within 500 years. Deltas located in dry climates are more resistant to decreases in groundwater recharge.

4. The number and placement of rivers in a delta play an important role in determining the fresh groundwater volume. In dry climates, rivers are responsible for most of the freshening that has occurred in the past 8 ky of modern delta formation. In wet climates, the role of the river network to supply or remove water from the shallow subsurface is highly sensitive to changes in groundwater removal and supply when channels are not abundant throughout the delta.

5. The freshwater lens that develops in the shallow subsurface is often deepest surrounding the river networks in fluvial and tidal deltas. In wave deltas, the freshwater lens is deepest adjacent to the river network in the subaerial levees. Salinity is most likely found in areas with low hydraulic conductivity that are not near a river channel.

## 5.2. Contributions

Research undertaken in this thesis builds upon the current scientific literature through the following contributions:

- ***Developing morphodynamic models with varying wave and tidal influence.*** Even though many of the 2D and 3D morphodynamic models have the capability to include fluvial, wave, and tidal processes within the modeling framework (Overeem et al., 2011), Edmonds et al. (2021) stated “we are unaware of any single model that can reproduce the diversity of river, wave, and tide dominated features that Galloway tried to explain”. The models created in Chapter 2 incorporate the range fluvial discharge, wave height, and tidal amplitude seen in coastal deltas around the world. The resulting sediment structures depict the morphologies expected in a fluvial, wave, and tidal influenced delta.

- ***Determining the range of morphodynamic influences and basin conditions that result in the formation of coastal deltas.*** Although Galloway’s ternary diagram (Galloway, 1975) is a useful tool to compare delta morphology, it does not explain why some combinations of fluvial, wave, and tidal influences result in delta formation while others do not. In Chapter 2, I showed that delta formation is overall most sensitive to incoming fluvial discharge. However, the sensitivity of delta formation to fluvial discharge, wave heigh, tidal amplitude, bathymetric

gradient and sediment concentration is dependant on the morphodynamic balance within the basin.

- ***Investigating the role of tides in coastal delta formation.*** Previous research proposed that the ability of wave and tidal action to change fluvial constructive processes is largely unknown, but it was hypothesized that waves, and possibly tides, suppress delta formation (Caldwell et al., 2019). The results in Chapter 2 suggest that tidal action increases the ability for a delta to form in the absence of waves or when wave influence is small compared to the fluvial and tidal influence; these results warrant further research to fully understand the role of tides in delta formation.

- ***Linking delta morphology to subsurface permeability and groundwater salinity within shallow deltaic aquifers.*** Recently research has shown that channelization impacts the subsurface structure of a delta and creates permeable pathways for contaminant transport (Kolker et al., 2013; Hariharan et al., 2021; Xu et al., 2021, 2022; Steel et al., 2022a). Although the generic models used in those studies allow for a deeper understanding of the interactions between delta morphology and the groundwater system, the influence of waves and tides had not yet been considered in coupled morphodynamic-groundwater models. The modeling methods developed in Chapters 3 and 4 incorporate wave and tidal deltas. I show that deltaic permeability, hydraulic gradient, and the volume of freshwater within a delta is sensitive to changes in morphodynamic influences as well as geomorphic characteristics of a delta (i.e., variations in the channel network and shoreline rugosity). These results are novel and suggest that the subsurface properties and distribution of groundwater salinity within a delta can be inferred by simply identifying if the delta is fluvial, wave, or tidal.

- ***Exploring the range of subsurface permeability, how permeability changes spatially, and how connective highly permeable bodies are in deltas with varying morphologies.*** Considering that there are likely over 2,000 coastal deltas estimated to exist around the world (Syvitski et al., 2022), the spatial quantification of the subsurface permeability and groundwater flow through the delta has been thoroughly studied in a handful of deltas, including the Ganges-Brahmaputra (Michael and Voss, 2009; Khan et al., 2016; Michael and Khan,

2016), Mekong (Minderhoud et al., 2015; Van Pham et al., 2019), Red River (Tran et al., 2012; Larsen et al., 2017), Nile (van Engelen et al., 2019), Po (Mollema et al., 2013; Antonellini et al., 2015), and Rhine-Meuse (Post et al., 2003; de Louw et al., 2010; Oude Essink et al., 2010; Delsman et al., 2014). The use of generalized delta models in Chapter 3 provides insights into the range of permeability in deltas globally and allows for investigation of how permeability is impacted by variations in morphodynamic influences. Chapter 3 also shows that high permeability bodies are highly connective within the subsurface and are associated with channelization.

- ***Estimating fresh groundwater volume in coastal deltas and determining which deltas are most susceptible to groundwater salinity.*** Subsurface salinization is the biggest factor limiting freshwater resources in coastal areas, making it imperative to understand how much salinity exists and how it is transported in the subsurface. Half of the 60 deltas evaluated in Chapter 4 have known groundwater salinity that was emplaced during previous marine transgressions (Larsen et al., 2017; van Engelen, 2020). I estimate that the volume of saline water in the shallow subsurface within deltas around the world varies between 36% and 89%, depending on the morphodynamic influences and the amount of recharge the delta receives. Results of the groundwater flow and solute transport modeling in Chapter 4 show that deltas located in dry climates are most susceptible to salinity within the shallow subsurface and that deltas classified as a wave or fluvial delta are especially susceptible.

- ***Determining the vulnerability of large coastal deltas around the world to salinization of shallow groundwater systems.*** Given the high population density of deltas and the importance of deltas from an ecological perspective, many recent review papers have summarized the current risk to deltaic land and evaluated the sustainability of these landscapes (Syvitski, 2008; Giosan et al., 2014; Ingebritsen and Galloway, 2014; Elliott et al., 2019). Dewatering of aquifers due to over pumping of groundwater promotes coastal subsidence through the collapse of pore space within the porous media, making sustainable groundwater abstraction a priority in many populated deltas. So far, scientific studies have overlooked the potential threat groundwater salinization poses to the sustainability of population centers living on coastal deltas. Results of Chapter 4

show that vulnerability to groundwater salinization in the shallow subsurface is greatest in the: 1) Vistula, 2) Ganges-Brahmaputra, 3) Yangtze, 4) Mekong, 5) Niger, 6) Pearl, 7) Song Hong, 8) Nile, 9) Irrawaddy, and 10) Mahanadi deltas. Out of these ten deltas, seven are tidal deltas located in Southern Asia. Although these deltas receive abundant groundwater recharge, the population living on these deltas makes up 65% of the global population living on coastal deltas.

## 5.3. Recommendations

While this research provides important contributions to the field, future efforts building upon this work are encouraged. Recommendations to refine and expand on this research include:

- ***Incorporating variable forcings in the morphodynamic modeling.*** Over the past 8.5 ky, deltas have experienced variability in fluvial and marine influence on a variety of temporal scales ranging from hours to decades. For instance, reductions in fluvial discharge during periods of drought can supress delta building, while seasonal monsoons and extreme weather events can result in flooding and large influxes of fluvial sediment to the delta. The morphodynamic models created in Chapter 2 and the groundwater models created in Chapter 4 only consider steady boundary conditions and do not account for extreme weather events, seasonality variability, or changes in the long-term averages over the Holocene. Although it does not appear that this variability is necessary to form a delta; variability through time may be responsible for giving deltas their unique character and shape. Seasonal variability and extreme weather events have not yet been included in long time scale groundwater modeling due to the computational requirements, so it is unclear how the inclusion of this variability may impact the fresh-saline groundwater interface and the amount of freshwater in deltaic subsurface. The inclusion of increased variability in the boundary conditions would more accurately reproduce the environments that coastal deltas form in.

- ***Quantification of delta morphology that better aligns with qualitative observations.*** Traditionally, the morphodynamics of a delta has been described qualitatively based on the identification and interpretation of deltaic structures

and sediment deposition patterns in comparison the Galloway ternary diagram (Galloway, 1975). Although recent work has made progress toward a goal of quantifying the ternary diagram (Nienhuis et al., 2020; Broaddus et al., 2022), discrepancies exist between the proposed quantitative morphodynamics and the qualitative morphodynamic features of certain deltas. For instance, the Po Delta exhibits a cuspate shape, has a smooth shoreline, and only have a few channels cutting through the delta plain, suggesting that the delta is primarily wave influenced when analyzed qualitatively. Nienhuis et al. (2020) shows that the Po Delta is primarily fluvial delta and has secondary tidal and wave influences (Figure 1.2 and Figure 4.3). Syvitski et al. (2022) points out that the computed sediment fluxes calculated in Nienhuis et al. (2020) are “unreliable” due to the use of converging-flow theory, which is often not applicable in coastal deltas where there is divergence in river flow through the distributary channels. Converging-flow theory predicts the sediment flux over all the distributary channels in a delta and assumes this flux occurs at one distributary mouth, concentrating the fluvial sediment fluxes in a narrow portion of the delta. The results of the vulnerability analysis in Chapter 4 are dependant upon the morphodynamic classification of the deltas included. The results of the vulnerability analysis would change significantly if the primary morphodynamic influence of delta changes, making it critical to have accurate quantifications of the delta morphodynamics. Yet, the models and vulnerability analysis method developed in Chapter 4 can be used to reproduce the vulnerability analysis if other ways of quantifying delta morphodynamics becomes available.

- ***Using more sophisticated modeling software to incorporate system feedbacks.*** Feedbacks between the morphodynamic and groundwater systems are not accounted for in this study because a one-way coupling was used, whereby the output of the morphodynamic model at the end of the simulation was used as an input into the groundwater model; this neglects the impacts groundwater can have on shaping delta morphology. To fully account for feedbacks between the surface and subsurface, integrated morphodynamic, surface water, and groundwater models are needed. The CSDMS repository is making progress toward integration of models capable of simulating these complex systems (Community Surface Dynamics Modeling System, 2009). There

is also potential for the integration of iMod with Delft3d since both softwares are developed under the umbrella of Deltares and use two of the most widely recognized codes for morphodynamic modeling and variable-density groundwater flow and solute transport modeling.

- ***Increasing observational data.*** The morphodynamic models built in Chapter 2 are based on morphodynamic and basin parameters gathered from 51 deltas around the world. Unfortunately, observations of the median grain size of sediment supplied to deltas are limited; only 19 deltas in the dataset have this information. I chose to use the same median grain size for all delta types because of the limited data. However, closer investigation shows that some fluvial deltas (the Mississippi and Waipaoa) have a grain size considerably larger than the median grain size used in the fluvial models. Since fluvial deltas do not have the natural sorting properties that exist within tidal and wave deltas, a higher median grain size would likely change the permeability within the fluvial model, in turn impacting groundwater freshening/salinization. More observations of sediment supply grain size around the world would allow for more accurate representation of the sediment, permeability, and groundwater salinity within fluvial deltas with minimal wave and tidal influence.

- ***Incorporating vertical heterogeneity.*** The use of a depth averaged sediment transport model to create the deltas in Chapter 2 captures the horizontal heterogeneity in sediment deposits but does not accurately represent the sediment horizons vertically. As such, I was unable to consider interactions of the shallow groundwater system with deeper aquifers in Chapter 4, which can have a significant impact on the salinity within the shallow subsurface, especially where groundwater pumping and land subsidence have changed the vertical hydraulic gradient within a delta. Vertical groundwater flow is also primarily responsible for contamination in the shallow groundwater systems in the Rhine-Meuse Delta, The Netherlands (Delsman et al., 2014). Deltf3D has the capability to preserve sedimentation vertically within the depth-averaged models and would be a good tool for investigating vertical heterogeneity with deltas.

- ***Comparative case-studies between generic modeling and real-world deltas.*** The results of the groundwater modeling in Chapter 4 are not validated because

generic modeling is used to explore processes rather than recreating accurate groundwater systems. One way to validate the modeling methods used would be to first create a morphodynamic model using the morphology and basin conditions specific to a real delta. The spatially varying permeability of the modeled delta could be calculated using the methods in Chapter 3, and the evolution of the groundwater system throughout the Holocene could be investigated using the methods in Chapter 4. The resulting spatially variable groundwater system could then be compared to groundwater salinity measurements collected from the real delta. This additional research may provide insights on how to improve the methods used in Chapters 2-4.

- ***Including more variation in delta morphology in the groundwater modeling.*** The groundwater models created in Chapter 4 are representative of end-member delta geomorphologies for a fluvial, wave, and tidal influenced delta. Although scientific literature tends to pigeon-hole deltas into one of these end-member archetypes, most deltas have a unique mixture of the three influences, in addition to other basin conditions (such as bathymetry, incoming sediment concentration, and grain size). The groundwater modeling in Chapter 4 would benefit from the addition of more delta structures representing the combination of morphodynamic influences.

- ***Calculation of risk in coastal deltas.*** Considering that the mitigation of groundwater resource degradation is often costly, it is critical to recognize that wealthy countries can effectively limit environmental hazards through investment into mitigation infrastructure (Tessler et al., 2015). Effective mitigation strategies to reduce subsidence and salinization from groundwater abstraction include using alternative water sources (piped water, high quality surface water, or desalinized water), relocating/distributing groundwater abstraction to areas that are less exploited or where subsidence is less harmful, and employing managed aquifer recharge/groundwater injection (Minderhoud et al., 2020). Although it was outside the scope of this thesis, quantifying economic means to mitigate groundwater salinization would be beneficial and provide a more accurate list of the deltas that are at risk for groundwater salinization.

# References


Anderson, M.P., Woessner, W.W., and Hunt, R.J., 2015, Applied Groundwater Modeling; Simulation of Flow and Advective Transport: Elsevier Inc.

Antonellini, M., Allen, D.M., Mollema, P.N., Capo, D., and Greggio, N., 2015, Groundwater freshening following coastal progradation and land reclamation of the Po Plain, Italy: Hydrogeology Journal, v. 23, p. 1009–1026, doi:10.1007/s10040-015-1263-0.

Antonellini, M., Mollema, P., Giambastiani, B., Bishop, K., Caruso, L., Minchio, A., Pellegrini, L., Sabia, M., Ulazzi, E., and Gabbianelli, G., 2008, Salt water intrusion in the coastal aquifer of the southern Po Plain, Italy: Hydrogeology Journal, v. 16, p. 1541–1556, doi:10.1007/s10040-008-0319-9.

Barlow, P.M., and Reichard, E.G., 2010, Saltwater intrusion in coastal regions of North America: Hydrogeology Journal, v. 18, p. 247–260, doi:10.1007/s10040-009-0514-3.

Bates, C., 1953, Rational theory of delta formation, *in* AAPG Bulletin, p. 2119–2162.

BenSaïda, A., 2021, Shapiro-Wilk and Shapiro-Francia normality tests:, https://www.mathworks.com/matlabcentral/fileexchange/13964-shapiro-wilk-and-shapiro-francia-normality-tests.

Beven, K., and Binley, A., 1992, The future of distributed models: Model calibration and uncertainty prediction: Hydrological Processess, v. 6, p. 279–298.

Bridger, D.W., and Allen, D.M., 2006, An investigation into the effects of diffusion on salinity distribution beneath the Fraser River Delta, Canada: Hydrogeology Journal, v. 14, p. 1423–1442, doi:10.1007/s10040-006-0060-1.

Broaddus, C.M., Vulis, L.M., Nienhuis, J.H., Tejedor, A., Brown, J., Foufoula-Georgiou, E., and Edmonds, D.A., 2022, First-order River Delta Morphology is Explained by the Sediment Flux Balance from Rivers, Waves, and Tides: Geophysical Research Letters, p. 1–10, doi:10.1029/2022gl100355.

Caldwell, R.L., and Edmonds, D.A., 2014, The effects of sediment properties on deltaic processes and morphologies: A numerical modeling study: Journal of Geophysical Research: Earth Surface, v. 119, p. 961–982, doi:10.1002/2013JF002965.

Caldwell, R.L., Edmonds, D.A., Baumgardner, S., Paola, C., Roy, S., and Nienhuis, J.H., 2019, A global delta dataset and the environmental variables that predict delta formation on marine coastlines: Earth Surface Dynamics, v. 7, p. 773–787, doi:10.5194/esurf-7-773-2019.

Cao, G., Han, D., and Moser, J., 2013, Groundwater exploitation management under land subsidence constraint: Empirical evidence from the hangzhou-jiaxing-huzhou plain, China: Environmental Management, v. 51, p. 1109–1125, doi:10.1007/s00267-013-0037-5.

Chawla, A., Spindler, D.M., and Tolman, H.L., 2013, Validation of a thirty year wave hindcast using the Climate Forecast System Reanalysis winds: Ocean Modelling, v. 70, p. 189–206, doi:10.1016/j.ocemod.2012.07.005.

Community Surface Dynamics Modeling System, 2009, CSDMS Model Repository:, https://csdms.colorado.edu/wiki/Model_download_portal.

Costanza, R. et al., 1997, The value of the world's ecosystem services and natural capital. LK - https://royalroads.on.worldcat.org/oclc/4592801201: Nature TA - TT -, v. 387, p. 253–260, https://www-nature-com.ezproxy.royalroads.ca/articles/387253a0.pdf.

Custodio, E., 2002, Aquifer overexploitation: What does it mean? Hydrogeology Journal, v. 10, p. 254–277, doi:10.1007/s10040-002-0188-6.

Custodio, E., and Bruggeman, G.A., 2013, Groundwater problems in coastal areas: Internatinal Hydrological Programme, v. 53, p. 1689–1699, doi:10.1017/CBO9781107415324.004.

Dalrymple, R.W., and James, N.P., 2010, Facies Models 4: Geological Association of Canada, v. 4.

Davis, R.A., 1983, Depositional Systems: An Genetic Approach to Sedimentary

Geology: Englewood Cliffs, New Jersey, Prentice-Hall, Inc.

Davis, K.F., Bhattachan, A., D'Odorico, P., and Suweis, S., 2018, A universal model for predicting human migration under climate change: examining future sea level rise in Bangladesh: Environmental Research Letters, v. 13, p. 064030, doi:10.1088/1748-9326/aac4d4.

Davis, R.A., and Fitzgerald, D.M., 2003, River Deltas: The Source of Most of our Coastal Sediments, *in* Beaches and Coasts, Wiley-Blackwell, p. 432.

Day, J.W. et al., 2016, Approaches to defining deltaic sustainability in the 21st century: Estuarine, Coastal and Shelf Science, v. 183, p. 275–291, doi:10.1016/j.ecss.2016.06.018.

Day, J.W., Ramachandran, R., Giosan, L., Syvitski, J., and Kemp, G.P., 2019, Delta Winners and Losers in the Anthropocene: , p. 149–165.

Delsman, J.R., Hu-a-ng, K.R.M., Vos, P.C., de Louw, P.G.B., Oude Essink, G.H.P., Stuyfzand, P.J., and Bierkens, M.F.P., 2014, Paleo-modeling of coastal saltwater intrusion during the Holocene: An application to the Netherlands: Hydrology and Earth System Sciences, v. 18, p. 3891–3905, doi:10.5194/hess-18-3891-2014.

Delsman, J.R., Winters, P., Vandenbohede, A., Essink, G.H.P.O., Lebbe, L., Oude Essink, G.H.P., and Lebbe, L., 2016, Global sampling to assess the value of diverse observations in conditioning a real-world groundwater flow and transport model: Water Resources Research, v. 52, p. 1652–1672, doi:10.1002/2014WR016476.

Deltares, 2013, Delft3D-Flow: Simulation of Multi-Dimensional Hydrodynamic Flows and Transport Phenomena, Including Sediments-User Manual: , p. 614, https://oss.deltares.nl/web/delft3d/download (accessed April 2021).

Deltares, 2021, iMOD:, https://deltares.github.io/iMOD-Documentation/viewer_index.html.

Deltares, 2012, User manual Delft3D-FLOW: , p. 676.

Döll, P., and Fiedler, K., 2008, Global-scale modeling of groundwater recharge:

Hydrology and Earth System Sciences, v. 12, p. 863–885, doi:10.5194/hess-12-863-2008.

Domenico, P.A., and Schwartz, F.W., 1990, Physical and Chemical Hydrogeology: New York, John Wiley & Sons, Inc., 824 p.

Dunn, F.E., Darby, S.E., Nicholls, R.J., Cohen, S., Zarfl, C., and Fekete, B.M., 2019, Projections of declining fluvial sediment delivery to major deltas worldwide in response to climate change and anthropogenic stress: Environmental Research Letters, v. 14, doi:10.1088/1748-9326/ab304e.

Edmonds, D.A., Caldwell, R.L., Brondizio, E.S., and Siani, S.M.O., 2020, Coastal flooding will disproportionately impact people on river deltas: Nature Communications, v. 11, p. 1–8, doi:10.1038/s41467-020-18531-4.

Edmonds, D.A., Chadwick, A.J., Lamb, M.P., Lorenzo-Trueba, J., Murry, B.A., Nardin, W., Salter, G., and Shaw, J.B., 2021, Morphodyanmic Modeling of River-Dominated Deltas: A Review and Future Perspectives, *in* Treatise on Geomorphology, Uncorrected Proof, doi:10.1016/B978-0-12-818234-5.00076-6.

Edmonds, D.A., and Slingerland, R.L., 2010, Significant effect of sediment cohesion on deltamorphology: Nature Geoscience, v. 3, p. 105–109, doi:10.1038/ngeo730.

Egbert, G.D., and Erofeeva, S.Y., 2002, Efficient inverse modeling of barotropic ocean tides: Journal of Atmospheric and Oceanic Technology, v. 19, p. 183–204, doi:10.1175/1520-0426(2002)019<0183:EIMOBO>2.0.CO;2.

Elliott, M., 2009, A burst of energy: Industrial Engineer, v. 41, p. 28–29, doi:10.5194/hessd-10-10873-2013.

Elliott, T., 2005, Sedimentary Environments- Deltas, *in* Encyclopedia of Geology, Amsterdam, The Netherlands, Elsevier, p. 528–539.

Elliott, M., Day, J.W., Ramachandran, R., and Wolanski, E., 2019, A Synthesis: What Is the Future for Coasts, Estuaries, Deltas and Other Transitional Habitats in 2050 and Beyond? Coasts and Estuaries, p. 1–28, doi:10.1016/b978-0-12-814003-1.00001-0.

van Engelen, J., 2020, Fresh Groundwater Reserves in Major Deltas: Evolution and Current State of Deltaic Groundwater Resources: Utrecht, 194 p.

van Engelen, J., Essink, G.O., and Bierkens, M.F.P., 2022, Sustainability of fresh groundwater resources in fifteen major deltas around the world: Environmental Research Letters, doi:10.1088/1748-9326/aca16c.

van Engelen, J., Oude Essink, G.H.P., Kooi, H., and Bierkens, M.F.P., 2018, On the origins of hypersaline groundwater in the Nile Delta aquifer: Journal of Hydrology, v. 560, p. 301–317, doi:10.1016/j.jhydrol.2018.03.029.

van Engelen, J., Verkaik, J., King, J., Nofal, E.R., Bierkens, M.F.P.P., and Oude Essink, G.H.P., 2019, A three-dimensional palaeohydrogeological reconstruction of the groundwater salinity distribution in the Nile Delta Aquifer: Hydrology and Earth System Sciences, v. 23, p. 5175–5198, doi:10.5194/hess-23-5175-2019.

Erban, L.E., Gorelick, S.M., and Zebker, H.A., 2014, Groundwater extraction, land subsidence, and sea-level rise in the Mekong Delta, Vietnam: Environmental Research Letters, v. 9, doi:10.1088/1748-9326/9/8/084010.

Ericson, J.P., Vörösmarty, C.J., Dingman, S.L., Ward, L.G., Meybeck, M., Vorosmarty, C.J., Dingman, S.L., Ward, L.G., and Meybeck, M., 2006, Effective sea-level rise and deltas: Causes of change and human dimension implications: Global and Planetary Change, v. 50, p. 63–82, doi:10.1016/j.gloplacha.2005.07.004.

Fenwick, D., Scheidt, C., and Caers, J., 2014, Quantifying Asymmetric Parameter Interactions in Sensitivity Analysis: Application to Reservoir Modeling: Mathematical Geosciences, v. 46, p. 493–511, doi:10.1007/s11004-014-9530-5.

Ferguson, G., and Gleeson, T., 2012, Vulnerability of coastal aquifers to groundwater use and climate change: Nature Climate Change, v. 2, p. 342–345, doi:10.1038/nclimate1413.

Fisher, W.L., Brown, L.F., Scott, A.J., and McGowen, J.H., 1969, Delta Systems in the Exploration for Oil and Gas, *in* A Research Colloquium., Austin, Texas, Bureau of Economic Geology, p. 102.

Galloway, W.E., 1975, Process Framework for Describing the Morphological and Stratigraphic Evolution of Deltaic Depositional Systems: Deltas: Models for Exploration, p. 87–98.

Geleynse, N., Storms, J.E.A., Stive, M.J.F., Jagers, H.R.A., and Walstra, D.J.R., 2010, Modeling of a mixed-load fluvio-deltaic system: Geophysical Research Letters, v. 37, p. 1–7, doi:10.1029/2009GL042000.

Geleynse, N., Storms, J.E.A., Walstra, D.J.R., Jagers, H.R.A., Wang, Z.B., and Stive, M.J.F., 2011, Controls on river delta formation; insights from numerical modelling: Earth and Planetary Science Letters, v. 302, p. 217–226, doi:10.1016/j.epsl.2010.12.013.

Gibbs, R.J., Matthews, M.D., and Link, D.A., 1971, The relationship between sphere size and settling velocity: Journal of Sedimentary Research, v. 41, p. 7–18, https://doi.org/10.1306/74D721D0-2B21-11D7-8648000102C1865D.

Giosan, L., Syvitski, J., Constantinescu, S., and Day, J., 2014, Climate change: Protect the world's deltas: Nature, v. 516, p. 31–33, doi:10.1038/516031a.

Gleeson, T., Marklund, L., Smith, L., and Manning, A.H., 2011, Classifying the water table at regional to continental scales: Geophysical Research Letters, v. 38, p. 1–6, doi:10.1029/2010GL046427.

Golder Associates, 2014, Poverty Bay Groundwater Management: MAR Feasibility Stage 1A-Conceptual Model.:

Haitjema, H.M., and Mitchell-Bruker, S., 2005, Are water tables a subdued replica of the topography? Ground Water, v. 43, p. 781–786, doi:10.1111/j.1745-6584.2005.00090.x.

Hariharan, J., Passalacqua, P., Xu, Z., Michael, H.A., Steel, E., Chadwick, A., Paola, C., and Moodie, A.J., 2022, Modeling the Dynamic Response of River Deltas to Sea-Level Rise Acceleration: Journal of Geophysical Research: Earth Surface, v. 127, p. 1–21, doi:10.1029/2022jf006762.

Hariharan, J., Xu, Z., Michael, H.A., Paola, C., Steel, E., and Passalacqua, P., 2021,

Linking the Surface and Subsurface in River Deltas—Part 1: Relating Surface and Subsurface Geometries: Water Resources Research, v. 57, p. 1–31, doi:10.1029/2020WR029282.

Hazen, A., 1911, Discussion of dams on sand foundations: Transactions of the American Society of Civil Engineers, v. 73, p. 199–203.

Hoitink, A., Buschman, F., Sassi, M., De Brye, B., Tarya, A., Hidayat, H., Vermeulen, B., Van der Vegt, M., Hoekstra, P., and Deleersnijder, E., 2011, River-tide interactions observed from novel measurement methods and modelling: implications for pathways of sediment and delta morphology, *in* American Geophysical Union, Fall Meeting 2011, abstract id. EP44A-03,.

Hoitink, A.J.F., Nittrouer, J.A., Passalacqua, P., Shaw, J.B., Langendoen, E.J., Huismans, Y., and van Maren, D.S., 2020, Resilience of River Deltas in the Anthropocene: Journal of Geophysical Research: Earth Surface, v. 125, p. 1–24, doi:10.1029/2019JF005201.

Hoitink, A.J.F., Wang, Z.B., Vermeulen, B., Huismans, Y., and Kästner, K., 2017, Tidal controls on river delta morphology: Nature Geoscience, v. 10, p. 637–645, doi:10.1038/ngeo3000.

Holding, S., and Allen, D.M., 2016, Risk to water security for small islands: an assessment framework and application: Regional Environmental Change, v. 16, p. 827–839, doi:10.1007/s10113-015-0794-1.

Ingebritsen, S.E., and Galloway, D.L., 2014, Coastal subsidence and relative sea level rise: Environmental Research Letters, v. 9, doi:10.1088/1748-9326/9/9/091002.

Isikdogan, F., Bovik, A., and Passalacqua, P., 2017, RivaMap: An automated river analysis and mapping engine: Remote Sensing of Environment, v. 202, p. 88–97, doi:10.1016/j.rse.2017.03.044.

Jaworska-Szulc, B., 2009, Groundwater flow modelling of multi-aquifer systems for regional resources evaluation: The Gdansk hydrogeological system, Poland: Hydrogeology Journal, v. 17, p. 1521–1542, doi:10.1007/s10040-009-0473-8.

Khan, M.R. et al., 2016, Megacity pumping and preferential flow threaten groundwater quality: Nature Communications, v. 7, p. 1–8, doi:10.1038/ncomms12833.

Kim, J.H., Kim, K.H., Thao, N.T., Batsaikhan, B., and Yun, S.T., 2017, Hydrochemical assessment of freshening saline groundwater using multiple end-members mixing modeling: A study of Red River delta aquifer, Vietnam: Journal of Hydrology, v. 549, p. 703–714, doi:10.1016/j.jhydrol.2017.04.040.

Klassen, J., and Allen, D.M., 2017, Assessing the risk of saltwater intrusion in coastal aquifers: Journal of hydrology, v. 551, p. 730–745, doi:10.1016/j.jhydrol.2017.02.044.

Kolker, A.S., Cable, J.E., Johannesson, K.H., Allison, M.A., and Inniss, L. V., 2013, Pathways and processes associated with the transport of groundwater in deltaic systems: Journal of Hydrology, v. 498, p. 319–334, doi:10.1016/j.jhydrol.2013.06.014.

Kooi, H., Bakr, M., Lange, G. de, Haan, E. den, and Erkens, G., 2018, User Guide to SUB-CR- a MODFLOW package for land subsidence and aquifer system compaction that includes creep:, papers2://publication/uuid/07BB64DA-4396-46EB-BB50-3F3D4C8B4833.

Langevin, C., 2009, SEAWAT: A Computer Program for Simulation of Variable-Density Groundwater Flow and Multi-Species Solute and Heat Transport.: U.S. Geological Survey Fact Sheet, v. 3047, p. 2, doi:10.1007/s10040-009-0511-6.Dausman.

Langevin, C.D., Thorne, D.T., Dausman, A.M., Sukop, M.C., and Guo, W., 2007, SEAWAT Version 4: A Computer Program for Simulation of Multi-Species Solute and Heat Transport: U.S. Geological Survey Techniques and Methods Book 6, Chapter A22: , p. 39.

Larsen, F., Tran, L.T.L.V., Van Hoang, H., Tran, L.T.L.V., Christiansen, A.V., and Pham, N.Q., 2017, Groundwater salinity influenced by Holocene seawater trapped in incised valleys in the Red River delta plain: Nature Geoscience, v. 10, p. 376–381, doi:10.1038/ngeo2938.

Lee, J.-Y. et al., 2021, Future Global Climate: Scenario-Based Projections and Near-

Term Information, *in* Masson-Delmotte, V. et al. eds., Climate Change 2021: The Physical Science Basis. Contribution of Working Group I to the Sixth Assessment Report of the Intergovernmental Panel on Climate Change, Cambridge, United Kingdom and New York, NY, USA, Cambridge University Press, p. 553–672, doi:10.1017/9781009157896.006.

Li, C., Tang, X., and Ma, T., 2006, Land subsidence caused by groundwater exploitation in the Hangzhou-Jiaxing-Huzhou plain, China: Hydrogeology Journal, v. 14, p. 1652–1665, doi:10.1007/s10040-006-0092-6.

Liang, M., Geleynse, N., Edmonds, D.A., and Passalacqua, P., 2015, A reduced-complexity model for river delta formation - Part 2: Assessment of the flow routing scheme: Earth Surface Dynamics, v. 3, p. 87–104, doi:10.5194/esurf-3-87-2015.

de Louw, P.G.B., Oude Essink, G.H.P., Stuyfzand, P.J., and van der Zee, S.E.A.T.M., 2010, Upward groundwater flow in boils as the dominant mechanism of salinization in deep polders, The Netherlands: Journal of Hydrology, v. 394, p. 494–506, doi:10.1016/j.jhydrol.2010.10.009.

Mabrouk, M., Jonoski, A., Oude Essink, G.H.P., and Uhlenbrook, S., 2018, Impacts of sea level rise and groundwater extraction scenarios on fresh groundwater resources in the Nile Delta Governorates, Egypt: Water (Switzerland), v. 10, doi:10.3390/w10111690.

Mazzotti, S., Lambert, A., Van der Kooij, M., and Mainville, A., 2009, Impact of anthropogenic subsidence on relative sea-level rise in the Fraser River delta: Geology, v. 37, p. 771–774, doi:10.1130/G25640A.1.

Michael, H.A., and Khan, M.R., 2016, Impacts of physical and chemical aquifer heterogeneity on basin-scale solute transport: Vulnerability of deep groundwater to arsenic contamination in Bangladesh: Advances in Water Resources, v. 98, p. 147–158, doi:10.1016/j.advwatres.2016.10.010.

Michael, H.A., Russoniello, C.J., and Byron, L.A., 2013, Global assessment of vulnerability to sea-level rise in topography-limited and recharge-limited coastal groundwater systems: Water Resources Research, v. 49, p. 2228–2240, doi:10.1002/wrcr.20213.

Michael, H.A., and Voss, C.I., 2009, Estimation of regional-scale groundwater flow properties in the Bengal Basin of India and Bangladesh: Hydrogeology Journal, v. 17, p. 1329–1346, doi:10.1007/s10040-009-0443-1.

Minderhoud, P.S.J., Erkens, G., Pham, V.H., Vuong, B.T., and Stouthamer, E., 2015, Assessing the potential of the multi-Aquifer subsurface of the Mekong Delta (Vietnam) for land subsidence due to groundwater extraction: Proceedings of the International Association of Hydrological Sciences, v. 372, p. 73–76, doi:10.5194/piahs-372-73-2015.

Minderhoud, P., Erkens, G., Pham, V.H., Vuong, B.T., and Stouthamer, E., 2017, Impacts of 25 years of groundwater extraction on subsidence in the Mekong Delta, Vietnam: v. 9, p. 2015.

Minderhoud, P.S.J., Middelkoop, H., Erkens, G., and Stouthamer, E., 2020, Groundwater extraction may drown mega-delta: Projections of extraction-induced subsidence and elevation of the mekong delta for the 21st century: Environmental Research Communications, v. 2, doi:10.1088/2515-7620/ab5e21.

Minnema, B., Vermeulen, P., Riddell, J., Palombi, D., Wallace, S., and Aimo, N., 2013, Utilization of interactive MODeling (iMOD) to facilitate stakeholder engagement in model development usinga sustainable approach with fast,flexible and consistent sub-domain modeling techniques, *in* MODFLOW and More 2013: Translating Science into Practice, Colorado, USA.

Mishra, S.K., and Singh, V.P., 2003, Soil Conservation Service Curve Number (SCS-CN) Methodology: Springer Dordrecht, 516 p., doi:https://doi.org/10.1007/978-94-017-0147-1.

Mollema, P.N., Antonellini, M., Dinelli, E., Gabbianelli, G., Greggio, N., and Stuyfzand, P.J., 2013, Hydrochemical and physical processes influencing salinization and freshening in Mediterranean low-lying coastal environments: Applied Geochemistry, v. 34, p. 207–221, doi:10.1016/j.apgeochem.2013.03.017.

Mulligan, M., van Soesbergen, A., and Sáenz, L., 2020, GOODD, a global dataset of more than 38,000 georeferenced dams: Scientific Data, v. 7, p. 1–8, doi:10.1038/s41597-020-0362-5.

Nicholls, R.J., Adger, W.N., Rahman, M.M., Hutton, C.W., Hanson, S.E., and Salehin, M. (Eds.), 2018, Ecosystem Services for Well-being in Deltas: Integrated Assessment for Policy Analysis: Springer Nature Switzerland AG, 615 p.

Nicholls, R.J., Lincke, D., Hinkel, J., Brown, S., Vafeidis, A.T., Meyssignac, B., Hanson, S.E., Merkens, J.L., and Fang, J., 2021, Author Correction: A global analysis of subsidence, relative sea-level change and coastal flood exposure (Nature Climate Change, (2021), 11, 4, (338-342), 10.1038/s41558-021-00993-z): Nature Climate Change, v. 11, p. 634, doi:10.1038/s41558-021-01064-z.

Nienhuis, J.H., Ashton, A.D., Edmonds, D.A., Hoitink, A.J.F., Kettner, A.J., Rowland, J.C., and Törnqvist, T.E., 2020, Global-scale human impact on delta morphology has led to net land area gain: Nature, v. 577, p. 514–518, doi:10.1038/s41586-019-1905-9.

Nienhuis, J.H., Ashton, A.D., and Giosan, L., 2015, What makes a delta wave-dominated? Geology, v. 43, p. 511–514, doi:10.1130/G36518.1.

Nienhuis, J.H., Hoitink, A.J.F., and Tornqvist, T.E., 2018, Future Change to Tide-Influenced Deltas: Geophysical Research Letters, v. 45, p. 3499–3507, doi:10.1029/2018GL077638.

Nienhuis, J.H., and van de Wal, R.S.W., 2021, Projections of Global Delta Land Loss From Sea-Level Rise in the 21st Century: Geophysical Research Letters, v. 48, p. 1–9, doi:10.1029/2021GL093368.

Orton, G.J., and Reading, H.G., 1993, Variability of deltaic processes in terms of sediment supply, with particular emphasis on grain size: Sedimentology, v. 40, p. 475–512, doi:10.1111/j.1365-3091.1993.tb01347.x.

Oude Essink, G.H.P., 1996, Impact of sea level rise on groundwater flow regimes:

Oude Essink, G.H.P., 1998, MOC3D adapted to simulate 3D density-dependent groundwater flow, *in* Proceedings of MODFLOW ’ 98 Conference at the International Ground Water Modeling Center, Golden, Colorado, USA, v. I, p. 291–303.

Oude Essink, G.H.P., 2001, Salt water intrusion in a three-dimensional groundwater system in the Netherlands: A numerical study: Transport in Porous Media, v. 43, p. 137–158, doi:10.1023/A:1010625913251.

Oude Essink, G.H.P., 1999, Simulating density dependent ground- water flow: the adapted MOC3D, *in* Proceedings of the 15th Salt Water Intrusion Meeting, Ghent, Belgium, p. 69–79.

Oude Essink, G.H.P., van Baaren, E.S., and de Louw, P.G.B., 2010, Effects of climate change on coastal groundwater systems: A modeling study in the Netherlands: Water Resources Research, v. 46, p. 1–16, doi:10.1029/2009WR008719.

Overeem, I., and Syvitski, J.P.M., 2009, Dynamics and Vulnerability of Delta Systems: LOICZ Reports & Studies, v. 35, p. 9–54, doi:10.13140/RG.2.1.5183.6644.

Overeem, I., Syvitski, J.P.M.M., and Hutton, E.W.H.H., 2011, Three-Dimensional Numerical Modeling of Deltas: River Deltas-Concepts, Models, and Examples, p. 11–30, doi:10.2110/pec.05.83.0011.

Peel, M.C., Finlayson, B.L., and Mcmahon, T.A., 2007, Updated world map of the Köppen-Geiger climate classification: Hydrology and Earth System Sciences, p. 1633–1644, www.hydrol-earth-syst-sci.net/11/1633/2007.

Van Pham, H., Van Geer, F.C., Bui Tran, V., Dubelaar, W., and Oude Essink, G.H.P., 2019, Paleo-hydrogeologic reconstruction of the fresh-saline groundwater distribution in the Vietnamese Mekong Delta since the late Pleistocene: Journal of Hydrology: Regional Studies, v. 23, p. 1–22.

Post, V., and Abarca, E., 2010, Saltwater and freshwater interactions in coastal aquifers: Hydrogeology Journal, v. 18, p. 1–4, doi:10.1007/s10040-009-0561-9.

Post, V.E.A., Van der Plicht, H., and Meijer, H.A.J., 2003, The origin of brackish and saline groundwater in the coastal area of the Netherlands: Geologie en Mijnbouw/Netherlands Journal of Geosciences, v. 82, p. 133–147, doi:10.1017/S0016774600020692.

Pratson, L.F. et al., 2007, Seascape Evolution on Clstic Continental Shelves and Slopes,

*in* Nittrouer, C.A., Austin, J.A., Field, M.E., Kravitz, J.H., Syvitski, J.P.M., and Wiberg, P.L. eds., Continental Margin Sedimentation: From Sediment Transport to Sequence Stratigraphy, p. 339–380, doi:10.1002/9781444304398.

Ravenscroft, P., and Mcarthur, J.M., 2004, Mechanism of regional enrichment of groundwater by boron : the examples of Bangladesh and Michigan , USA: v. 19, p. 1413–1430, doi:10.1016/j.apgeochem.2003.10.014.

Richardson, C., and Wright, A., 1984, WGEN: A Model for Generating Daily Weather Variables:

van Rijn, L.C., 1993, Principles of Sediment Transport in Rivers, Estuaries and Coastal Seas: Amsterdam, The Netherlands, Aqua Publications.

Rossi, V.M., Kim, W., López, J.L., Edmonds, D.A., Geleynse, N., Olariu, C., Steel, R.J., Hiatt, M., and Passalacqua, P., 2016, Impact of tidal currents on delta-channel deepening, stratigraphic architecture, and sediment bypass beyond the shoreline: Geology, v. 44, p. 927–930, doi:10.1130/G38334.1.

Scheidt, C., Li, L., and Caers, J., 2018, Quantifying Uncertainty in Subsurface Systems: American Geophysical Union, 304 p.

Schwanghart, W., 2021, Experimental (Semi-) Variogram: MATLAB Central File Exchange, https://www.mathworks.com/matlabcentral/fileexchange/20355-experimental-semi-variogram (accessed April 2021).

Seybold, H., Andrade, J.S., and Herrmann, H.J., 2007, Modeling river delta formation: Proceedings of the National Academy of Sciences, v. 104, p. 16804–16809, doi:10.1073/pnas.0705265104.

Shaw, J.B., Wolinsky, M.A., Paola, C., and Voller, V.R., 2008, An image-based method for shoreline mapping on complex coasts: Geophysical Research Letters, v. 35, p. 1–5, doi:10.1029/2008GL033963.

Simpson, M.W.M., Allen, D.M., and Journeay, M.M., 2014, Assessing risk to groundwater quality using an integrated risk framework: Environmental Earth Sciences, v. 71, p. 4939–4956, doi:10.1007/s12665-013-2886-x.

Socioeconomic Data and Applications Center, 2020, Gridded Population of the World (GPW), v4: Population Count, v4.11, https://sedac.ciesin.columbia.edu/data/set/gpw-v4-population-count-rev11/data-download (accessed October 2022).

Spear, R., and Hornberger, G., 1980, Eutrophication in peel inlet—II. Identification of critical uncertainties via generalized sensitivity analysis: Water Resesarch, v. 14, p. 43–49, https://doi.org/10.1016/0043-1354(80)90040-8.

Stanley, D.J., and Warne, A.G., 1994, Worldwide Initiation of Holocene Marine Deltas by Deceleration of Sea-Level Rise: Science, v. 265, p. 228–231, doi:10.1126/science.265.5169.228.

Steel, E., Paola, C., Chadwick, A.J., Hariharan, J., Passalacqua, P., Xu, Z., Michael, H.A., Brommecker, H., and Hajek, E.A., 2022a, Reconstructing subsurface sandbody connectivity from temporal evolution of surface networks: Basin Research, p. 1–21, doi:10.1111/bre.12668.

Steel, E., Paola, C., Chadwick, A.J., Hariharan, J., Passalacqua, P., Xu, Z., Michael, H.A., Brommecker, H., and Hajek, E.A., 2022b, Reconstructing subsurface sandbody connectivity from temporal evolution of surface networks: , p. 1–21, doi:10.1111/bre.12668.

Syvitski, J.P.M., 2008, Deltas at risk: Sustainability Science, v. 3, p. 23–32, doi:10.1007/s11625-008-0043-3.

Syvitski, J.P.M. et al., 2009, Sinking deltas due to human activities: Nature Geoscience, v. 2, p. 681–686, doi:10.1038/ngeo629.

Syvitski, J., Anthony, E., Saito, Y., Zăinescu, F., Day, J., Bhattacharya, J.P., and Giosan, L., 2022, Large deltas, small deltas: Toward a more rigorous understanding of coastal marine deltas: Global and Planetary Change, v. 218, doi:10.1016/j.gloplacha.2022.103958.

Syvitski, J.P.M., and Saito, Y., 2007, Morphodynamics of deltas under the influence of humans: Global and Planetary Change, v. 57, p. 261–282, doi:10.1016/j.gloplacha.2006.12.001.

Syvitski, J.P.M., Slingerland, R.L., Burgess, P., Meiburg, E., Murray, A.B., Wiberg, P., Tucker, G.E., and Voinov, A.A., 2010, Morphodynamic models : An overview: River, Coastal and Estuarine Morphodynamics, p. 3–20.

Szpakowski, W., 2007, Numerical simulation of the Quaternary Aquifer groundwater flow of Northern Vistula delta plain.: TASK Quarterly, v. 11, p. 411–424.

Tessler, Z.D. et al., 2015, Profiling risk and sustainability in coastal deltas of the world: Science, v. 349, p. 638–643, doi:10.1126/science.aab3574.

Tolman, H.L., 2009, User manual and system documentation of WAVEWATCH-IIITM version 3.14: Technical note, p. 220, http://polart.ncep.noaa.gov/mmab/papers/tn276/MMAB_276.pdf%5Cnpapers2://publication/uuid/298F36C7-957F-4D13-A6AB-ABE61B08BA6B.

Trafford, J., Lawrence, A., Macdonald, D., van Dan, N., Tran, D.N., and Thia Ha, N., 1996, The effect of urbanisation on the groundwater quality beneath the city of Hanoi, Vietnam.:

Tran, L.T., Larsen, F., Pham, N.Q., Christiansen, A. V., Tran, N., Vu, H. V., Tran, L. V., Hoang, H. V., and Hinsby, K., 2012, Origin and extent of fresh groundwater, salty paleowaters and recent saltwater intrusions in Red River flood plain aquifers, Vietnam: Hydrogeology Journal, v. 20, p. 1295–1313, doi:10.1007/s10040-012-0874-y.

United States Environmental Protection Agency, 1984, Hydrologic Evaluation of Landfill Performance (HELP) Model:, https://www.epa.gov/land-research/hydrologic-evaluation-landfill-performance-help-model.

Vandenbohede, A., Luyten, K., and Lebbe, L., 2008, Effects of Global Change on Heterogeneous Coastal Aquifers: A Case Study in Belgium: Journal of Coastal Research, v. 2, p. 160–170, doi:10.2112/05-0447.1.

Vermeulen, P.T.M., Heemink, A.W., Delft, T.U., and Tu Delft, D.U. of T., 2006, Model-reduced inverse modeling: v. PhD, 177 p., doi:urn:NBN:nl:ui:24-uuid:e1736a50-057a-46f5-8bf3-6200279b5ed4.

Wada, Y., van Beek, L.P.H., van Kempen, C.M., Reckman, J.W.T.M., Vasak, S., and Bierkens, M.F.P., 2010, Global depletion of groundwater resources: Geophysical Research Letters, v. 37, p. 1–5, doi:10.1029/2010GL044571.

Waelbroeck, C., Labeyrie, L., Micheal, E., Duplessy, J.C., McManus, J.F., Lambeck, K., Balbon, E., and Labracherie, M., 2002, Sea-level and deep water temperature changes derived from benthic foraminifera isotopic records: Quaternary Science Reviews, v. 21, p. 295–305.

Wagner, F., Bui Tran, V., and Renaud, F.G., 2012, Groundwater Resources in the Mekong Delta: Availability, Utilization and Risks, *in* Renaus, F.G. and Kuenzer, C. eds., The Mekong Delta System: Interdisciplinary Analyses of a River Delta, Springer Environmental Science and Engineering, p. 201–220, doi:10.1007/978-94-007-3962-8_7.

Wagner, G., and Mahrwald, R., 1980, Synthese Von S-Glucuroniden Von 5-Halogen-2-Thiouracilen, Und Von 5-Halogen-4-Thiouracilen: Pharmazie, v. 35, p. 663–668, doi:10.1002/2013WR013725.Received.

van Weert, F., and van der Gun, J., 2012, Saline and Brackish groundwater at shallow and intermediate depths: Genesis and World Wide Occurrence: 2012 Congress of the Canadian branch of the International Association of Hydrogeologists (IAH), p. 1–9, https://www.un-igrac.org/es/resource/saline-and-brackish-groundwater-shallow-and-intermediate-depths-genesis-and-world-wide.

Williamson, A.K., Grubb, H.F., and Weiss, J.S., 1990, Ground-Water Flow in the Gulf Coast Aquifer Systems, South Central United States a Preliminary Analysis: U.S. Geological Survey Water-Resources Investigations Report, v. 89–4071.

Wright, L.D., 1978, River Deltas, *in* Coastal Sedimentary Environments, p. 5–68.

Wright, L.D., 1977, Sediment transport and deposition at river mouths: A synthesis: Bulletin of the Geological Society of America, v. 88, p. 857–868, doi:10.1130/0016-7606(1977)88<857:STADAR>2.0.CO;2.

Wright, L.D., and Coleman, J.M., 1972, River Delta Morphology: Wave Climate and the Role of the Subaqueous Proffile: Science, v. 176, p. 282–284,

doi:10.1126/science.176.4032.282.

Wright, L.D., and Coleman, J.M., 1973, Variations in morphology of major river deltas as functions of ocean wave and river discharge regimes: American Association of Petroleum Geologists Bulletin, v. 57, p. 370–398, doi:10.1306/819A4274-16C5-11D7-8645000102C1865D.

Wright, L.D., Coleman, J.M., and Erickson, M.W., 1974, Analysis of Major River Systems and Thier Deltas: Morphologic and Process Comparisons: Technical report, v. 156, p. 114.

Wright, L.D., Coleman, J.M., and Thom, B.G., 1975, Sediment Transport and Deposition in a Macrotidal River Channel: Ord River, Western Australia: Geology and Engineering, p. 309–321.

Xu, Z., Hariharan, J., Passalacqua, P., Steel, E., Chadwick, A., Paola, C., Paldor, A., and Michael, H.A., 2022, Effects of Geologic Setting on Contaminant Transport in Deltaic Aquifers: Water Resources Research, doi:10.1029/2022wr031943.

Xu, Z., Hariharan, J., Passalacqua, P., Steel, E., Paola, C., and Michael, H.A., 2021, Linking the Surface and Subsurface in River Deltas—Part 2: Relating Subsurface Geometry to Groundwater Flow Behavior: Water Resources Research, v. 57, doi:10.1029/2020WR029281.

Yu, X., and Michael, H.A., 2019, Offshore pumping impacts onshore groundwater resources and land subsidence: Geophysical Research Letters, p. 1–10, doi:10.1029/2019gl081910.

Zamrsky, D., Essink, G.H.P.O., and Bierkens, M.F.P., 2018, Estimating the thickness of unconsolidated coastal aquifers along the global coastline: , p. 1–19.

Zhou, Y.Q., Sawyer, A.H., David, C.H., and Famiglietti, J.S., 2019, Fresh Submarine Groundwater Discharge to the Near-Global Coast: Geophysical Research Letters, v. 46, p. 5855–5863, doi:10.1029/2019GL082749.

# Appendix A.

# Supplemental information for Chapter 2

## Global delta data

The Syvitski and Saito (2007) dataset has 51 deltas, the Caldwell et al. (2019) dataset has 2,174, and the Nienhuis et al. (2020) dataset has 10,848 deltas. Variables of interest in the Syvitski and Saito (2007) dataset include discharge, wave height, tidal range, area of the delta plain, sediment concentration, and grain size. The Caldwell et al. (2019) dataset is used to gather more information on wave height, tidal range, and bathymetric gradient. The Nienhuis et al. (2020) dataset is used for the latitude and longitudinal point of the delta, discharge, and tidal range. Only one data point from each dataset is used to characterize a delta. The datasets are joined based on latitude and longitude by selecting the datapoint closest to the location of each delta. A joined datapoint is excluded from this study if it fell outside the delta plain, defined by the distance between the data point and the delta being more than the square root of the distance of the delta plain.

More than one dataset includes information on the wave and tidal conditions within the 51 selected deltas. The Caldwell et al. (2019) wave height data are collected from wave hindcasts (Tolman, 2009; Chawla et al., 2013) and exhibit overall higher values than the wave height data in Syvitski and Saito (2007) which are maximum-monthly wave heights from the Wave-WatchIII model (http://polar.ncep.noaa.gov/waves/main_int.html). The tidal data published in the Syvitski and Saito (2007) exhibit the highest values of the three datasets. The median tidal range of the Syvitski and Saito (2007), Caldwell et al. (2019), and Nienhuis et al. (2020) datasets for the 51 selected deltas used in this study are 2 m, 0.9 m, and 0.7 m, receptively. The Caldwell et al. (2019) dataset was generated from a tidal inversion model (Egbert and Erofeeva, 2002) and exhibits the second highest values. The Nienhuis et al. (2020) dataset is also generated from the same tidal inversion model (Egbert and Erofeeva, 2002), but exhibits slightly smaller values for each delta. Multiple values of wave height and tidal range for each delta are averaged to provide a single value for each delta. The distributions of the averaged wave and tidal data are

comparable to the distributions shown in Caldwell et al. (2019). Therefore, it is unlikely that unrealistic wave or tidal heights are created due to averaging.

# Modeling domain

## Domain size

The area of the modeling domain (Figure A1) impacts the ability of a model to run without producing errors. Initial modeling found that the domain needs to be large enough to accommodate the highest fluvial input. If the domain is too small, too much sediment erodes from one cell and the simulation terminates due to runtime errors. In this study, the modeling domain was chosen to accommodate the majority of deltas built in models with the largest fluvial discharge (Qav = 22,000 $m^3/s$). This resulted in models that took weeks to run on a single core. Initial research indicates that scaling the model domain and discharge down to reduce runtimes may result in changes in delta morphology and the potential for delta formation. This change in morphology may be supported by recent work suggesting that small and large deltas do not respond the same to certain processes and that they should be considered separately. More research is needed to determine how model domain size impacts delta formation and if these models are accurately representing deltaic processes at a variety of spatial scales.

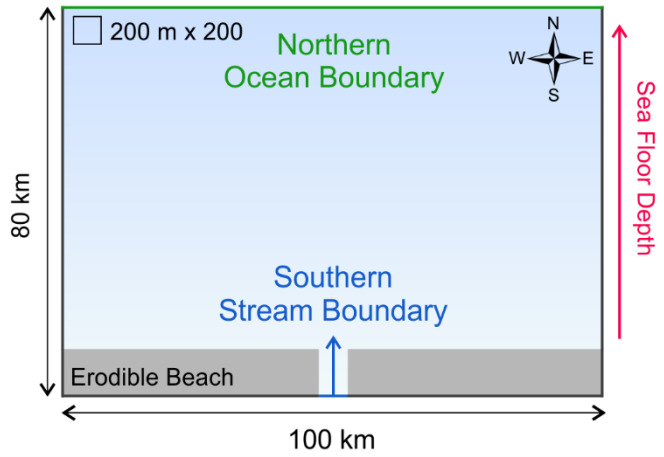


**Figure A1. Modeling domain setup.**

## Water boundary conditions

The modeling domain has four boundaries: the stream, northern, eastern, and western boundary Initial modeling indicates that the specification of the eastern and western boundary conditions impacts delta formation within the models. When waves or tides are assigned to the eastern and western boundaries (i.e. assigning the same conditions as to the eastern and western boundaries as is specified in the northern boundary), interference patterns appear as constructive or decoctive effects in the water level between the eastern and northern or western and northern boundaries. The interference patterns are most notable in models with high tidal ranges, resulting from the water level rising along all three boundaries simultaneous and propagating radially toward the middle of the modeling domain rather than perpendicular to the shoreline, as would be expected in a simplified real-world scenario (not accounting for directionality of waves). The radial direction of water level rise toward the middle of the modeling domain decreases the likelihood of sediment deposition, especially when Pf is low compared to Pw and Pt. In some cases when Pt is high, sediment builds along the eastern and western boundary in addition to the southern (Figure A2). Changing the eastern and western boundaries to no-flux boundaries (the default when no boundary conditions are specified) results in water level changes that propagates toward the shoreline and allows for sediment deposition in models with high wave height and tidal range. Since the water level undulation in models where the eastern and western boundaries are no-flux boundaries is more realistic, this is what is used in the models analyzed in this study.

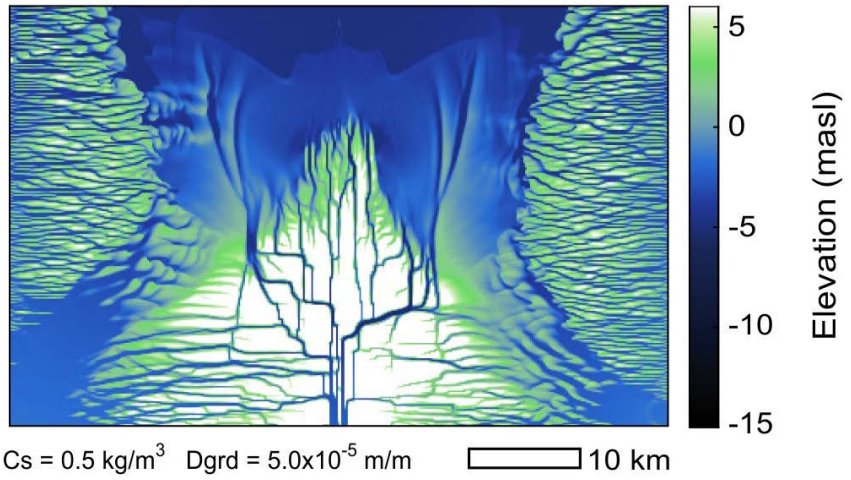


**Figure A2. Delta formation and morphology for a tidal-influenced model with the eastern and western boundaries specified with the same tidal amplitude as the northern boundary (Pf = 0.9, Pw = 0, and Pt = 0.9).**

Initial modeling also indicates that the width of the initial river in each model is shown to impact the ability of a model to finish the simulation without producing errors. The river width in each model must be large enough to accommodate the fluvial and sediment discharge coming into the basin. If the river width is not large enough, discharge overtops the initial riverbanks, and the river erodes into the beach until a sufficient path is formed to accommodate the high discharge rates. If the discharge rates are high, such as those in the 90 percentiles of discharge, too much erosion occurs in cells that tend to be around the river boundary and produces errors in the modeling output. While small river width does not inhibit delta formation in the modeling environment, it may affect characteristics of the morphology, such as area of the delta plain and number of distributary channels.

## Sediment boundary conditions

Sediment within the model enters through the river total discharge boundary. The incoming sediment distribution includes six sediment types ranging in size from clay ($2x10^{-3}$ µm) to coarse sand (2 mm) and follows a simplistic unimodal normal distribution. Each sediment type is defined with a particle size, settling velocity for non-cohesive particles, and a dry bulk density. Particle sizes under $6.4x10^{-2}$ mm are treated as cohesive particles in the model (Deltares, 2013). The settling velocity of the non-cohesive sediment types are defined by the relations in Gibbs et al. (1971) and the

settling velocities for cohesive sediment are computed using the van Rijn (1993) method. The default values for dry-bulk density, 1600 kg/m$^3$ for non-cohesive and 500 kg/m$^3$ for cohesive sediment. Table A1 outlines the sediment types and their associated properties.

Sediment transport is computed using van Rijn (1993) equations for bedload and suspended sediment transport. The effect of salinity on sediment transport and settling is accounted for in this study. The incoming river discharge has a salinity concentration of 0 ppt while the ocean boundaries have a constant salinity concentration of 35 ppt, representing average oceanic salinity.

**Table A1. Description of sediment type and their properties.**

| Sediment | Grain Size (mm) | Settling Velocity (mm/s) | Dry-bulk Density (kg/m$^{-3}$) |
|---|---|---|---|
| **Very coarse sand** | 2 | $8.5 \times 10^{-1}$ | 1600 |
| **Medium sand** | $6 \times 10^{-1}$ | $4.4 \times 10^{-2}$ | 1600 |
| **Fine sand** | $1 \times 10^{-1}$ | $8.9 \times 10^{-4}$ | 1600 |
| **Medium silt** | $3 \times 10^{-2}$ | - | 500 |
| **Find silt** | $8 \times 10^{-3}$ | - | 500 |
| **Clay** | $2 \times 10^{-3}$ | - | 500 |

The distribution of sediment coming into the model through the stream boundary follows a simplistic unimodal distribution (Figure A3). The distribution has a mean of $1.3 \times 10^{-1}$ mm in the base-case model, a mean of $3.1 \times 10^{-2}$ mm in the low Dmm model, and a mean of $6.4 \times 10^{-1}$ mm in the high Dmm model. All three of the distributions have a standard deviation of 0.1 mm.

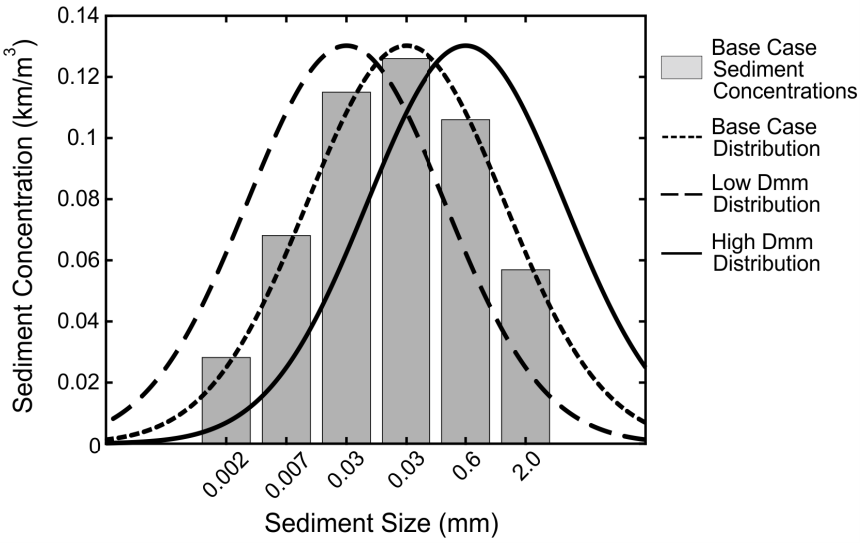


**Figure A3. Normal distributions that the base case, low Dmm, and high Dmm models are based on. The histogram indicates the percent of each sediment type that is present within the fluvial discharge entering the base case models.**

The concentration of each sediment type in the base case, low Dmm, and high Dmm models (Table A2) are based on the distributions shown in Figure A3. The base case model has 37% cohesive sediments, the low Dmm models have 64% cohesive sediments, and the high Dmm models have 18% cohesive sediments. A visual representation of the sediment distributions in the base case, low Dmm, and high Dmm models is provided in Figure A3.

**Table A2. Concentration (kg/m$^3$) of each sediment type in the base case, low Dmm, and high Dmm models. The percent of each grain size compared to the total sediment input within each mode is listed next to the concentration value in brackets.**

| Sediment | Base case | Low Dmm | High Dmm |
|---|---|---|---|
| **Very coarse sand** | 0.0057 [11%] | 0.026 [5%] | 0.11 [23%] |
| **Medium sand** | 0.11 [21%] | 0.061 [12%] | 0.16 [31%] |
| **Fine sand** | 0.13 [25%] | 0.098 [20%] | 0.12 [25%] |
| **Medium silt** | 0.12 [23%] | 0.13 [27%] | 0.068 [14%] |
| **Find silt** | 0.068 [14%] | 0.11 [22%] | 0.024 [5%] |
| **Clay** | 0.0028 [6%] | 0.070 [14%] | 0.015 [3%] |

## Modeling results

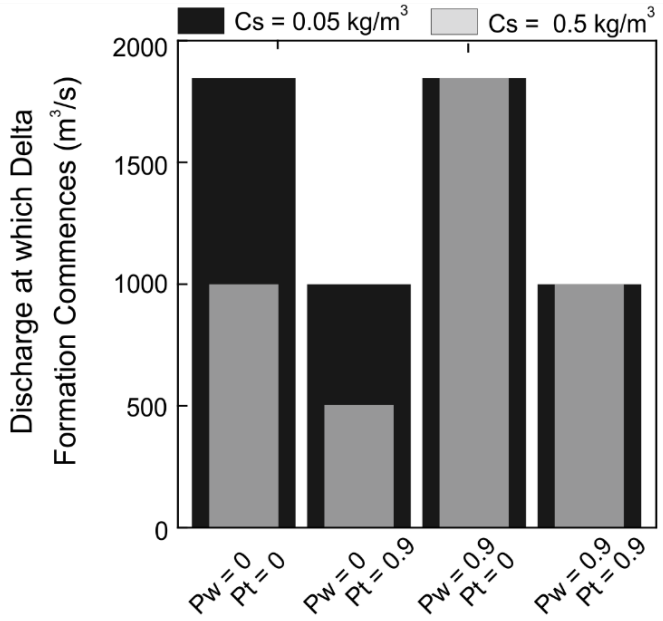


**Figure A4.** **Discharge at which delta formation commences for fluvial (Pw = 0, Pt = 0), tidal (Pw = 0, Pt = 0.9), wave (Pw = 0.9, Pt = 0), and mixed environments (Pw = 0.9, Pt = 0.9). Black bars represent models with a Cs = 0.05 kg/m$^3$ and grey bars represent models with a Cs = 0.5 kg/m$^3$.**

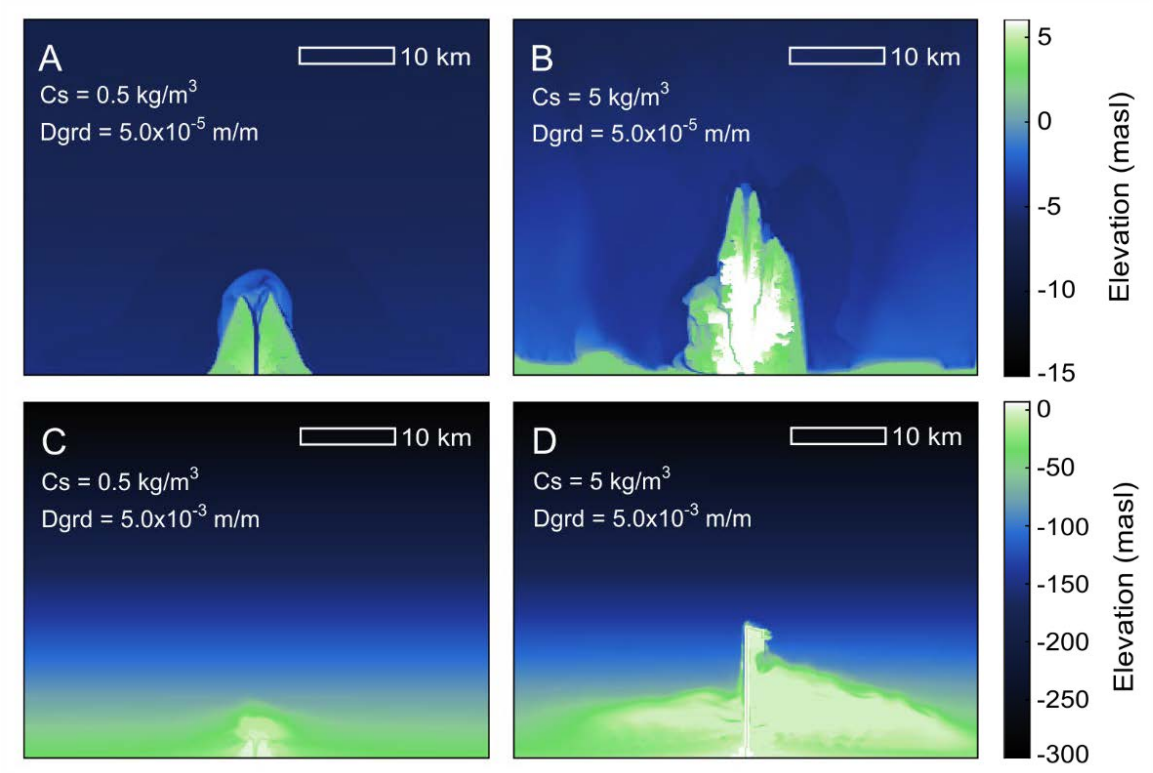


**Figure A5.** **Delta formation and morphology for four models with the same morphodyanmic influence ratio of 0.35, 0.42, and 0.23 for nMlf, nMlw, and nMlt, respectively: A) small bathymetric gradient, B) small bathymetric gradient and high sediment concentration, C) large bathymetric gradient, and D) large bathymetric gradient and high sediment concentration.**

# Appendix B.

# Supplemental data for Chapter 2

The accompanying Excel spreadsheet (AA_AppendixB.xlsx) shows the input parameters for the 229 models created in Chapter 2. results. The spreadsheet includes for following columns:

ID, Name, Sed_formed, Qav, Wa, Ti, nMIr, nMIw, nMIt, Cs, Dgrd, River_width, Sed_discharge(m3/2), Dmm.

In the Sed_formed column, 1 means that a delta formed, 0 means that a delta did not form, and NaN means that the simulation did not finish.

**Filename: AA_AppendixB.xlsx**

# Appendix C.

# Supplemental information for Chapter 3

## Modeling domain

The initial model setup, described in Chapter 2, is based on the modeling protocol described in Caldwell and Edmonds (2014). The models mimic a sediment-carrying river debouching into an oceanic basin with waves and tides. The initial shoreline is located along the southern boundary of the model and consists of an erodible beach 5 meters above sea level (m asl). The shoreline protrudes 5 km into the basin. The beach and the basin floor are 0.5 m thick and consist of homogenously mixed sediments that have the same distribution of sizes as the incoming sediment. A channel cuts through the initial shoreline half-way along the southern boundary. The depth of the sea floor is shallowest at -5 m asl in the channel at the southern boundary and deepens to the north with a uniform gradient that ranges from $5.0 \times 10^{-5}$ m/m to $5.0 \times 10^{-3}$.

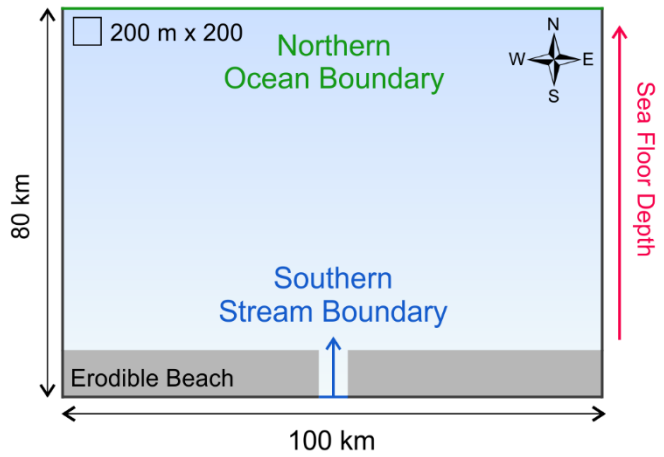


**Figure C1. Modeling domain.**

## Sediment in the models

Sediment in the model is represented with six sediment types, ranging from very coarse sand to clay (Table C1). Particle sizes under $6.4 \times 10^{-2}$ mm are treated as cohesive particles in the model. The default values for dry-bulk density, 1600 $\mathrm{kg\,m^{-3}}$ for non-cohesive and 500kg/m$^3$ for cohesive sediment, are used to calculate the sediment

thickness. Settling velocities for cohesive sediments follows the relation defined by Gibbs et al. (1971) (Table C1, column 3) and the settling velocities non-cohesive sediments is computed using the van Rijn (1993) method. Models in this study consider three unimodal grain-size distributions that center around a median grain size (Dmm): 1) base case (Dmm = 31 μm; Table C1, column 5), low Dmm (Dmm = 0.13 mm; Table C1, column 6), and high Dmm (Dmm = 0.5 mm; Table B1, column 7). Each delta model starts with a thin layer of sediment (0.5 m thick) that contains the six grain sizes in a proportion equal to the concentration of incoming sediment within the stream boundary (Table C1, columns 5-7).

Throughout the model simulation, sediment is transported throughout the model based on the grain size of sediment and the sediment transport equations used (Deltares, 2013). In general, coarse-grained sediments are deposited within the delta plain and fine-grained sediments are transported out of the delta plain, depositing farther into the receiving basin where the water velocity is lower (Figure C2).

**Table C1. Description of sediment type and their properties.**

| Sediment | Grain Size (mm) | Settling Velocity (mm/s) | Dry-bulk Density ($kg/m^{-3}$) | Concentration of sediment in models | | |
|---|---|---|---|---|---|---|
| | | | | Base case | low Dmm | high Dmm |
| **Coarse sand** | 2 | $8.5x10^{-1}$ | 1600 | $5.7x10^{-2}$ | 0.026 | 0.11 |
| **Medium sand** | $6.4x10^{-1}$ | $4.4x10^{-2}$ | 1600 | $1.1x10^{-1}$ | 0.061 | 0.16 |
| **Fine sand** | $1.3x10^{-1}$ | $8.9x10^{-4}$ | 1600 | $1.3x10^{-1}$ | 0.098 | 0.12 |
| **Medium silt** | $3.1x10^{-2}$ | - | 500 | $1.2x10^{-1}$ | 0.13 | 0.07 |
| **Fine silt** | $7.8x10^{-3}$ | - | 500 | $6.8x10^{-2}$ | 0.11 | 0.024 |
| **Clay** | $2.0x10^{-3}$ | - | 500 | $2.8x10^{-2}$ | 0.07 | 0.015 |

## Permeability heterogeneity and anisotropy

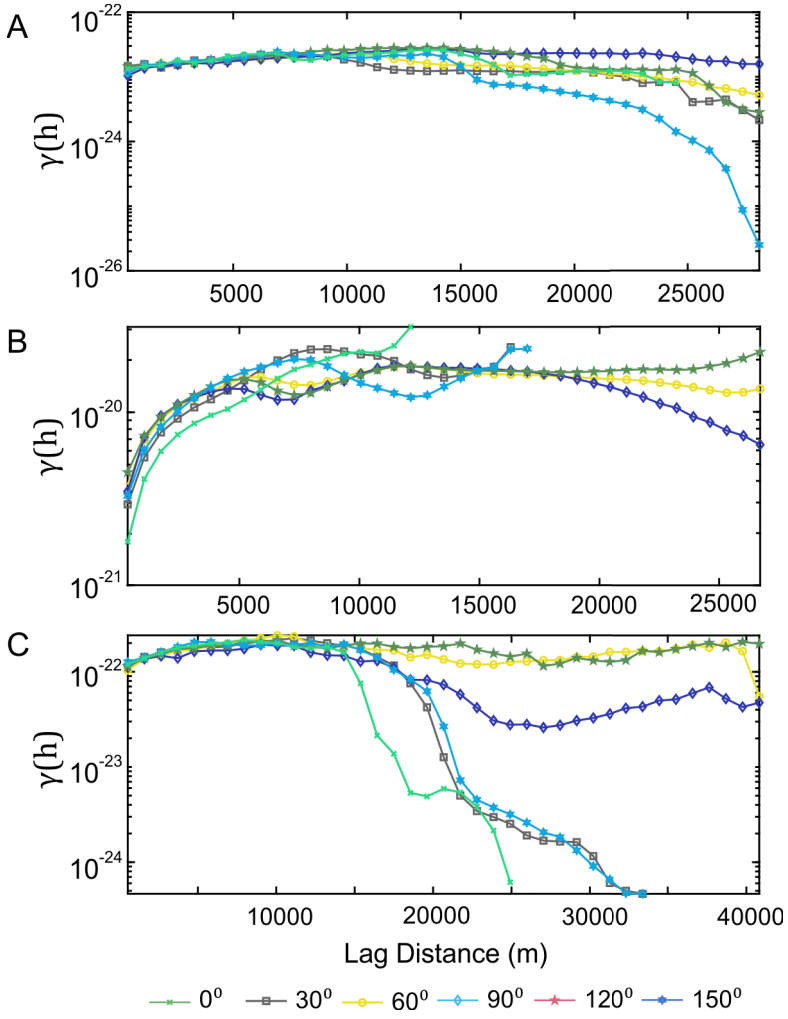


**Figure C2.** **Directional semivariograms (in units of $(m^2)^2$) for a A) fluvial, B) wave, and C) tidal delta permeability map. The angles are measured as the angle of deviation from the initial shoreline in the model (i.e. 90 degrees is perpendicular to the initial shoreline and parallel to the incoming river channel). Note that the scales on the horizontal and vertical axis are different in each plot.**

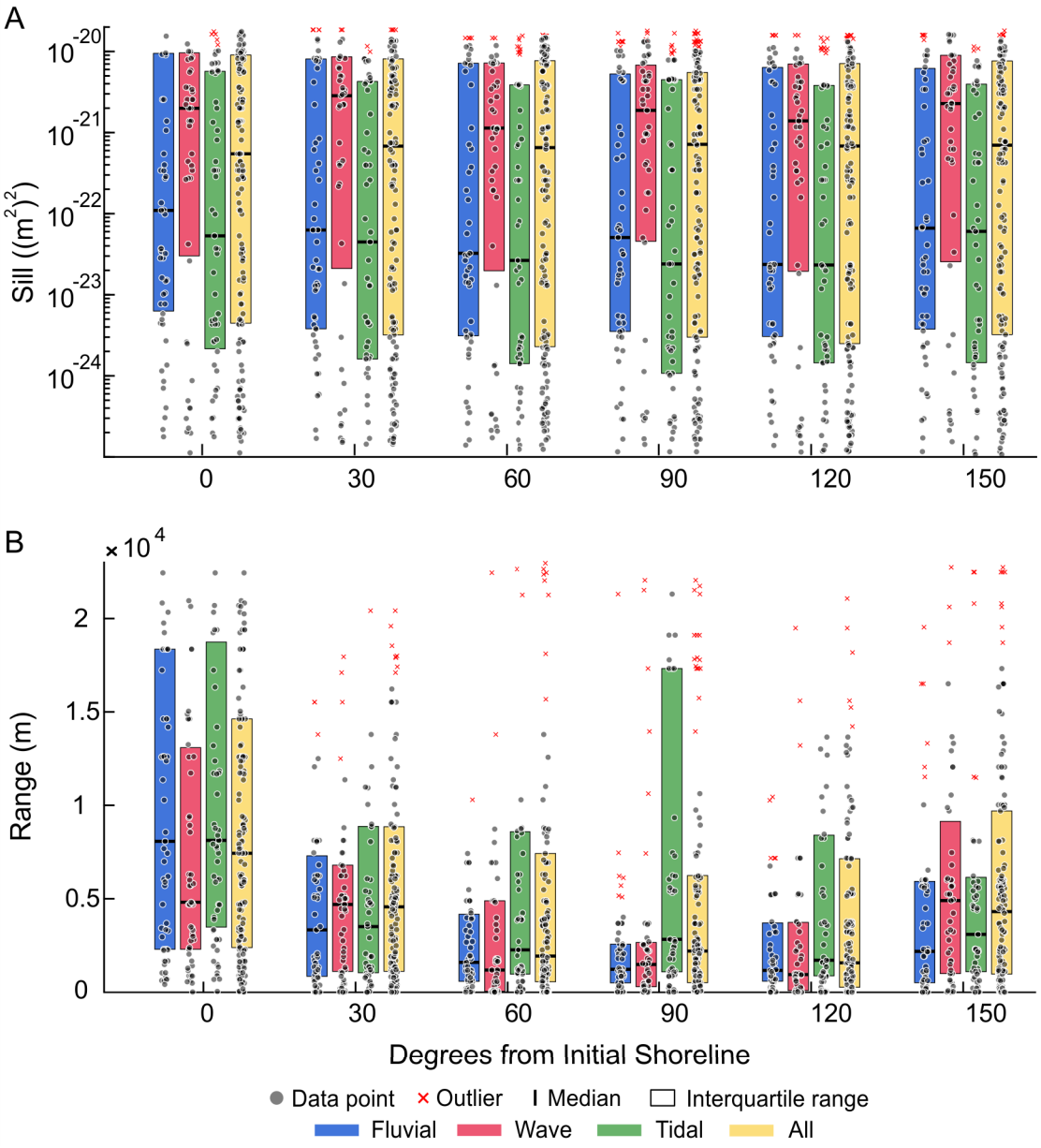


**Figure C3.** **The average A) range and B) sill for directional semivariograms of the permeability in fluvial, wave, tidal, and all models.**

## Distribution of each sediment type

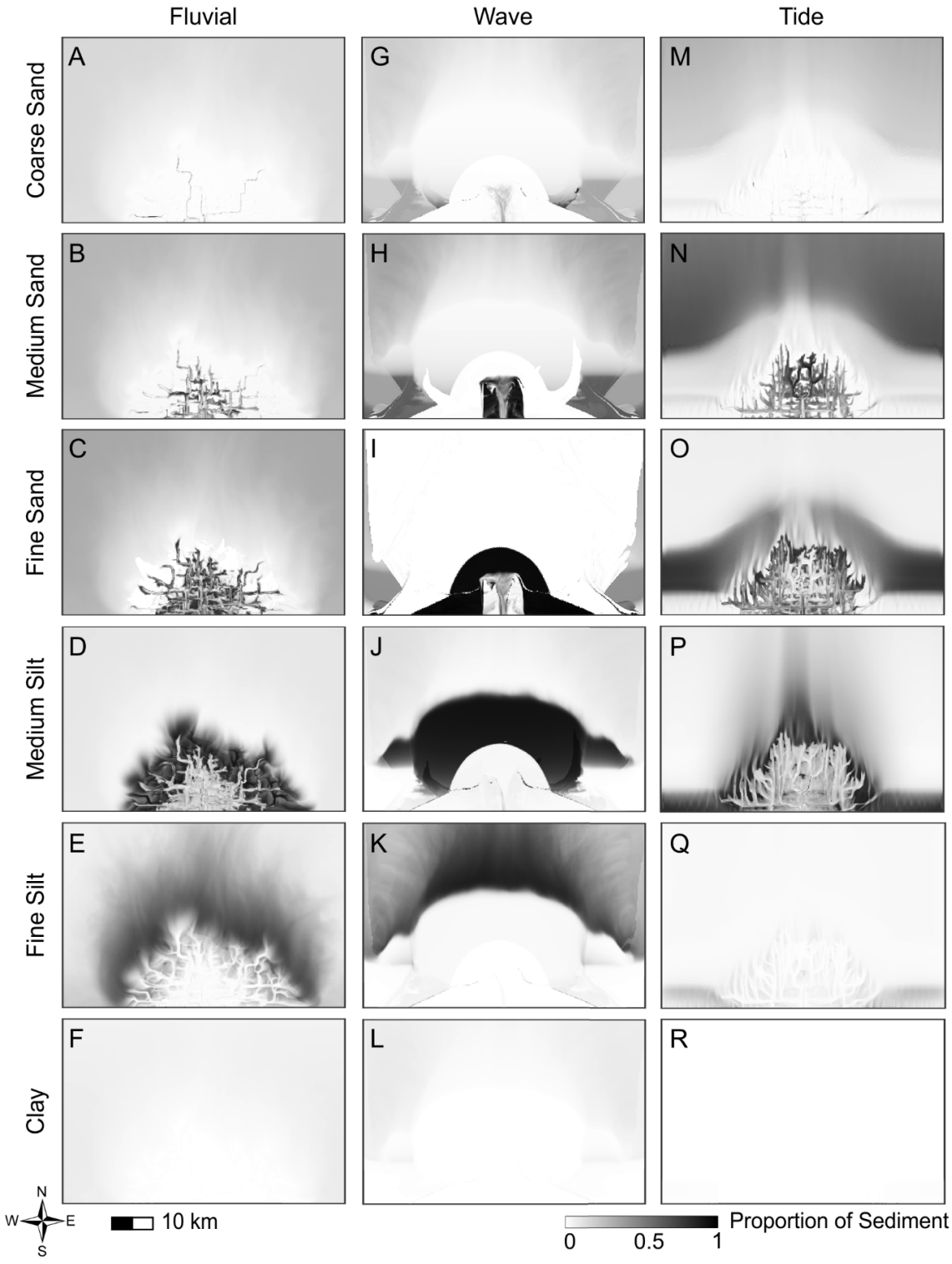


**Figure C4.** **Percent accumulation maps for each grain size in a A-F) fluvial, G-L) wave, and M-R) tidal delta model.**

# Appendix D.

# Supplemental data for Chapter 3

The accompanying Excel spreadsheet (AA_AppendixD.xlsx) shows the input parameters for the 229 models created in Chapter 2 along with the geomorphic and hydrogeologic parameters calculated for each delta model in Chapter 3. The spreadsheet includes for following columns:

ID, Name, Sed_formed, Qav, Wa, Ti, Cs, Dgrd, Dmm, Ad, Cn, Tcl, L, Ncw, Sh, Sr, k, K, d10, Co, NumCo, SizeCo, 90th_percentile_of_k, hp_in_cn, dh/dl, q, q_min, q_max, Ahp, Range_0, Range_30, Range_60, Range_90, Range_120, Range_150, Sill_0, Sill_30, Sill_60, Sill_90, Sill_120, Sill_150.

In the Sed_formed column, 1 means that simulation formed a delta formed, 0 means that a delta did not form, and NaN means that the simulation did not finish.

Some of the variables in this spreadsheet are not discussed in Chapter 3. As such, a definition of the additional variables is given:

| | |
|---|---|
| Tcl | Total channel length |
| L | Length of the longest channel |
| Ncw | Channel width normalized by the number of channels |
| NumCo | Number of connective bodies |
| SizeCo | Size of the largest connective body |
| q_min | Specific discharge calculated using the smallest dh/dl |
| q_max | Specific discharge calculated using the largest dh/dl |
| hp_in_cn | Percent of high permeability area contained within the channel network |

**Filename: AA_AppendixD.xlsx**

# Appendix E.

# Supplemental information for Chapter 4

## Numerical Modeling Methods

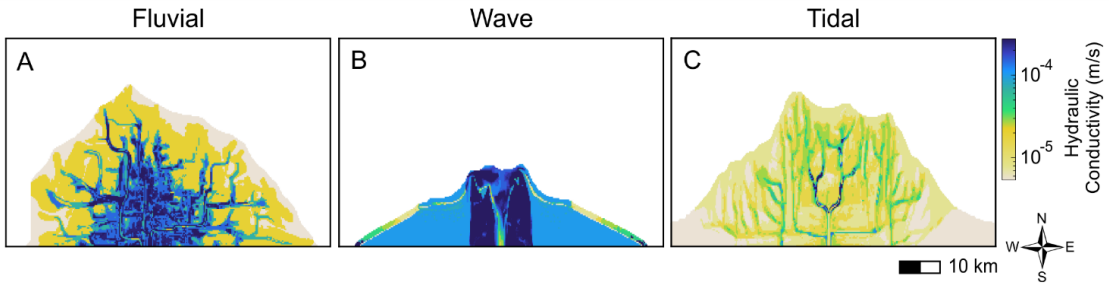


**Figure E1.** **Hydraulic conductivity for the A) fluvial, B) wave, and C) tidal influenced deltas.**

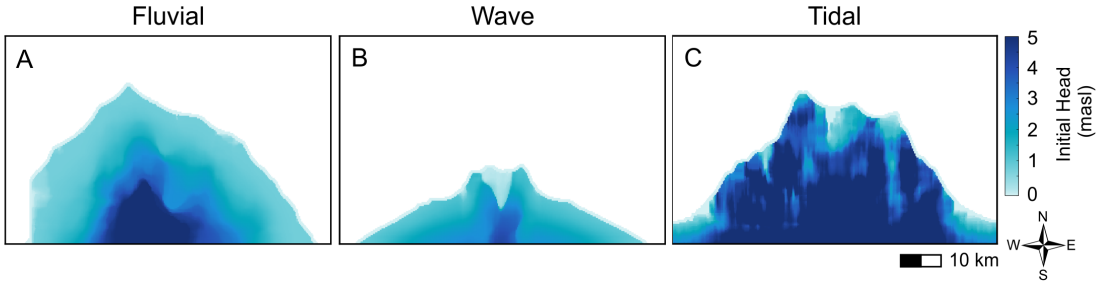


**Figure E2.** **Initial freshwater head for the A) fluvial, B) wave, and C) tidal influenced deltas.**

# HELP Water Balance Modeling Methods

**Table E1. Weather generator representative climate station and evapotranspiration parameters.**

| | Arid | Temperate | Tropical |
|---|---|---|---|
| **Station name** | Damascus Airport | Venezia/b Tesser | Saigon (Ho Chi Min) |
| **Station longitude** | 34.445 | 12.385 | 106.825 |
| **Station latitude** | 31.195 | 44.929 | 9.934 |
| **Station distance from delta shoreline (km)** | 470 | 60 | 100 |
| **Evaporative zone depth (cm)** | 38 | 25 | 25 |
| **Maximum leaf area Index** | 2 | 5 | 5 |
| **Growing season start day** | 323 | 74 | 111 |
| **Growing season end day** | 38 | 319 | 348 |
| **Average wind speed (km/h)** | 13 | 123 | 14 |
| **First quarter relative humidity (%)** | 70 | 75 | 72 |
| **Second quarter relative humidity (%)** | 62 | 70 | 71 |
| **Third quarter relative humidity (%)** | 61 | 68 | 77 |
| **Fourth quarter relative humidity (%)** | 68 | 77 | 75 |

**Table E2. Weather generator station climate normals by month.**

| | Precipitation (mm) | | | Temperature (°C) | | |
|---|---|---|---|---|---|---|
| | Tropical | Temperate | Arid | Tropical | Temperate | Arid |
| **Jan** | 4.3 | 42 | 16 | 27 | 2.6 | 6.5 |
| **Feb** | 2.5 | 47 | 20 | 28 | 4.1 | 8.1 |
| **Mar** | 5.6 | 58 | 28 | 29 | 8.3 | 11 |
| **Apr** | 29 | 53 | 10 | 30 | 12 | 16 |
| **May** | 74 | 65 | 1.9 | 30 | 17 | 20 |
| **Jun** | 130 | 83 | 1.2 | 29 | 20 | 24 |
| **Jul** | 14038.9 | 69 | 0.3 | 28 | 23 | 27 |
| **Aug** | 130 | 64 | 0.6 | 28 | 22 | 26 |
| **Sep** | 160 | 64 | 0.7 | 28 | 19 | 23 |
| **Oct** | 160 | 75 | 16 | 28 | 14 | 18 |
| **Nov** | 60 | 59 | 20 | 27 | 7.6 | 12 |
| **Dec** | 11 | 48 | 21 | 26 | 3.9 | 7.7 |

**Table E3. Vertical percolation column parameters.**

| | Low Conductivity | Medium Conductivity | High Conductivity |
|---|---|---|---|
| **Total porosity (vol/vol)** | 0.43 | 0.46 | 0.42 |
| **Field capacity (vol/vol)** | 0.32 | 0.08 | 0.05 |
| **Wilting point (vol/vol)** | 0.22 | 0.033 | 0.018 |
| **Saturated hydraulic conductivity (m/s)** | $3.3 \times 10^{-7}$ | $3.1 \times 10^{-5}$ | $1.0 \times 10^{-4}$ |
| **Subsurface inflow (m/s)** | 0.00 | 0.00 | 0.00 |

# Results

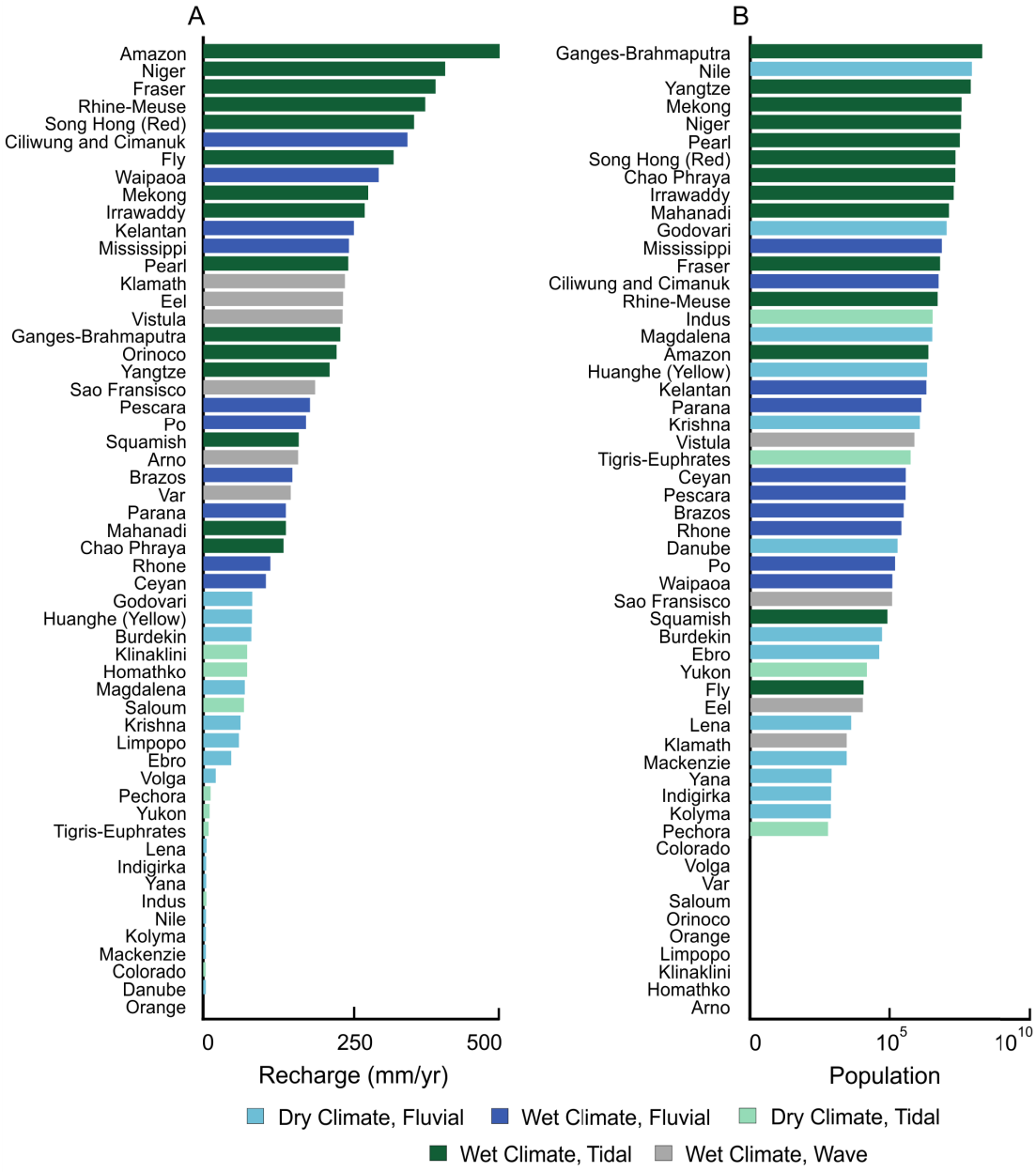


**Figure E3. A) Recharge and B) population for 60 of the largest and most populated coastal deltas around the world.**

# Appendix F.

# Supplemental Data for Chapter 4

The accompanying Excel spreadsheet (AA_AppendixF.xlsx) shows the morphodynamic, recharge, population, and groundwater salinity information for the 60 deltas investigated in Chapter 4. Calculated susceptibility, hazard, and vulnerability are also included. The spreadsheet includes for following columns:

Delta_ID, Lat, Long, Delta, Country, Name, Qfluvial, Qtide, Qwave, Rfluvial, Rtide, Rwave, Delta_type, R, P, Salinity.

In the Delta_type column, 1 means that the delta is fluvial, 2 means that the delta is wave, 3 means that the delta is tidal, and 4 means that the delta is mixed.

In the Salinity column, 1 means that there is known groundwater salinity from pervious marine transgressions in the delta and 0 means that there is no scientific research demonstrating the presence of salinity from previous transgressions.

**Filename: AA_AppendixF.xlsx**